FACILITY FORM 602

N66 35745
(ACCESSION NUMBER)

116
(PAGES)

CR-76473
(NASA CR OR TMX OR AD NUMBER)

[redacted]1
(THRU)

(CODE)

30
(CATEGORY)

NORTHROP

A STUDY ON SENSOR SYSTEMS FOR INITIATING PARACHUTE DEPLOYMENT FOR A MARS ENTRY VEHICLE

PREPARED FOR

JET PROPULSION LABORATORY

CALIFORNIA INSTITUTE OF TECHNOLOGY

CONTRACT NAS-7-100

NVR-4062

A STUDY ON SENSOR SYSTEMS FOR INITIATING PARACHUTE DEPLOYMENT FOR A MARS ENTRY VEHICLE

Prepared for

Jet Propulsion Laboratory
California Institute of Technology
Under Contract 951174

Prepared by

Fred E. Mickey

This work was performed for the Jet Propulsion Laboratory, California Institute of Technology, sponsored by the National Aeronautics and Space Administration under Contract NAS7-100.

Approved by

Chas Green

Charles H. Green, Chief
Analytical Engineering Group

Issued:
June 1966

NORTHROP CORPORATION, VENTURA DIVISION
1515 Rancho Conejo Boulevard
Newbury Park, California 91320

FOREWORD

This is the final report presenting the results of a study performed during Fiscal Year 1966 at Northrop Ventura, Newbury Park, California. The study was performed for the Jet Propulsion Laboratory, California Institute of Technology, under the authority of Contract No. 951174. Mr. Jay W. Stuart, Jr., of the Jet Propulsion Laboratory, served as the Technical Representative.

The work was performed under the general direction of Mr. George F. Douglas, Vice President and General Manager, and Mr. George C. Grogan, Jr., Vice President and Manager, Technical Department. At Northrop Ventura, the study was identified as Project 6037.

The technical effort was carried out with direction from the Analysis Group under Mr. Charles H. Green. Program direction was provided by Mr. Robert N. Worth, Program Manager. The electrical design contributions were made by Mr. Graham Judge and Mr. Francis A. Morse. The reliability analysis contributions were made by Mr. Ben W. Pankratz. The performance analyses were carried out by Fred Mickey who was also the chief contributor to this report.

ABSTRACT

3/933

The results of a study, encompassing the analysis of sensor systems suitable for initiating parachute deployment on a Mars entry vehicle, are presented. It is shown that a variety of sensor concepts are feasible in various degrees. Several of these concepts are analyzed, preparatory to selecting two for use as parallel subsystems in a "Final System." The performance of the Final System is analyzed in terms of ten independent variables, and it is found that the largest altitude-uncertainty component is due to the current lack of good definition for the Martian atmosphere. An electrical design for the Final System is presented, and it is shown conclusively that today's technology and hardware can provide a sensor system with sufficient flexibility to assure accurate sensing over the wide range of possible Martian atmospheres, entry conditions and environmental conditions currently postulated for the mission. A reliability analysis, presenting guidelines for additional reliability improvement, is also included as part of the study.

CONTENTS

PAGE NO.

FOREWORD iii

ABSTRACT v

1.0 INTRODUCTION 1

1.1 The Sensor Problem 1

1.2 The Program Plan 3

2.0 SCOPE OF STUDY 7

2.1 The Trajectory Data 7

2.2 The Lander Vehicle 10

2.3 The Planet Mars and Its Atmosphere 15

2.4 The Entry Conditions 15

2.5 The Specified Parachute Deployment Conditions 18

2.6 The Environmental Conditions 18

2.7 The Operational Errors 18

3.0 FEASIBLE SYSTEMS STUDY (PHASE 1) 23

3.1 Feasible Systems' Descriptions 23

3.2 Ideas for Other Systems 29

3.3 Feasible Systems Analyses 29

4.0 CANDIDATE SYSTEMS STUDY (PHASE 2) 35

4.1 Performance Analysis Approach 36

4.2 Subsystem Definitions 39

4.2.1 Acceleration Subsystem 39

4.2.2 Base Pressure Subsystem 41

4.2.3 Base Pressure to Acceleration Ratio Subsystem 42

4.2.4 Acceleration Function Subsystem . . . 42

4.2.5 Ideal M = 1.0 System 43

4.3 Matrix Equation Defined 43

4.4 Performance Analysis Results 43

CONTENTS (Concluded)

PAGE NO.

4.5 Prime Sensor Trade Studies 47

4.5.1 Accelerometers 49

4.5.2 Pressure Transducers 49

4.6 Candidate Systems Ranking 52

5.0 FINAL SYSTEM STUDY (PHASE 3) 55

5.1 Performance Analysis 55

5.1.1 Performance Analysis Approach . . . 55

5.1.2 Final System Performance Analysis Results 59

5.2 Electrical Design 67

5.2.1 Introductory Remarks 67

5.2.2 Arming of the Primary Subsystem 67

5.2.3 Circuit Operation 69

5.2.4 Error Analysis 77

5.2.5 Parts List and Weight Estimate 81

5.3 Reliability Analysis 81

5.3.1 Redundancy Considerations 83

5.3.2 System Design 85

5.3.3 Failure Mode and Effects Analysis 87

5.3.4 Reliability Recommendations 89

6.0 CONCLUSIONS 93

7.0 RECOMMENDATIONS 95

REFERENCES 97

APPENDIX A: NOMENCLATURE 99

TABLES

PAGE NO.

TABLE 1a	-	SUMMARY OF THE TRAJECTORY RUNS.	8
TABLE 1b	-	SUMMARY OF TRAJECTORY DATA AT M = 1.0 . .	9
TABLE 2	-	ENTRY CONDITION ASSUMPTIONS	19
TABLE 3	-	MODEL ENVIRONMENTS FOR THE SENSOR SYSTEMS STUDY	20
TABLE 4	-	SENSOR SYSTEMS ANALYSED FOR FEASIBILITY .	24
TABLE 5	-	LISTING OF SENSOR SYSTEMS NOT ANALYSED FOR FEASIBILITY	28
TABLE 6	-	SUMMARY OF FEASIBLE SYSTEMS' PERFORMANCE, SPECIFIED MACH NUMBER M = 1.0	31
TABLE 7	-	SUMMARY OF FEASIBLE SYSTEMS' PERFORMANCE, SPECIFIED MACH NUMBER M = 2.5	32
TABLE 8	-	SUMMARY OF FEASIBLE SYSTEMS' PERFORMANCE, SPECIFIED MACH NUMBER M = 5.0	33
TABLE 9	-	EQUATIONS USED TO COMPUTE THE FIRST THREE ALTITUDE-UNCERTAINTY COMPONENTS	38
TABLE 10	-	EQUATIONS USED TO COMPUTE THE REMAINING FIVE ALTITUDE-UNCERTAINTY COMPONENTS. . .	40
TABLE 11	-	SUMMARY OF THE FIVE SYSTEMS/SUBSYSTEMS AND EIGHT INDEPENDENT VARIABLES	45
TABLE 12	-	SUMMARY OF ALTITUDE ERROR PERFORMANCE RESULTS FOR FIVE SYSTEMS/SUBSYSTEMS STUDIED IN PHASE 2.	46
TABLE 13	-	SUMMARY OF VALUES FOR INDEPENDENT VARIABLES GIVING THE NULL ALTITUDE AND THE MINIMUM ALTITUDE IN PHASE 2 STUDY CONDITIONS. . .	48
TABLE 14	-	TRADE STUDY MATRIX FOR SIX ACCELEROMETERS	50
TABLE 15	-	TRADE STUDY MATRIX FOR FIVE TYPES OF PRESSURE TRANSDUCERS.	51

TABLES (concluded)

			PAGE NO.
TABLE 16	-	EVALUATION MATRIX FOR THE CANDIDATE SYSTEMS	53
TABLE 17	-	SUMMARY OF THE TEN INDEPENDENT VARIABLES CONSIDERED IN THE FINAL SYSTEM STUDY. . .	56
TABLE 18	-	EQUATIONS FOR COMPUTING TWO ADDITIONAL LOW ALTITUDE-UNCERTAINTY COMPONENTS	58
TABLE 19	-	EQUATIONS FOR COMPUTING SEVEN HIGH ALTITUDE-UNCERTAINTY COMPONENTS	58
TABLE 20	-	EQUATIONS FOR THE SECONDARY COMPUTATIONS.	60
TABLE 21	-	SUMMARY OF LOW ALTITUDE ERROR PERFORMANCE RESULTS (Altitudes Below H_o).	61
TABLE 22	-	SUMMARY OF HIGH ALTITUDE ERROR PERFORMANCE RESULTS (Altitudes Above H_o).	61
TABLE 23	-	SUMMARY OF VALUES FOR INDEPENDENT VARIABLES GIVING MINIMUM, NULL AND MAXIMUM TRIGGER ALTITUDES	64
TABLE 24	-	SUMMARY OF TRIGGER AND PREDICTED ALTITUDES FOR THE EXTREME CASES (RUNS 94-97). . . .	65
TABLE 25	-	PARTS LIST AND WEIGHT ESTIMATE FOR FINAL SYSTEM.	80
TABLE 26	-	SYSTEM RELIABILITY AS A FUNCTION OF COMPONENT CONFIGURATION.	86
TABLE 27	-	SUMMARY OF FAILURE MODE AND EFFECTS ANALYSIS	90

ILLUSTRATIONS

PAGE NO.

FIGURE 1 - ACTIVITY NETWORK FOR THE STUDY. 4

FIGURE 2 - SIDE VIEW OF LANDER VEHICLE 11

FIGURE 3 - AXIAL FORCE VERSUS MACH NUMBER. 12

FIGURE 4 - NORMAL FORCE VERSUS MACH NUMBER 12

FIGURE 5 - CENTER OF PRESSURE VERSUS MACH NUMBER . . 12

FIGURE 6 - BASE PRESSURE ON BODIES OF REVOLUTION VERSUS FREE STREAM MACH NUMBER. 14

FIGURE 7 - ALTITUDE VERSUS DENSITY FOR THE SIX MARS MODEL ATMOSPHERES 16

FIGURE 8 - ALTITUDE VERSUS PRESSURE FOR THE SIX MARS MODEL ATMOSPHERES 16

FIGURE 9 - ALTITUDE VERSUS TEMPERATURE FOR THE SIX MARS MODEL ATMOSPHERES. 17

FIGURE 10 - ERROR IN AXIAL ACCELEROMETER VERSUS TOTAL ANGLE OF ATTACK 41

FIGURE 11 - ACCELERATION AT M = 1.0 VERSUS MAXIMUM ACCELERATION FOR EIGHT CORNER RUNS 44

FIGURE 12 - SCHEMATIC DIAGRAMS ILLUSTRATING THE PERFORMANCE RESULTS. 62

FIGURE 13 - BLOCK DIAGRAM OF FINAL SYSTEM 66

FIGURE 14 - CIRCUIT DIAGRAM FOR FINAL SYSTEM. 71

FIGURE 15 - SCHEMATIC DIAGRAM FOR TYPICAL CAPACITIVE PRESSURE TRANSDUCER 74

FIGURE 16 - SCHEMATIC DIAGRAM FOR TYPICAL STRAIN GAUGE ACCELEROMETER 74

FIGURE 17 - SCHEMATIC DIAGRAM FOR TYPICAL DIFFERENTIAL AMPLIFIER 76

FIGURE 18 - SCHEMATIC DIAGRAM FOR TYPICAL "NAND" GATE 76

ILLUSTRATIONS (concluded)

			PAGE NO.
FIGURE 19	-	SCHEMATIC DIAGRAM FOR TYPICAL DARLINGTON RELAY DRIVER.	76
FIGURE 20	-	FOUR SENSOR CONFIGURATIONS FEATURING AT LEAST ONE EACH OF: AN INITIATING RELAY, BOTH A P_b/a' SENSOR AND A P_b SENSOR, A PYRO RELAY, AND A PYRO BATTERY	82
FIGURE 21	-	THREE MODES OF REDUNDANCY	83
FIGURE 22	-	TYPICAL CROSSOVER NETWORK FOR PYROTECHNIC INITIATION.	88

1.0 INTRODUCTION

A Mars lander vehicle is being planned for flight sometime during the early 1970's. Present plans call for this vehicle to be directed into a Mars entry trajectory either from a "fly-by spacecraft" or from an "orbiter-bus." In order to achieve high payload capability for this lander (entry) vehicle, it is planned to employ, in succession, different modes of deceleration between the time it starts its entry trajectory and the time it comes to rest on the surface of the planet. These different modes of deceleration will include most, if not all, of the following types:

1) Deceleration due to the aerodynamic drag of the entry vehicle to slow it from the initial hypersonic entry speed to a supersonic or subsonic speed,

2) Deceleration by means of one or more parachutes to reduce the descent speed to a low subsonic value,

3) Deceleration with the aid of landing retro-rockets to reduce the speed of the vehicle to essentially zero at a point several feet above the surface, and

4) Deceleration at the time of impact with honey-comb and/or other impact attenuation structure on the bottom of the vehicle.

The subject of this report is the sensor system that is to initiate the deployment of the parachute.

1.1 THE SENSOR PROBLEM

At the present time, the Mars atmosphere is defined only within rather broad limits (1).* These limits represent an uncertainty range, and their effect on the flight profile and vehicle design for the first Mars landers is profound. An example of this is the need for a rather sophisticated sensor system to determine when parachute deployment should be initiated. This is, in fact, very largely the reason for the study presented in this report.

* Numbers in parentheses refer to references

A number of ideas have been presented in prior literature on how to measure various flight and atmospheric conditions from onboard an entry vehicle while it is descending through the Martian atmosphere. Some of these are:

a) The velocity and altitude can be obtained by integrating data from accelerometers (2) - (6). During the terminal portion of the descent, such a scheme can be augmented by a more direct measurement method employing the ratio of two vehicle surface pressures.

b) Density can be measured directly by a back-scattering technique (7) or computed with the aid of accelerometer data (2) - (6).

c) During the terminal descent phase, both ambient and stagnation pressures and temperatures can be measured by sensors located judiciously on the surface of the entry vehicle.

Also of interest in regard to making measurements from onboard a vehicle while traveling at supersonic speed, although not concerned with Martian entry, is Reference 8.

At least two previous studies have dealt with the central question considered in this report: What is the best method, in a Mars entry vehicle, to sense the flight condition at which parachute deployment should be initiated? Boobar and McElhoe (9) analytically derived the following expression to show how a simple accelerometer, aligned with the longitudinal axis of a non-lifting entry vehicle, could be used for this purpose:

$$\frac{a_{dep}}{a_{max}} = -2e\left(\frac{V_{dep}}{V_E}\right) \log_e\left(\frac{V_{dep}}{V_E}\right)$$

The quantities a and V are for acceleration and velocity respectively; the subscripts dep, max, and E stand for deployment initiation, maximum and initial entry respectively. Foreknowledge of the velocity ratio (V_{dep}/V_E) permits the right hand side of this equation to be evaluated prior to entry. Thus, it is seen that the deployment initiation condition occurs at the time the acceleration is equal to a predetermined fraction of the maximum acceleration. Furthermore, it may be noted that it is not required to know the atmosphere's scale height, the entry flight path angle or the ballistic coefficient of the entry vehicle in order to use the concept.

A similar idea was proposed by Worth (10). He found that reasonable accuracy could be obtained by using a relationship of the following form

$$a'_{dep} = C_1 + C_2 \, a'_{max}$$

Here, a' is "sensed" acceleration* and C_1 and C_2 are predetermined constants associated with the entry velocity and the Mach number at which it is desired to initiate parachute deployment.

1.2 THE PROGRAM PLAN

The various activities that constituted this study are summarized in Figure 1. This figure shows an activity network. Blocks with solid boundaries mark the activities in which Northrop Ventura had primary responsibility. The circled numbers in the following discussion refer to the activities in this figure.

The first activity was the preparation of specific recommendations on the scope of the study and the preparation of program schedules ①. These were summarized in write-ups and submitted to JPL ②. The first phase of the study effort started with a rather general survey of the sensor problem ③. This was reported in the First Progress Report ④.

A number of computer generated trajectories including both tabulated data listings and plots were provided by JPL ⑤. These were analyzed to determine possible trends that might be useful to a sensing system ⑥. Also, an investigation was undertaken to establish the prime sensors that would be available for this application ⑦. In addition, an expanded investigation determined which flight parameters can be derived with combinations of prime sensors ⑧. The results of these investigations were presented in the Second Progress Report ⑨.

---

* "Sensed" acceleration a' is related to acceleration a by a vector equation, $\underline{a}' = \underline{a} - \underline{G}$, where G is the planet's gravitational specific force (11).

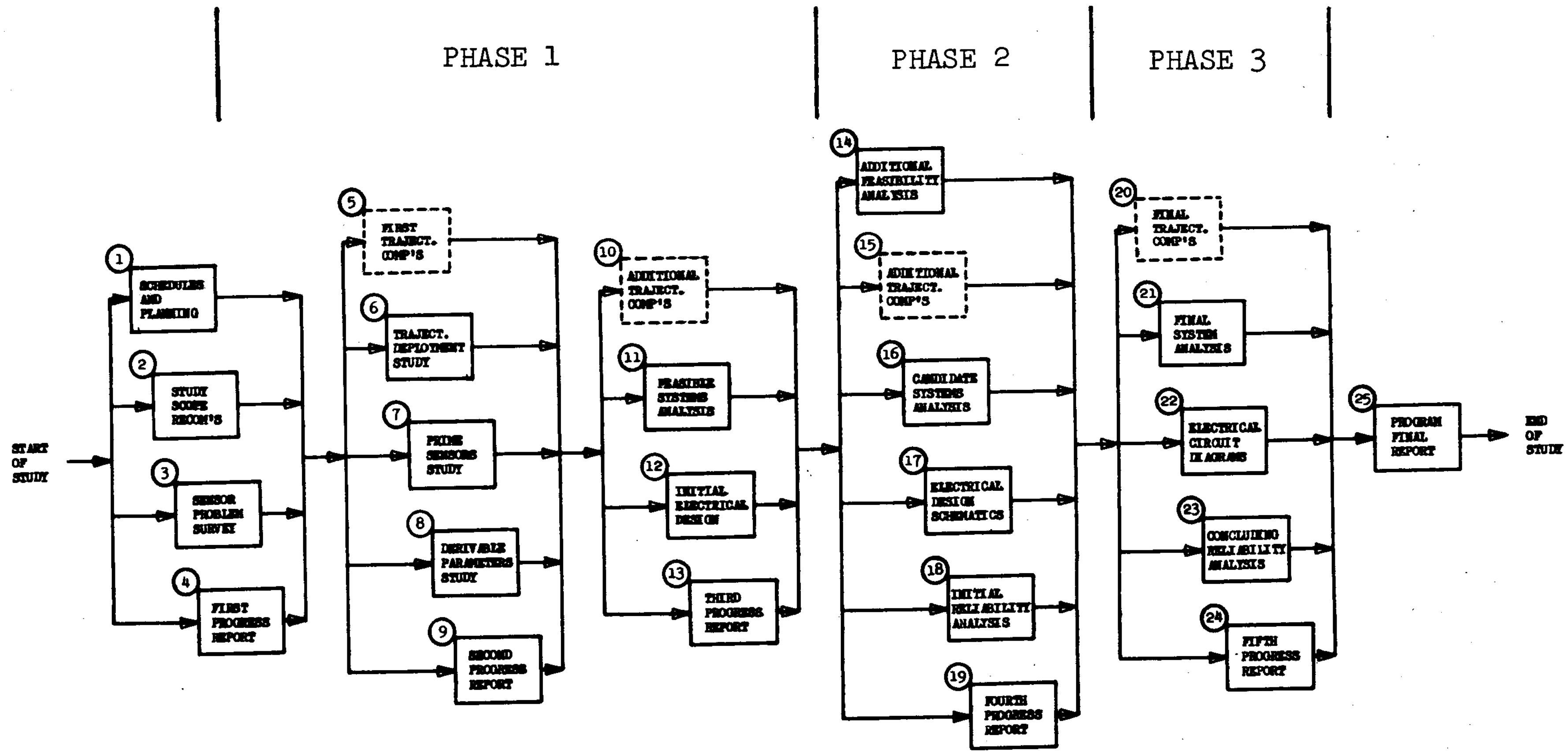

FIGURE 1, ACTIVITY NETWORK FOR THE STUDY

Additional trajectories were provided by JPL [10]. The feasibilities of 13 sensor system ideas were established [11]. Block diagrams illustrating how these ideas could be mechanized were prepared [12]. This information was presented in the Third Progress Report [13], and the first study phase ended.

The second phase of the study started with an analysis to establish the feasibility of three additional sensor system ideas [14]. More trajectories were provided by JPL [15]. Three Candidate Systems were selected and performance analyses were made [16]. The mechanization and logic for these systems were developed in preliminary form [17]. Consideration was given to the matter of how their reliability could be enhanced [18]. The results of this study phase were summarized and presented in the Fourth Progress Report [19].

The Final System was selected and the third and final phase of the study was started. More trajectories were provided by JPL [20]. Additional performance analysis was undertaken [21]. Circuit diagrams for the Final System were prepared [22]. Additional reliability analysis was performed [23]. The Fifth Progress Report was prepared [24]. And finally, the Final Report was prepared [25].

2.0 SCOPE OF STUDY

This section discusses the scope of the study. The underlying conditions, restraints and assumptions used to develop the results presented in the subsequent sections are indicated. These include the lander vehicle characteristics, the Mars atmosphere models, the trajectory entry conditions and the specified parachute deployment conditions. Most of these conditions are common to all three study phases; however, some are restricted to only one or two phases. In general, limited restrictions are indicated both here and in the sections of the report where they specifically apply.

2.1 THE TRAJECTORY DATA

A basic decision was made at the start of the study that trajectory aspects of the analyses would be based on computer generated trajectories (as opposed to approximate analytic solutions). The decision was based on the belief that a more comprehensive and accurate analysis would result. By and large, this belief was verified during the course of the study.

All trajectory data were provided by JPL. The computer program used to generate these data featured six degrees of freedom for the vehicle; an oblate, rotating planet; and two-dimensional tables of aerodynamic coefficients. In addition to detailed print-outs, in which all the important trajectory parameters were listed at discrete points along the flight path, selected plots were also provided.

A total of 41 computer generated trajectories (runs) were used during the course of the study. These are summarized in terms of the variables that distinguish them in Table 1a. These variables are (a) the entry mode -- orbital or hyperbolic, (b) the atmosphere model, (c) the entry velocity V_E, (d) the entry flight path angle γ_E, (e) the entry angle of attack α_E, (f) the entry rolling velocity p_E, and (g) the entry azimuth angle χ_E. Table 1b presents a summary of selected items of data appearing in the computer generated trajectories nearest Mach number M = 1.0.

TABLE 1a, SUMMARY OF THE TRAJECTORY RUNS

RUN	ENTRY MODE	ATMOS-PHERE MODEL	V_E (FPS)	γ_E (DEG)	α_E (DEG)	p_E (RAD/SEC)	χ_E (DEG)	STUDY PHASE	COMMENTS
TYPICAL ORBITAL ENTRY TRAJECTORIES, ALL SIX MODEL ATMOSPHERES									
44	Orbital	VM-3	16,000	-16	-50	0	+ 90	1,2,3	γ = 1.38
43	Orbital	VM-1	16,000	-16	-50	0	+ 90	1	γ = 1.38
45	Orbital	VM-7	16,000	-16	-50	0	+ 90	1	γ = 1.38
42	Orbital	VM-4	16,000	-16	-50	0	+ 90	1	γ = 1.43
40	Orbital	VM-2	16,000	-16	-50	0	+ 90	1	γ = 1.37
41	Orbital	VM-8	16,000	-16	-50	0	+ 90	1,2,3	γ = 1.37
60	Orbital	VM-3	12,500	-14	-50	0	+ 90	1,2,3	
59	Orbital	VM-1	12,500	-14	-50	0	+ 90	1	
61	Orbital	VM-7	12,500	-14	-50	0	+ 90	1	
58	Orbital	VM-4	12,500	-14	-50	0	+ 90	1	
56	Orbital	VM-2	12,500	-14	-50	0	+ 90	1	
57	Orbital	VM-8	12,500	-14	-50	0	+ 90	1,2,3	
TYPICAL HYPERBOLIC ENTRY TRAJECTORIES									
55	Hyperb.	VM-3	23,000	-20	-50	0	+ 90	1	
53	Hyperb.	VM-4	23,000	-20	-50	0	+ 90	1	
54	Hyperb.	VM-8	23,000	-20	-50	0	+ 90	1	
52	Hyperb.	VM-4	23,000	-40	-50	0	+ 90	1	
51	Hyperb.	VM-8	23,000	-40	-50	0	+ 90	1	
THE EIGHT "CORNER RUNS"									
60	Orbital	VM-3	12,500	-14	-50	0	+ 90	1,2,3	
70	Orbital	VM-3	12,500	-20	-50	0	+ 90	2,3	
72	Orbital	VM-3	16,000	-14	-50	0	+ 90	2,3	
78	Orbital	VM-3	16,000	-20	-50	0	+ 90	2,3	
57	Orbital	VM-8	12,500	-14	-50	0	+ 90	1,2,3	
69	Orbital	VM-8	12,500	-20	-50	0	+ 90	2,3	
77	Orbital	VM-8	16,000	-14	-50	0	+ 90	2,3	
71	Orbital	VM-8	16,000	-20	-50	0	+ 90	2,3	
ENTRY ROLL VELOCITY, p_E = 1 RAD/SEC									
24	Orbital	VM-3	16,000	-16	-50	1	+ 90	3	
20	Orbital	VM-8	16,000	-16	-50	1	+ 90	2,3	
ENTRY ANGLE OF ATTACK, α_E = -5 AND -105 DEG									
74	Orbital	VM-3	12,500	-14	-5	0	+ 90	3	
75	Orbital	VM-8	16,000	-20	-5	0	+ 90	2,3	
73	Orbital	VM-3	12,500	-14	-105	0	+ 90	3	
76	Orbital	VM-8	16,000	-20	-105	0	+ 90	2,3	
ENTRY ANGLE OF AZIMUTH, χ_E = -90 DEG (RETROGRADE ENTRY)									
79	Orbital	VM-3	12,500	-14	-50	0	- 90	3	
80	Orbital	VM-8	16,000	-20	-50	0	- 90	2,3	
WIND ONSET INSTANTANEOUS WITH CONSTANT WIND VELOCITY TO SURFACE									
81	Orbital	VM-8	12,500	-20	-50	0	+ 90	3	V_w = 220 FPS; h_s = 16,100 ft.
82	Orbital	VM-3	16,000	-14	-50	0	+ 90	3	V_w = 155 FPS; h_s = 72,700 ft.
83	Orbital	VM-3	16,000	-14	-50	0	+ 90	3	V_w = 223 FPS; h_s = 211,700 ft.
84	Orbital	VM-8	12,500	-20	-50	0	+ 90	3	V_w = 151 FPS; h_s = 61,600 ft.
LANDER VEHICLE C_A AND C_N VARIATION = ± 3% (NOMINAL)									
85	Orbital	VM-3	12,500	-14	-50	0	+ 90	3	ΔC_A, ΔC_N = +3% (NOMINAL)
86	Orbital	VM-8	16,000	-20	-50	0	+ 90	3	ΔC_A, ΔC_N = -3% (NOMINAL)
EXTREME CASES									
94	Orbital	VM-8	12,500	-20	-105	1	+ 90	3	
95	Orbital	VM-8	12,500	-20	-105	1	- 90	3	
96	Orbital	VM-3	16,000	-14	0	0	- 90	3	
97	Orbital	VM-3	16,000	-14	0	0	+ 90	3	

TABLE 1b, SUMMARY OF TRAJECTORY DATA AT M = 1.0

RUN	TIME FROM ENTRY PT	ALTITUDE	VELOCITY (AERO)	FL.PATH ANGLE (AERO)	ACCELER-ATION (SENS)	DYNAMIC PRESS.	STAGNA-TION PRESS.	PITCH ANGLE AMP.	PRESS. (AMB)	DENSITY (AMB)	TEMPERA-TURE (AMB)	MACH NUMBER (ACTUAL)
	t	h	V_A	γ_A	a'	q	P_{s2}	$\bar{\eta}$	P	$\rho \times 10^6$	T	M
	(sec)	(ft)	(fps)	(deg)	(fpss)	(psf)	(psf)	(Deg)	(psf)	(scf)	(^oR)	-
TYPICAL ORBITAL TRAJECTORIES, ALL SIX MODEL ATMOSPHERES												
44	315.463	72,452	890.25	- 47.75	16.665	3.7305	10.34	± 3.5	5.50	9.0	360	1.0004
43	321.296	57,134	911.27	- 46.86	16.303	3.6444	9.96	± 3.5	5.30	6.6	373	1.0058
45	327.696	42,111	948.96	- 46.07	15.654	3.4998	9.40	± 3.6	5.00	7.8	405	1.0052
42	303.163	40,610	620.03	- 43.88	15.026	3.3872	6.79	± 3.2	4.60	16.0	228	1.0039
40	311.382	31,666	645.87	- 45.88	14.752	3.3252	9.18	± 3.6	4.90	16.0	265	1.0054
41	317.666	23,374	679.54	- 45.91	14.782	3.3262	9.18	± 3.2	4.90	14.4	291	1.0123
60	349.119	71,528	899.04	- 47.22	17.378	3.8803	10.53	± 3.3	5.60	10.0	360	1.0103
59	355.126	55,170	911.18	- 46.83	16.759	3.7518	10.34	± 3.3	5.50	9.0	377	1.00[illegible]
61	360.278	39,933	952.79	- 46.03	16.124	3.6355	9.96	± 3.2	5.30	6.0	410	1.0035
58	332.336	39,359	627.43	- 42.11	16.103	3.6516	9.93	± 3.7	5.20	16.5	233	1.0057
56	336.664	30,422	656.75	- 43.40	16.016	3.5690	9.55	± 3.8	5.10	16.7	270	1.0153
57	345.559	21,252	680.27	- 44.45	15.779	3.5302	9.74	± 3.9	5.20	15.5	298	1.0027
TYPICAL HYPERBOLIC ENTRY TRAJECTORIES												
55	211.625	71,689	892.57	- 43.19	17.051	3.8115	10.53	± 3.5	5.60	[illegible]	360	1.0030
53	188.426	39,606	622.49	- 39.87	15.726	3.5471	9.55	± 3.4	5.00	1.67	232	.9995
54	200.904	21,756	676.55	- 42.05	15.397	3.4447	9.74	± 3.5	5.20	1.50	295	.9997
52	77.101	19,677	706.70	- 46.20	35.735	7.0759	21.56	± 3.6	11.30	31.5	295	1.0090
51	IMPACT	AT MACH	1.10 -	- - - -	- - - -	- - - -	- - - -	- - - -	- - - -	- - - -	- - - -	- - - -
THE EIGHT "CORNER RUNS"												
60	349.119	71,528	899.04	- 47.22	17.378	3.8803	10.53	± 3.3	5.60	10.0	360	1.0103
70	244.749	65,662	894.88	- 45.07	19.508	4.3579	12.03	± 3.3	6.40	11.2	360	1.0056
72	399.374	72,677	890.09	- 51.20	16.453	3.7113	10.34	± 3.5	5.50	9.0	360	1.0003
78	231.121	68,302	890.75	- 43.96	18.105	4.0809	11.26	± 3.3	6.00	10.5	360	1.0010
57	345.559	21,252	680.27	- 44.45	15.779	3.5302	9.74	± 3.9	5.20	15.5	298	1.0027
69	234.404	16,049	696.95	- 41.89	18.795	4.2447	11.61	± 4.2	6.20	17.5	313	1.0017
77	532.454	22,519	676.79	- 52.26	15.110	3.3770	9.18	± 3.4	4.90	14.7	294	1.0039
71	216.688	18,876	691.66	- 40.82	17.406	3.8864	10.49	± 3.9	5.60	16.4	305	1.0076
ENTRY ROLL VELOCITY P_E = 1 RAD/SEC												
24	317.000	69,660	892.97	- 47.95	16.811	3.9840	11.09	±15.2	5.90	10.3	360	1.0035
20	320.056	21,521	676.59	- 47.27	14.770	3.4876	9.55	±14.6	5.10	15.5	296	1.0015
ENTRY ANGLE OF ATTACK, a_E = -5 AND -105 DEG												
74	349.778	71,293	893.39	- 47.66	17.232	3.6510	10.62	± 1.2	5.65	10.0	360	1.0040
75	216.350	19,163	694.03	- 40.52	17.377	3.6835	10.49	± 0.9	5.60	16.2	304	1.0125
73	349.086	71,260	898.99	- 47.20	17.234	3.9021	10.62	± 6.2	5.65	10.0	360	1.0103
76	216.818	16,505	691.65	- 40.76	17.210	3.9239	10.56	± 6.7	5.65	16.5	305	1.0058
ENTRY ANGLE OF AZIMUTH, X_E = -90 DEG (RETROGRADE ENTRY)												
79	351.706	71,243	898.55	- 46.02	17.343	3.6998	10.72	± 3.2	5.70	10.0	360	1.0098
80	221.331	19,157	685.60	- 41.70	16.818	3.7904	10.49	± 3.1	5.60	16.5	304	1.0002
WIND ONSET INSTANTANEOUS WITH CONSTANT WIND VELOCITY TO SURFACE												
81	243.970	11,726	702.81	- 38.92	21.409	4.8087	13.30	±13.0	7.10	19.5	325	.9901
82	408.770	66,263	892.11	- 48.96	18.742	4.2756	11.56	± 9.8	6.15	11.0	360	1.0025
83	399.070	72,905	894.18	- 51.12	16.610	3.7272	10.04	± 3.6	5.34	9.5	360	1.0048
84	235.289	15,913	690.35	- 42.23	18.456	4.1790	11.61	± 4.2	6.20	17.5	314	.9916
LANDER VEHICLE C_A AND C_N VARIATION = ± 3% (NOMINAL)												
85	345.787	75,489	936.53	- 46.50	18.141	3.8857	9.59	± 4.0	5.10	9.0	360	1.0547
86	216.987	17,144	685.92	- 40.83	17.293	3.9975	11.24	± 3.2	6.00	17.2	310	.9910
EXTREME CASES												
94	235.470	13,575	704.07	- 42.39	18.850	4.6103	12.55	±19.7	6.70	18.5	320	1.0003
95	238.170	14,805	697.98	- 42.54	18.235	4.3934	12.10	±17.4	6.46	18.0	316	.9973
96	395.131	71,836	887.89	- 51.79	16.797	3.7598	10.30	±13.4	5.48	9.60	360	.9978
97	399.170	72,938	890.06	- 51.23	16.472	3.6903	10.04	± 0.6	5.34	9.50	360	1.0002

2.2 THE LANDER VEHICLE

The shape of the lander vehicle is that of a blunt cone with rounded shoulders and a flat base. A side view of the lander vehicle is shown in Figure 2. The lander vehicle is symmetrical about its longitudinal axis, both geometrically and with respect to its mass distribution. The moment center is located one quarter of a diameter aft of the nose.

The mass of the lander vehicle is assumed to be a constant 31.677 slugs (no mass loss due to ablation is considered). Its moments of inertia about the X, Y and Z axes are 300, 270 and 270 slug-ft^2, respectively and the products of inertia are zero. The base diameter (reference dimension) is taken to be $D = 12$ ft.

The lander vehicle's static aerodynamic characteristics were specified in the computer program by three two-dimensional tables organized as follows:

$$C_A = F_1\ (M,\alpha) \qquad M = 0.3,\ 0.5,\ ..\ ,\ 50.0$$

$$C_N = F_2\ (M,\alpha) \qquad \alpha = 0,\ 10,\ ..\ ,\ 180 \text{ deg}$$

$$\Delta X_N/D = F_3\ (M,\alpha)$$

where $\Delta X_N/D = (X_{nose} - X_{c.p.})/D$. The quantities X_{nose} and $X_{c.p.}$ are the distances along the X axis at which the nose of the vehicle and the center of pressure occur. (All values in this table were for an angle of sideslip $\beta = 0$.) For values of M and α not in the table, a linear interpolation was made.

Plots prepared from the aerodynamic tables are presented in Figures 3, 4 and 5. Figure 3 presents axial force coefficient C_A (positive in the $-X$ direction) versus Mach number for seven values of total angle of attack η from 0 to 180 degrees.* Figure 4 presents normal force coefficient C_N (positive in the $-Z$ direction) versus Mach number for seven values of angle of attack α from 0 to 180 degrees. Figure 5 presents similar curves for the center of pressure location C_m/C_N. This is, in effect, the position (in units of D) at

---

* The total angle of attack η is the resultant angle associated with α and β. In the strictest sense, it is computed with the relation

$$\eta = \arctan\ (\tan^2 \alpha + \tan^2 \beta)^{\frac{1}{2}}$$

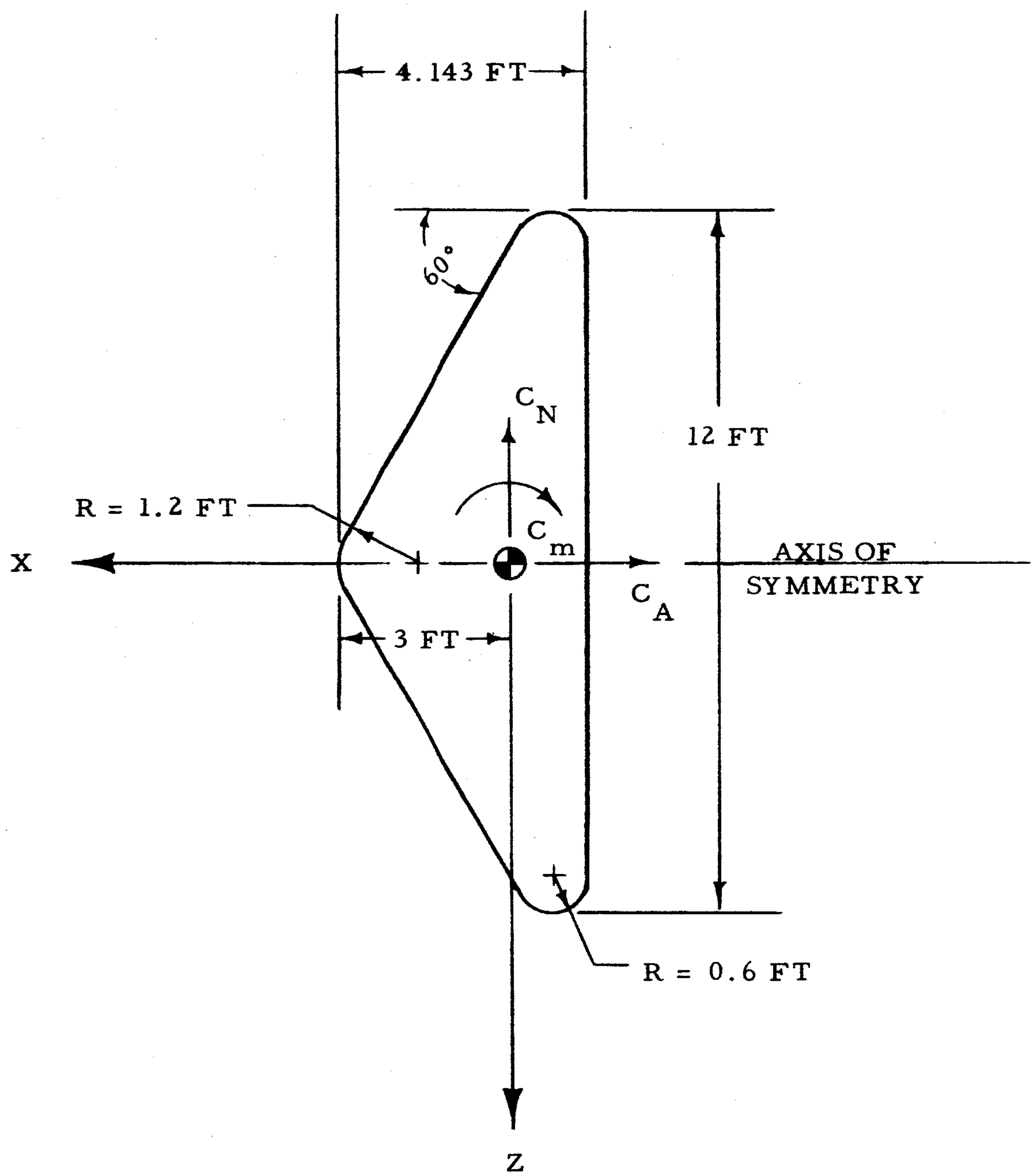

FIGURE 2, SIDE VIEW OF LANDER VEHICLE

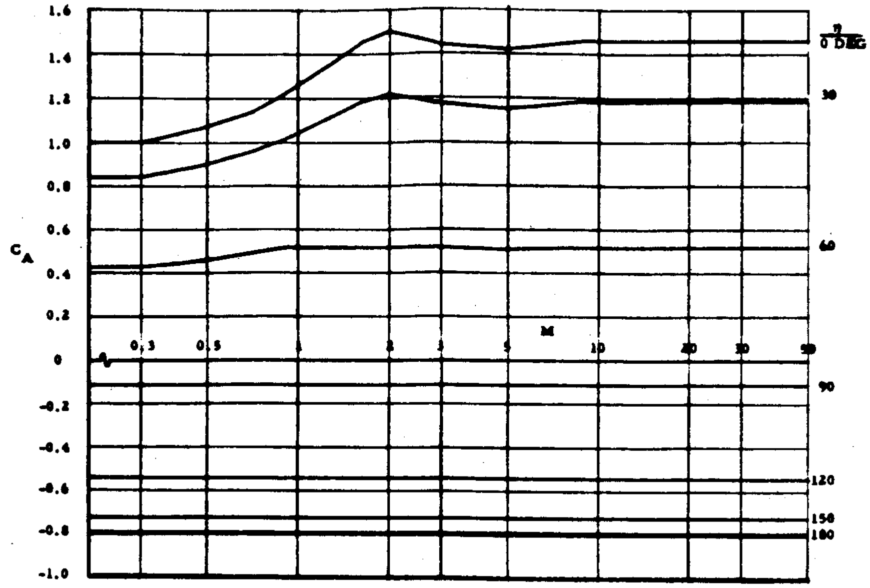

FIGURE 3, AXIAL FORCE VERSUS MACH NUMBER

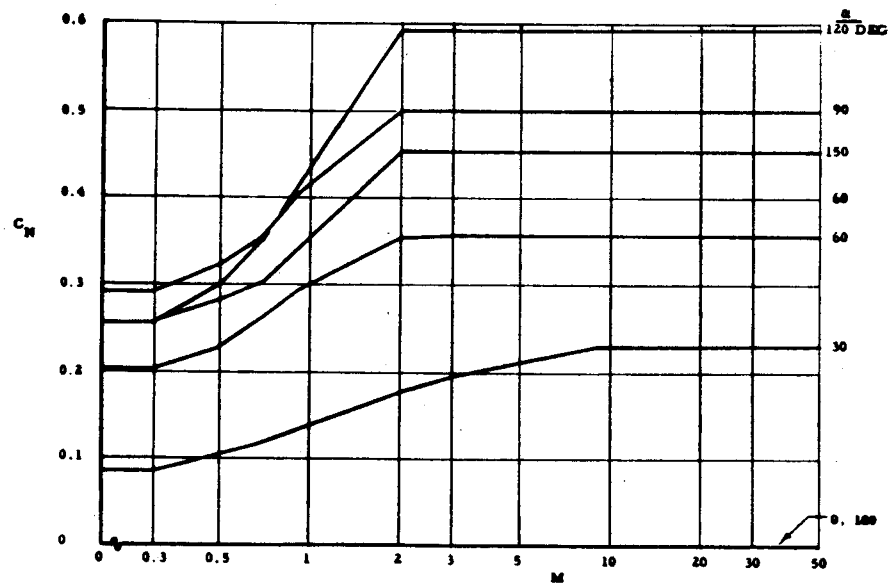

FIGURE 4, NORMAL FORCE VERSUS MACH NUMBER

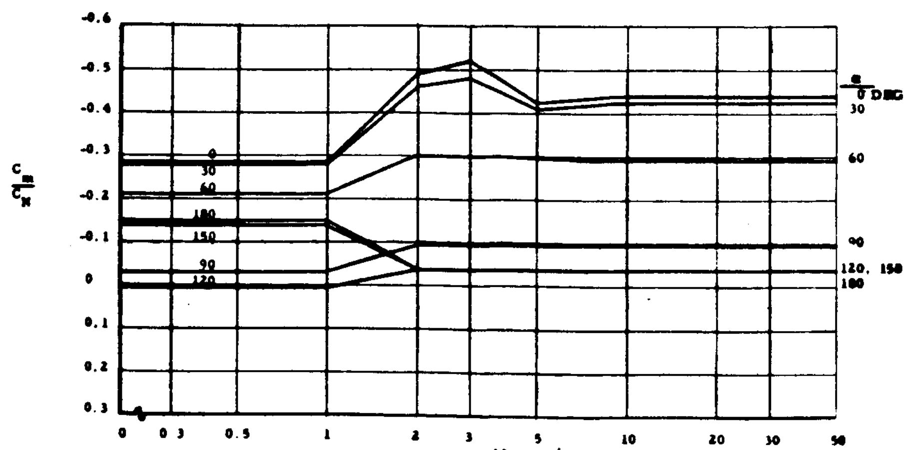

FIGURE 5, CENTER OF PRESSURE VERSUS MACH NUMBER which a force equal to the normal force will produce a moment (w/t the moment center) equal to the aerodynamic pitching moment. The ratio C_m/C_N is related to $\Delta X_N/D$ by the relation

$$\frac{C_m}{C_N} = \frac{1}{4} - \frac{\Delta X_N}{D}$$

The aerodynamic characteristics C_Y and C_n/C_Y are of course inferred by C_N and C_m/C_N.

In addition to the force and center of pressure data described above, one stability derivative is assumed; viz., $C_{m_q} = -0.145$. The stability derivative C_{n_r} is of course equal to C_{m_q}. All other stability derivatives such as C_{ℓ_p} are assumed equal to zero.

The base pressure coefficient and a range of uncertainty for this coefficient are assumed for the lander vehicle throughout all three study phases. These are shown in Figure 6 together with the limited amount of base pressure data found during the course of the study. There is little doubt that a suitable test program could reduce the uncertainty indicated by the spacing between the upper and lower curves in this figure.

During Phase 3, the uncertainty in the lander vehicle's aerodynamic force characteristics is considered. This uncertainty is assumed to be represented by a "band" of values for both the axial force coefficient and the nornal force coefficient. The center of the "band" is assumed to be the values given in Figures 3 and 4, and the width of the "band" is taken to follow the schedule given below.

VARIATION (Half-Band Width)	MACH NUMBER
± 3%	M = 0.3
± 3%	M = 2.01
± 4%	M = 3.02
± 6%	M = 5.01
± 10%	M = 9.02
± 10%	M = 50

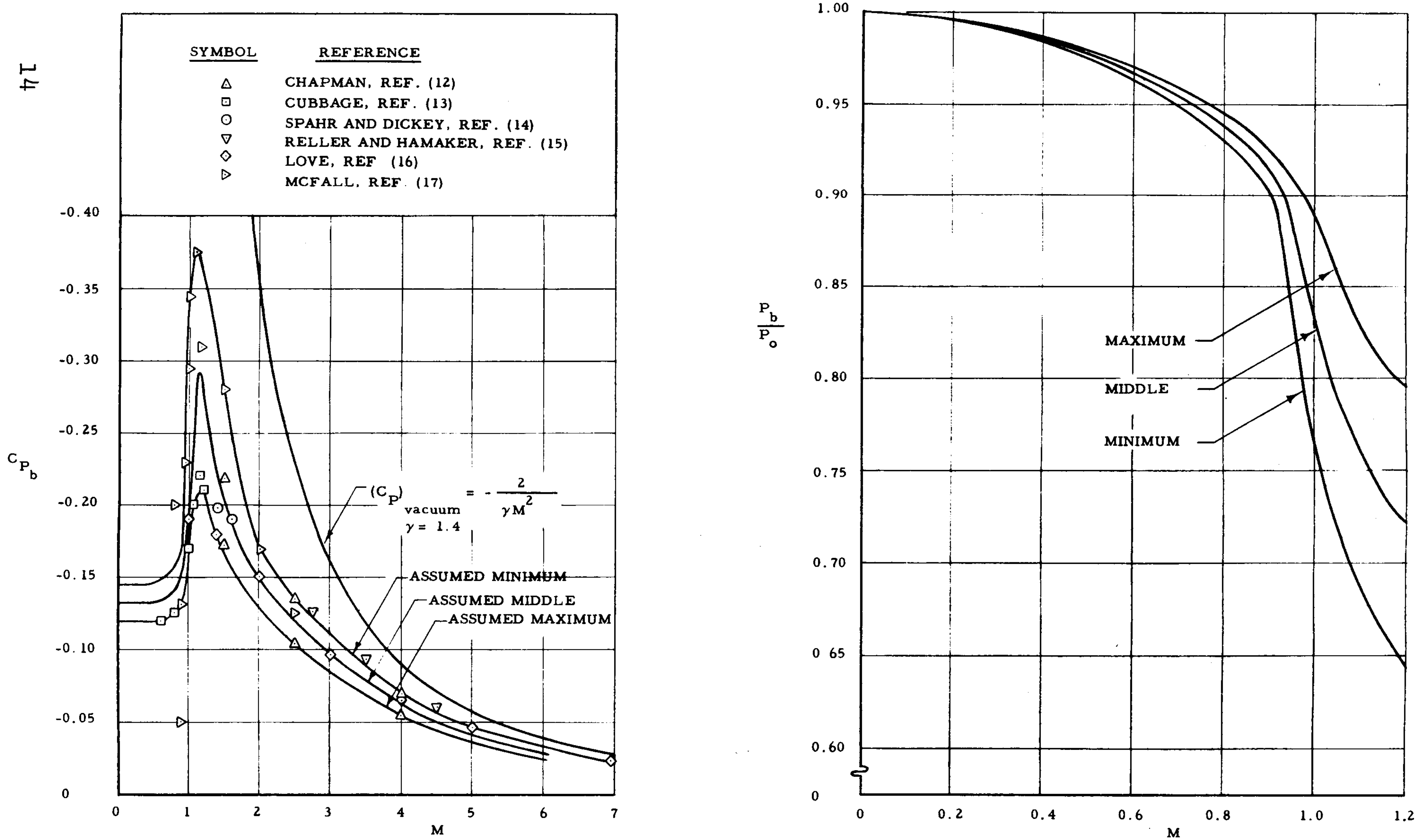

(a) BASE PRESSURE COEFFICIENT VERSUS MACH NUMBER

(b) EXTREME CURVES IN ILLUSTRATION (a) REPLOTTED AS BASE PRESSURE RATIO VERSUS MACH NUMBER

FIGURE 6, BASE PRESSURE ON BODIES OF REVOLUTION VERSUS FREE STREAM MACH NUMBER

2.3 THE PLANET MARS AND ITS ATMOSPHERE

The planet Mars was assumed to be an oblate spheroid with an equitorial radius of 11,180,000 feet. The gravitational constant (w/t inertial space) at the equator was taken to be $G = 12.3$ ft/sec^2. The acceleration due to gravity at points away from the equator was computed with an expression that included one oblateness term. The value used for the angular velocity of the planet was $\omega = 0.00007292$ rad/sec.

The Mars atmosphere is represented by six models: VM-1, VM-2, VM-3, VM-4, VM-7 and VM-8. These are each specified by an assumed gas composition and several constants such as the surface density, the lapse rate and the tropopause altitude (1). Each atmosphere model features an adiabatic troposphere and a constant temperature stratosphere. The density, pressure and temperature profiles for these atmospheres are shown in Figures 7 - 9. Except for the wind runs described immediately below, the atmospheres rotate with the planet.

During Phase 3, a special wind model is assumed in order to estimate the most adverse possible effect of wind. This model assumes the atmosphere above a certain altitude rotates with the planet; i.e., the "air" particles maintain constant longitude and latitude. This altitude is called the shear height h_s. Below the shear height, the atmosphere is assumed to act as a layer moving in a uniform manner either toward the East or toward the West. The velocity (w/t the planet) of this moving layer is called the wind speed. For Model Atmospheres VM-3 and VM-8, this wind speed is assumed to be 155.5 and 220 ft/sec, respectively. (Runs 83 and 84 unintentionally employed somewhat different wind speed values. However, the effects of these variations proved not to be important.)

Four trajectory runs feature a wind layer; viz., Runs 81 - 84. The shear heights for Runs 81 and 82 are altitudes slightly above the point at which the Mach number 1.0 flight condition would have occurred had there been no wind; the shear heights for Runs 83 and 84 are at altitudes slightly above the point at which the maximum "sensed" acceleration occurs.

2.4 THE ENTRY CONDITIONS

The point of entry "E" is defined as the point in the trajectory having an altitude of 805,000 ft. This altitude is the arbitrarily assumed outer edge of the planet's atmosphere,

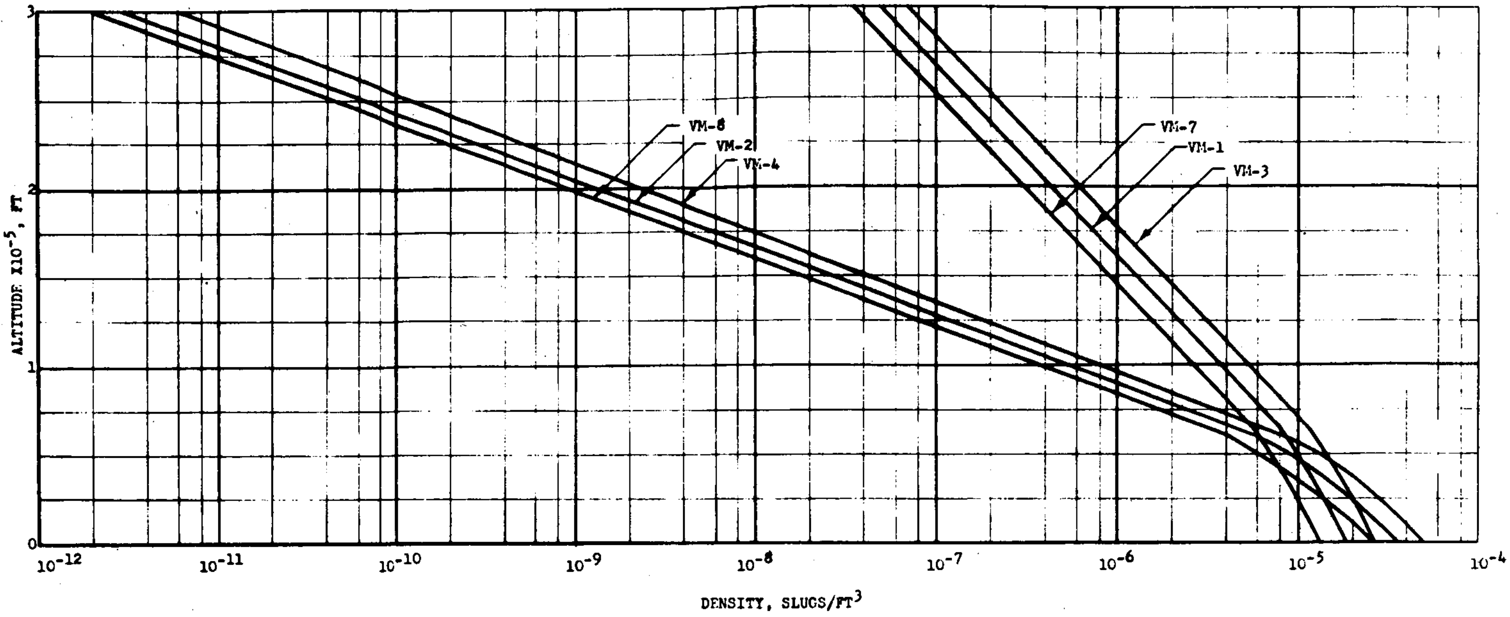

FIGURE 7, ALTITUDE VERSUS DENSITY FOR THE SIX MARS MODEL ATMOSPHERES

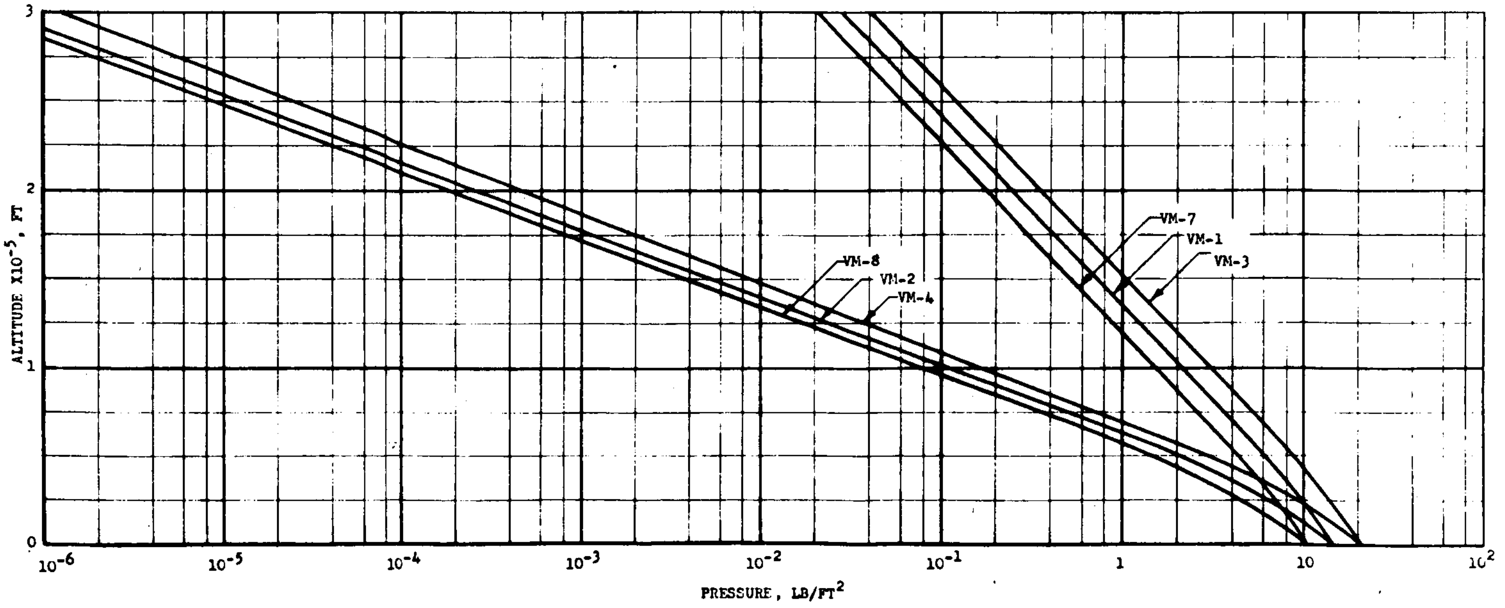

FIGURE 8, ALTITUDE VERSUS PRESSURE FOR THE SIX MARS MODEL ATMOSPHERES

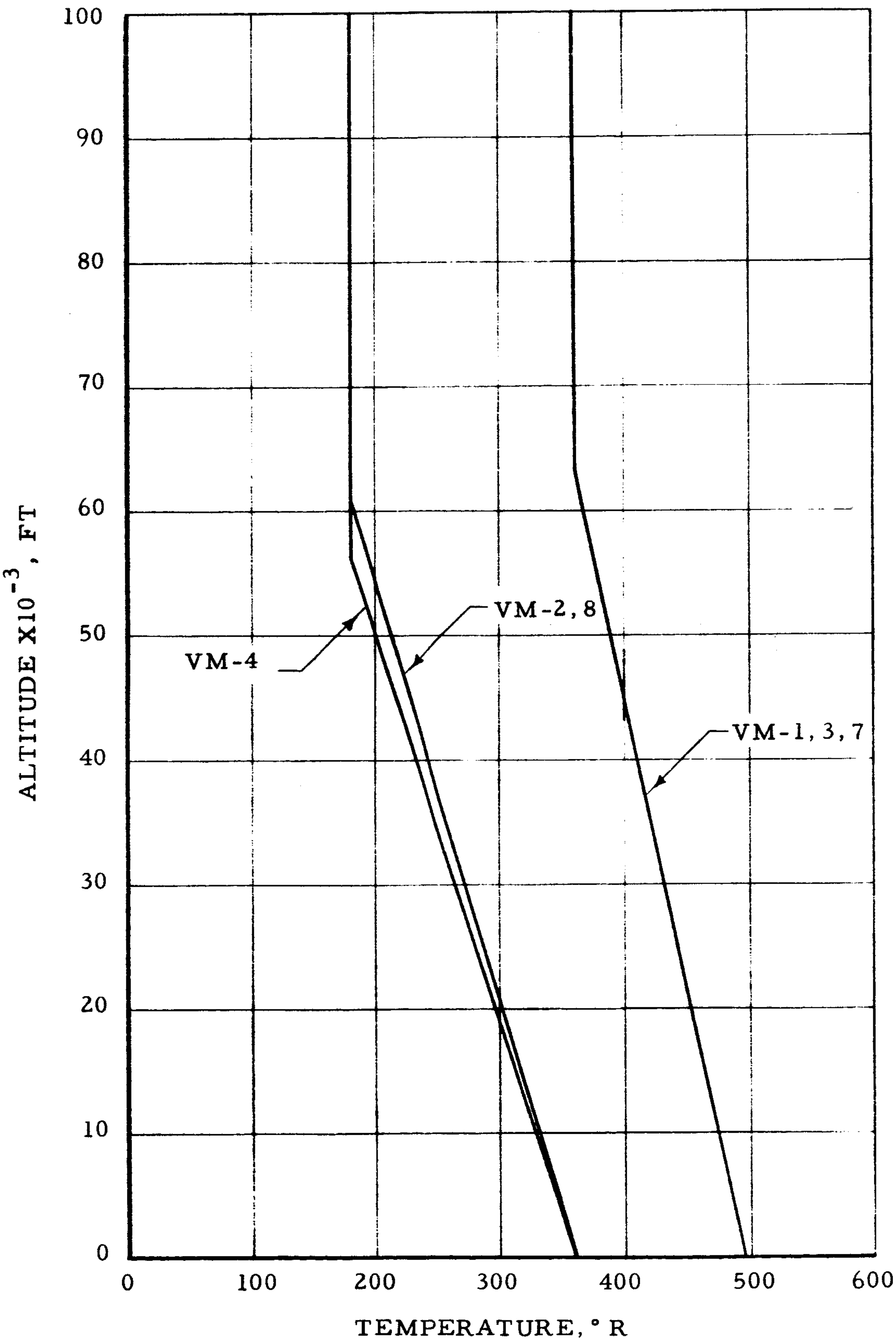

FIGURE 9, ALTITUDE VERSUS TEMPERATURE FOR THE SIX MARS MODEL ATMOSPHERES and all trajectory computations start at this point. Point E is in the equatorial plane for all trajectories considered in this study. Values and ranges for the lander vehicle orientation and velocity variables at Point E for each study phase are given in Table 2.

2.5 THE SPECIFIED PARACHUTE DEPLOYMENT CONDITIONS

Recent studies at Northrop Ventura have indicated flight Mach number to be the most suitable design criterion for the initiation of parachute deployment (10). These studies have indicated that heating should not be a problem for deployment Mach numbers less than 5.0. However, these studies have also indicated that certain canopy inflation and oscillation problems are strongly Mach number dependent and would merit consideration at the time a parachute design is selected. It was primarily for this reason that Mach number was selected for the parachute deployment initiation criterion.

During Phase 1, three initiation Mach numbers are considered. These are referred to as the <u>specified Mach numbers</u>. They are M_S = 1.0, 2.5 and 5.0.

During Phases 2 and 3, only one specified Mach number M_S = 1.0 is used.

It should be realized that the specified Mach number is an ideal Mach number in the sense that this is the flight condition at which a perfect sensor system would initiate parachute deployment. The true Mach number at which an actual (imperfect) sensor system would initiate parachute deployment is referred to as the <u>trigger Mach number</u>.

2.6 THE ENVIRONMENTAL CONDITIONS

The environmental conditions assumed for this study are presented in Table 3. Both preoperational and operational environments are listed. The preoperational environments are the conditions that the sensor systems are subjected to prior to the time that they perform their function. The operational environment is viewed as the conditions under which the sensor systems are required to function.

2.7 THE OPERATIONAL ERRORS

The operational errors are defined in this study as the errors due to imperfect functioning of the sensor system. These are viewed as being primarily due to environmental

TABLE 2, ENTRY CONDITION ASSUMPTIONS

ENTRY CONDITIONS	PHASE 1 ORBITAL ENTRY	PHASE 1 HYPERBOLIC ENTRY	PHASES 2 AND 3 (ORBITAL ENTRY)
1.0 Position (a)			
1.1 Longitude	$\lambda_E = 0$	$\lambda_E = 0$	$\lambda_E = 0$
1.2 Latitude	$\Lambda_E = 0$	$\Lambda = 0$	$\Lambda_E = 0$
1.3 Altitude (b)	h_E = 805,000-ft	h_E = 805,000-ft	h_E = 805,000-ft
2.0 Orientation (c)			
2.1 Angle of Attack	α_E = -50 deg	α_E = -50 deg	α_E = -105 to +105 deg
2.2 Angle of Sideslip	$\beta_E = 0$	$\beta_E = 0$	$\beta_E = 0$
3.0 Translational Velocity (d)			
3.1 Magnitude	V_E = 12,500 to 16,000 ft/sec	V_E = 21,000 to 23,000 ft/sec	V_E = 12,500 to 16,000 ft/sec
3.2 Angle of Flight Path	γ_E = -14 to -20 deg	γ_E = -20 to -40 deg	γ_E = -14 to -20 deg
3.3 Angle of Azimuth	χ_E = +90 deg	χ_E = +90 deg	χ_E = -90 to +90 deg
4.0 Rotational Velocity (d)			
4.1 Rolling Velocity	$p_E = 0$	$p_E = 0$	p_E = -1 to +1 rad/sec
4.2 Pitching Velocity	$q_E = 0$	$q_E = 0$	$q_E = 0$
4.3 Yawing Velocity	$r_E = 0$	$r_E = 0$	$r_E = 0$

NOTES:
(a) Position is w/t the (rotating) planet
(b) The point of entry is defined as the point in the trajectory at which the altitude is 805,000-ft
(c) Orientation is w/t local "air."
(d) Translational and rotational velocities are w/t inertial space

TABLE 3, MODEL ENVIRONMENTS FOR THE SENSOR SYSTEMS STUDY

ENVIRONMENT	OPERATIONAL MODE	DESCRIPTION
1.0 PREOPERATIONAL*		
1.1 Temperature	Sterilization:	257°F for 76 hours
	Launch:	60°F increasing to 100°F in 10 minutes
	Trans-Mars:	100°F for 260 days
	Entry:	100°F to 180°F to 0°F in 10 minutes
1.2 Chemical	Sterilization:	12% ETO and 88% Freon, 104°F for 28 hours (Unit remains sealed until entry)
	Entry:	100% CO_2
1.3 Pressure	Prelaunch:	14.7 $\pm$ 0.2 PSIA
	Launch:	14.7 PSIA to 10^{-8} torr in 140 seconds
	Trans-Mars:	10^{-8} torr
	Entry:	10^{-8} torr to 4.5 PSIA in 10 minutes
1.4 Acceleration	Launch:	7 "g" for 10 minutes
	Trans-Mars:	0 "g" for 260 days; three mid-course maneuvers at 7 "g" for 2 minutes total.
	Entry:	0 "g" to 22 "g" to 1/2 "g" in 10 minutes
1.5 Shock	Launch:	20 "g" max, 5 "g" av. for 10 milliseconds
	Trans-Mars and Entry:	Negligible
1.6 Vibration	Launch:	600 to 1000 cps with Spectral Power Density, SPD = 0.1 g^2/cps for 10 minutes
	Trans-Mars and Entry:	Negligible
1.7 Accoustical Noise	Launch:	150 db for 60 seconds
	Trans-Mars and Entry:	Negligible
1.8 Radiation	Trans-Mars:	X-rays decreasing from Earth environment level to 60% of this value in 260 days
1.9 Meteoroids	Trans-Mars:	Negligible (assumed protected)
1.10 Magnetic Fields	Trans-Mars:	0.7 gauss to 0 in 260 days
1.11 High Energy Particles	Trans-Mars:	300 rad total dose
2.0 OPERATIONAL*		
2.1 Temperature		T = -40°F to 40°F
2.2 Pressure		P = 3 PSFA to 6 PSFA
2.3 Acceleration	Oscillation Mode No. 1 (Planar Motion):	p = 0 $\alpha(\beta)$ = 8.7° sin (2π ft), f = 1.888 cps $\beta(\alpha)$ = 0
	Oscillation Mode No. 2 (Coning Motion):	p = 1 rad/sec α = 16° cos (2π ft), f = .275 cps β = 16° sin (2π ft), f = .275 cps (The coning frequency is .043 cps)

* These environmental conditions are based upon Northrop Venturas interpretation of JPL Spec VOL 50503-ETS "Voyager Capsule Equipment Environmental Specification" and NSL 62-152 "Handbook of Aerospace Environments and Missions, 1962," prepared for NASA by the Northrop Space Laboratories.

effects and are referred to as environmental uncertainties. The reason for this is as follows: Each sensor system component (or, for that matter, a whole sensor system) can be made to function with excellent repeatability under ideally controlled conditions such as a calibration laboratory might have. The reason a component would not function perfectly at the time of the Mars entry is due to either or both of two reasons. These are effects due to aging (the preoperational environment) and effects due to the conditions under which it is required to function (the operational environment).

In phase 1, no environmental uncertainties are assumed.

In Phase 2, specific environmental uncertainties are assumed. These are associated with the operation of the two prime sensors employed in the Candidate Systems; namely, an accelerometer and a pressure transducer. These uncertainties are ± 5% for the outputs of both units. In particular, it is assumed that

$$(P_b)_{ACT} = (1 \pm 0.05)(P_b)_{IND}$$

$$(a')_{ACT} = (1 \pm 0.05)(a')_{IND}$$

where P_b and a' are base pressure and "sensed" acceleration; and the subscripts ACT and IND stand for actual and indicated, respectively.

In Phase 3, the environmental uncertainties are handled in a manner similar to that used in Phase 2. In this phase, the environmental uncertainties are the result of a detailed error analysis and are as follows:

(a) For the Primary Subsystem,

$$(P_b/a')_{ACT} = (1 \pm 0.106)(P_b/a')_{IND}$$

(b) For the Secondary Subsystem,

$$(P_b)_{ACT} = (1 \pm 0.055)(P_b)_{IND}$$

3.0 FEASIBLE SYSTEMS STUDY (PHASE 1)

In this study phase, a sensor system is considered feasible if it can be shown to satisfy three criteria. These are that the functions it performs can be mechanized with existing technology; that the size, weight and reliability of its components are reasonably compatible with the lander vehicle and the mission requirements; and that a preliminary evaluation of the system's performance indicates that it is satisfactory. The last criterion means that the sensor system should neither trigger parachute deployment at too high a Mach number or at too low an altitude. Too high a Mach number is taken to be any Mach number greater than the specified value; too low an altitude is taken to be below 1000-ft. A system need satisfy the above criteria for only one entry mode and one specified Mach number in order to be considered feasible.

Table 4 presents a listing of the sensor systems found to be feasible in the sense of the preceding paragraph. No special significance should be attached to the listing order. Brief descriptions of these sensor systems are presented in the subsection immediately below. Following these descriptions, several other systems are suggested. Finally, the results of the performance analysis are presented.

3.1 FEASIBLE SYSTEMS' DESCRIPTIONS

A functional description for each of the sixteen sensor systems analyzed in this phase of the study are given in the following paragraphs (More detailed descriptions are presented in References 18 and 19).

<u>System B: Acceleration Matrix Fit</u>

An accelerometer in the lander vehicle is used to monitor the total sensed acceleration during entry. The maximum acceleration level is noted as is the acceleration level at each of two subsequent preset time intervals. The time interval required to reach the specified Mach number is computed as a simple function of these three acceleration values. The trigger pulse is generated after this time interval has elapsed.

TABLE 4, SENSOR SYSTEMS ANALYZED FOR FEASIBILITY

System Symbol	Name of System	Prime Sensors: Accelerometer	Radar	Base Pressure	Stag Press	Timer	Sun Sensor	Force Link
B	Acceleration Matrix Fit	X				X		
C	Altimeter and Timer		X			X		
D	Oscillation Counter	X						
F	Inertial Path Angle	X					X	
G	Radar Altimeter		X					
H	Towed Body	X				X		X
I	Stag to Base Press Ratio			X	X			
J	Base Press to Acceleration Ratio	X		X				
N	Acceleration	X						
O	Acceleration Function	X						
P	Time after Max Accel'n	X				X		
Q	Time Function of Max Acceleration	X				X		
R	Base Pressure			X				
T	Stagnation Pressure to Acceleration Ratio	X			X			
U	Stagnation Pressure				X			
V	Stag Press and Timer				X	X		

System C: Altimeter and Timer

A radar altimeter in the lander vehicle monitors the altitude during entry. When a preset value of the altitude is reached, a timer starts and runs for a preset interval associated with the specified Mach number. The trigger pulse is generated at the end of this interval.

System D: Oscillation Counter

The vehicle oscillates throughout the entry due in part to its initial angle of attack at entry and also to its low pitch damping characteristics. An accelerometer is used to sense these oscillations and a counter is used to count them. Another accelerometer is used to sense the maximum value of the total sensed acceleration. The number of oscillations required to reach the specified Mach number is computed as a simple function of the maximum acceleration. The trigger pulse is generated when the number of oscillations becomes equal to this computed number.

System F: Inertial Path Angle

The inertial path angle is monitored by sensing the angle between the acceleration vector and the Sun's direction during entry. This information, in combination with the maximum acceleration level, is used to compute the path angle associated with the specified Mach number. The trigger pulse is generated when the path angle becomes equal to the computed value.

System G: Radar Altimeter

The altitude of the lander vehicle is monitored with a radar altimeter during entry. The trigger pulse is generated when a preset altitude associated with the specified Mach number is sensed.

System H: Towed Body

An accelerometer is used to monitor the total sensed acceleration during entry. After a preset time interval following peak acceleration, a secondary body having a lower ballistic coefficient then the lander vehicle is deployed into the wake and coupled to the lander vehicle by a riser. The tension in the riser is sensed by a strain link. The trigger pulse is generated when the ratio of the tension to the total acceleration reaches a preset value associated with the specified Mach number.

System I: Stagnation to Base Pressure Ratio

The stagnation pressure, as sensed through a small hole at the nose, and the base pressure on the lander vehicle are monitored by separate pressure transducers during entry. The trigger pulse is generated when the ratio of these two pressures becomes equal to a preset value associated with the specified Mach number.

System J: Base Pressure to Acceleration Ratio

An accelerometer is used to sense the total sensed acceleration, and a pressure transducer is used to sense the base pressure on the lander vehicle during entry. The trigger pulse is generated when the base pressure to acceleration ratio reaches a preset value associated with the specified Mach number.

System N: Acceleration

An accelerometer is used to monitor the total sensed acceleration during entry. When a first preset acceleration level is exceeded, the trigger circuit is armed. The trigger pulse is generated when the acceleration level falls below a second preset acceleration level associated with the specified Mach number.

System O: Acceleration Function

An accelerometer is used to monitor the total sensed acceleration during entry. When a preset acceleration level is exceeded, the trigger circuit is armed. The maximum acceleration value is noted and used to compute the acceleration level associated with the specified Mach number. The trigger pulse is generated when the acceleration level drops to this computed level.

System P: Time After Maximum Acceleration

An accelerometer is used to monitor the total sensed acceleration during entry. A timer is started when the maximum acceleration time occurs. The trigger pulse is generated after a preset time interval associated with the specified Mach number.

System Q: Time Function of Maximum Acceleration

An accelerometer is used to monitor the total sensed acceleration during entry. The maximum acceleration level is noted and a timer is started. The time required to reach the specified Mach number is computed as a simple function of the maximum acceleration. The trigger pulse is generated after this time interval has passed.

System R: Base Pressure

The base pressure on the lander vehicle is monitored by a pressure transducer during entry. The trigger pulse is generated when a preset pressure level associated with the specified Mach number is sensed.

System T: Stagnation Pressure to Acceleration Ratio

The stagnation pressure, as sensed through a small hole at the nose, and the total sensed acceleration are sensed by appropriate transducers during entry. The trigger pulse is generated when the ratio of the stagnation pressure to acceleration reaches a preset value associated with the specified Mach number.

System U: Stagnation Pressure

The stagnation pressure, as sensed through a small hole at the nose, is monitored by a pressure transducer during entry. When a first preset pressure level is exceeded, the trigger circuit is armed. The trigger pulse is generated when the pressure level falls below a second preset level associated with the specified Mach number.

System V: Stagnation Pressure and Timer

The stagnation pressure, as sensed through a small hole at the nose, is monitored by a pressure transducer during entry. A timer is started when the stagnation pressure minimum occurs. The trigger pulse is generated after a preset time interval associated with the specified Mach number.

TABLE 5, LISTING OF SENSOR SYSTEMS <u>NOT</u> ANALYZED FOR FEASIBILITY

System Symbol	Name of System	Prime Sensors						
		Accelerometer	Radar/Radio	Pressure (s)	Timer	Sun Sensor	Temperature	Heat Rate
	Ejected-Spinning Body Plus Accelerometer	X	X					
	Ejected-Spinning Body		X					
	Inertial Path Angle (Modified)	X				X		
	2-Point Acceleration	X			X			
	Static Pressure Distribution change at M = 1.0			X				
	Base Pressure Change at M = 1.0			X				
	Acceleration Change at M = 1.0	X						
	Temperature						X	
	Heat Rate							X
	Altimeter and Rate of Descent		X					
	Altimeter and Accelerometer	X	X					

3.2 IDEAS FOR OTHER SYSTEMS

Table 5 presents a listing of sensor system concepts not analyzed for feasibility, but for which, a definite potential is felt to exist. Again, no special significance should be attached to the listing order. Most of these systems are apparently as simple as those described immediately above. Brief descriptions of these concepts are presented in Reference 18.

3.3 FEASIBLE SYSTEMS ANALYSES

Twelve orbital and five hyperbolic trajectories were available for Phase 1 as noted in Table 1. These were used to develop a common basis for comparison of the sixteen sensor systems described in the foregoing subsection.

Both orbital and hyperbolic type entry modes were considered. Also, for each entry mode, three specified Mach numbers were considered: $M_S = 1.0$, 2.5 and 5.0. Details of the analyses are presented in References 18 and 19.

The performance analyses were carried out as follows: First, each system was defined explicitly. The available trajectory data were used to optimize these definitions. Next, the trajectory data were used to determine the trigger altitudes for each combination of entry mode and specified Mach number. These data were then compared with the altitudes associated with the specified Mach number (referred to as the ideal altitudes). The differences between the ideal altitudes and the trigger altitudes were called the altitude reductions. Because the trigger altitudes never exceeded the ideal altitudes, the altitude reductions were always positive.

The performances of the feasible systems are summarized in Tables 6 - 8 in terms of altitude reduction for the 17 trajectories considered. Presenting the altitude performance in this fashion allows direct comparison of the systems for each of the specified Mach number deployment conditions.

For orbital entry and Mach number 1.0 specified, the best performance across the board is provided by the Base Pressure to Acceleration Ratio System (J), followed closely by the Stagnation to Base Pressure System (I). The Stagnation Pressure and Timer System (V) and the Stagnation Pressure to Acceleration Ratio System (T) yield approximately the same performance. The use of a preset acceleration value as in the Acceleration System (N) gives comparable results at the low altitude end but has poorer performance as the Mach number 1.0 altitude increases in the denser atmosphere models. Some improvement is obtained by computing the acceleration level as in the Acceleration Function System (O) or the Acceleration Matrix Fit System (B). It is interesting to note that the Altimeter and Timer System (C) and the Stagnation Pressure and Timer System (V) are feasible for the orbital entry, specified Mach number 1.0 conditions only.

For orbital entry and Mach number 2.5 specified, the best performance across the board is provided by the Acceleration System (N), the Stagnation to Base Pressure Ratio System (I), the Inertial Path Angle System (F), and the Base Pressure to Acceleration Ratio System (J). Showing somewhat less performance are the Stagnation Pressure System (U) and the Base Pressure System (R).

For orbital entry and Mach number 5.0 specified, the best performance across the board is provided by the Acceleration Function System (O) followed closely by the Acceleration System (N). Next, with significantly less performance, are the Time After Maximum Acceleration System (P), the Towed Body System (H), the Stagnation to Base Pressure Ratio System (I), and the Base Pressure to Acceleration Ratio System (J).

For hyperbolic entry, only the two specified Mach numbers of 2.5 and 5.0 are feasible. This is because Mach number 1.0 does not occur (above 1000 ft) in Run 51. The best performing systems for the hyperbolic entry mode are the Time Function of Maximum Acceleration System (Q), the Base Pressure to Acceleration Ratio System (J), and the Stagnation to Base Pressure Ratio System (I). Next, with somewhat less performance, are the Acceleration System (N), the Towed Body System (H), and the Acceleration Function System (O).

Comparison of all sixteen systems across the board for suitability at all Mach numbers and entry modes shows the Stagnation to Base Pressure Ratio System (I) and the Base Pressure to Acceleration Ratio System (J) to have the smallest altitude errors. The Acceleration Function System (O) also gives rather good performance across the board. It appears that sensor systems employing an accelerometer generally have the most satisfactory performance over the ranges of deployment conditions and entry modes studied.

TABLE 6, SUMMARY OF FEASIBLE SYSTEMS' PERFORMANCE, SPECIFIED MACH NUMBER M = 1.0

Run	Atmosphere Model	Entry Velocity (Inertial)	Entry Path Angle (Inertial)	Ideal Altitude (M = 1.0)	ALTITUDE REDUCTION (FT.) PERFORMANCE BY SYSTEM CONCEPT: Acceleration Matrix Fit	Altimeter and Timer	Oscillation Counter	Inertial Path Angle	Radar Altimeter	Towed Body	Stagnation to Base Pressure Ratio	Base Pressure To Acceleration Ratio	Acceleration	Acceleration Function	Time After Maximum Acceleration	Time Function of Maximum Acceleration	Base Pressure	Stagnation Pressure To Acceleration Ratio	Stagnation Pressure	Stagnation Pressure And Timer
	WM	V_{IE}	γ_{IE}	H_I	B	C	D	F	G	H	I	J	N	O	P	Q	R	T	U	V
		(FPS)	(DEG)	(FT)																
ORBITAL ENTRY MODE																				
44	-3	16,000	-16	72,452	7,233	18,150		3,614	51,200	45,220	3,610	2,710	17,230	9,940	0	0	5,430	4,515		0
43	-1			57,134	6,518	9,360		2,767	35,880	50,470	3,700	2,760	10,310	2,760	910	910	5,570	4,637		3,708
45	-7			42,111	6,861	960		0	20,860	--	3,900	2,910	6,860	0	0	1,940	5,880	4,880		965
42	-4			40,810	7,771	6,440		5,774	19,560	[illegible]	1,890	1,890	-1,250	1,250	[illegible]	4,470	3,810	3,159		4,465
40	-2			31,686	4,812	2,730		2,039	10,440	[illegible]	2,040	2,040	0	0	[illegible]	1,360	4,120	2,725		2,725
41	-8			23,374	5,055	0		0	2,120	--	2,860	2,140	710	710	[illegible]	0	5,050	2,863		2,863
60	-3	12,500	-14	71,528	883	22,430		8,892	50,280	[illegible]	4,440	3,550	18,880	9,780	[illegible]	16,990	2,660	4,436		1,778
59	-1			55,170	906	14,940		6,436	33,920	[illegible]	3,660	2,740	12,080	4,580	[illegible]	17,810	1,830	3,658		5,514
61	-7			39,933	1,907	8,710		3,834	18,680	--	3,830	2,870	9,700	1,900	[illegible]	17,690	2,870	4,805		4,805
58	-4			39,359	3,618	13,370		12,036	18,110	23,190	1,780	1,780	3,620	2,390	29,580	16,010	1,780	2,643		4,871
56	-2			30,422	626	10,700		8,615	9,170	27,120	1,910	1,910	3,220	3,220	29,770	13,470	2,570	2,569		5,885
57	-8			21,252	0	8,370		6,218	0	--	2,020	1,340	3,400	2,720	--	11,990	2,020	2,024		4,105
HYPERBOLIC ENTRY MODE																				
55	-3	23,000	-20	71,689						43,030	3,330	2,490		--	0	0	--			
53	-4			39,606						21,110	1,720	1,130		1,050	[illegible]	[illegible]	--			
54	-8			21,758						--	[illegible]	[illegible]		0	16,750	[illegible]	--			
52	-4	25,000	-40	19,877						8,670	960	960		0	--	0	--			
51	-8			Below S.L.						--	--	--		--	--	--	--			

TABLE 7, SUMMARY OF FEASIBLE SYSTEMS' PERFORMANCE, SPECIFIED MACH NUMBER M = 2.5

Run	Atmosphere Model	Entry Velocity (Inertial)	Entry Path Angle (Inertial)	Ideal Altitude (M = 2.5)	ALTITUDE REDUCTION (FT.) PERFORMANCE BY SYSTEM CONCEPT: Acceleration Matrix Fit	Altimeter And Timer	Oscillation Counter	Inertial Path Angle	Radar Altimeter	Towed Body	Stagnation To Base Pressure Ratio	Base Pressure To Acceleration Ratio	Acceleration	Acceleration Function	Time After Maximum Acceleration	Time Function Of Maximum Acceleration	Base Pressure	Stagnation Pressure To Acceleration Ratio	Stagnation Pressure	Stagnation Pressure And Timer
	VM	V_{IE}	γ_{IE}	H_I	B	C	D	F	G	H	I	J	N	O	P	Q	R	T	[illegible]	V
		(FPS)	(DEG)	(FT)																
ORBITAL ENTRY MODE																				
44	-3	16,000	-16	117,286	8,887			3,779	77,380	17,650	2,810	3,780	2,340	1,390	2,340	1,860	9,430	10,519	2,767	
43	-1			100,625	9,507			5,814	60,710	17,810	2,340	3,310	1,380	460	920	460	8,965	10,612	6,326	
45	-7			85,463	9,509			3,809	45,550	17,810	2,830	3,810	1,870	0	0	0	9,510	10,613	6,845	
42	-4			56,178	7,499			1,870	16,270	5,480	1,310	1,590	1,040	1,040	10,320	770	3,070	3,713	1,587	
40	-2			50,355	5,859			831	10,450	6,680	840	1,420	550	550	10,890	550	3,310	3,986	2,645	
41	-8			44,002	0			0	4,090	7,420	880	1,490	0	0	10,780	0	3,830	4,192	3,128	
60	-3	12,500	-14	114,255	8,942			4,597	74,350	17,370	2,510	3,550	4,600	3,560	10,640	14,210	7,290	10,648	4,072	
59	-1			97,732	9,449			2,505	57,820	17,890	3,010	4,050	4,570	3,530	11,160	14,120	7,780	11,158	5,097	
61	-7			81,778	9,462			0	41,870	17,940	9,510	4,060	4,580	3,020	10,600	13,550	7,250	11,176	5,103	
58	-2			53,131	12,087			3,173	13,220	4,880	1,080	1,360	2,550	2,240	15,550	8,210	1,650	3,500	0	
56	-2			46,676	12,694			1,785	6,770	6,020	880	1,170	2,100	2,100	16,880	7,720	1,790	3,420	286	
57	-8			39,906	20,678			301	0	6,700	920	1,230	2,210	2,210	16,700	7,570	2,210	1,944	916	
HYPERBOLIC ENTRY MODE																				
55	-3	23,000	-20	105,631					95,430	12,810	2,010	2,840	1,190	16,160	0	0	32,300	7,728	11,561	
53	-4			52,086					41,890	4,530	920	1,160	690	690	8,450	5,250	13,620	3,006	11,310	
54	-8			38,696					28,500	6,180	1,040	1,310	0	0	8,950	4,360	18,250	3,691	18,250	
52	-4	25,000	-40	28,976					18,780	3,950	1,030	1,030	6,390	0	22,250	0	1,380	2,812	0	
51	-8			10,197					0	5,150	1,130	1,500	7,840	750	--	2,290	1,900	3,482	750	

TABLE 8, SUMMARY OF FEASIBLE SYSTEMS' PERFORMANCE, SPECIFIED MACH NUMBER M = 5.0

Run	Atmosphere Model	Entry Velocity (Inertial)	Entry Path Angle (Inertial)	Ideal Altitude (M = 5.0)	Acceleration Matrix Kit	Altimeter And Timer	Oscillation Counter	Inertial Path Angle	Radar Altimeter	Towed Body	Stagnation To Base Pressure Ratio	Base Pressure To Acceleration Ratio	Acceleration	Acceleration Function	Time After Maximum Acceleration	Time Function of Maximum Acceleration	Base Pressure	Stagnation Pressure To Acceleration Ratio	Stagnation Pressure	Stagnation Pressure And Timer
					ALTITUDE REDUCTION (FT.) PERFORMANCE BY SYSTEM CONCEPT															
	VM	V_{IE}	γ_{IE}	H_I	B	C	D	F	G	H	I	J	N	O	P	Q	R	T	U	V
		(FPS)	(DEG)	(FT)																
ORBITAL ENTRY MODE																				
44	-3	16,000	-16	144,973	14,005		1,561	19,979	95,240	9,320	9,710	9,750	1,560	1,170	1,560	1,560	21,200	36,041	11,656	
43	-1			129,090	11,602		1,552	17,495	79,400	9,660	10,050	10,050	780	780	1,170	1,170	21,520	36,890	12,380	
45	-7			113,869	11,165		0	14,673	64,180	9,620	10,010	10,010	0	0	0	0	21,880	37,370	12,719	
42	-4			64,565	7,656		390	5,852	14,870	2,750	3,550	3,550	1,950	780	4,790	190	6,720	11,773	1,761	
40	-2			58,843	6,012		0	5,337	9,150	2,570	2,780	2,780	1,370	390	4,890	190	6,470	11,457	2,172	
41	-8			53,398	10,274		612	4,896	3,710	2,920	2,920	3,130	1,020	0	4,900	0	7,260	12,870	2,913	
60	-3	12,500	-14	145,837	16,388		31,089	9,200	96,150	11,010	11,460	11,460	940	1,870	12,810	15,050	23,120	40,524	14,149	
59	-1			129,221	16,352		30,998	5,092	79,530	10,980	11,430	11,880	930	1,870	13,220	15,460	23,060	40,377	14,565	
61	-7			113,200	16,299		30,442	0	63,510	10,940	11,390	11,840	460	1,400	12,730	14,960	22,990	40,323	14,071	
58	-4			61,383	6,754		18,755	2,688	11,690	2,910	3,580	3,580	3,800	2,910	9,610	6,280	5,140	11,107	0	
56	-2			55,705	3,974		21,173	2,095	6,010	2,790	3,020	3,020	3,260	320	10,190	6,390	5,410	11,275	1,163	
57	-8			49,691	0		22,874	0	0	2,950	3,190	3,190	3,190	2,210	10,390	6,470	5,700	13,015	735	
HYPERBOLIC ENTRY MODE																				
55	-3	23,000	-20	126,335					107,370	6,780	7,210	7,550	0	17,660	0	0	29,880	27,041	24,830	
53	-4			58,243					39,280	2,120	2,660	2,660	880	700	5,110	3,020	9,760	8,880	6,607	
54	-8			46,502					27,540	2,570	2,570	2,570	190	0	5,470	2,970	12,520	10,556	9,675	
52	-4	25,000	-40	36,196					17,240	2,350	3,010	3,010	8,250	0	19,680	0	2,680	9,664	0	
51	-8			18,963					0	2,990	2,990	3,360	9,890	0	--	1,510	5,170	11,446	763	

4.0 CANDIDATE SYSTEMS STUDY (PHASE 2)

The performance results obtained in the Feasible Systems Study were combined with other considerations preparatory to deciding on the specific sensor configurations to be analyzed in Phase 2 of the study. These other considerations included reliability and development risk factors. On this basis, three configurations of sensor systems were selected. Each was selected to consist of two independent subsystems acting in parallel; i.e., each candidate system comprises two sensor subsystems. For convenience sake, these subsystems are identified as primary and secondary, although in reality, they act in parallel. The three candidate systems are as follows:

Candidate System Number	Primary Subsystem	Secondary Subsystem
1	Acceleration (Feasible System N)	Base Pressure (Feasible System R)
2	Base Pressure To Acceleration Ratio (Feasible System J)	Base Pressure (Feasible System R)
3	Acceleration Function (Feasible System O)	Base Pressure (Feasible System R)

It may be noted that each candidate system uses the same two types of prime sensors: an accelerometer and a base pressure sensor.

At this point in the study, the specified Mach number for initiating parachute deployment was restricted to the one Mach number, $M_S = 1.0$. Also, it was decided that a one-stage parachute system could be assumed for the remainder of the study.

The error performances for the candidate systems are determined by analyzing the performances of the four subsystems. In the feasible systems study, these are Systems J, N, O and R as noted above. Following an explanation of the approach used in the analysis, the results of the performance analysis and the results of trade studies on the two types of prime sensors are presented.

4.1 PERFORMANCE ANALYSIS APPROACH

The performance analysis used in this phase of the study expresses the maximum altitude reduction due to the uncertainty in each of the independent variables acting individually. These are utilized to estimate the maximum overall altitude reduction due to the uncertainty in all the independent variables acting simultaneously.

The Assumed Functionality

Let the initiation altitude due to the operation of a sensor system be referred to as the trigger altitude, h_T. In this analysis, this trigger altitude is viewed as a function of eight independent variables as follows:

$$h_T = h_T\,(Atm,\ V_E,\ \gamma_E,\ \alpha_E,\ p_E,\ \chi_E,\ C_{P_b},\ Env) \qquad (1)$$

where, in addition to the symbol meanings given in Table 2, the symbols Atm, C_{P_b} and Env are used to represent atmosphere model, base pressure coefficient and environmental effects respectively.

Equation (1) states that the trigger altitude is a function of eight independent variables: atmosphere model, entry velocity, etc. Assuming that this functionality is "well behaved", Eq. (1) can be written as a Taylor expansion about an altitude h_o as follows:

$$h_T = h_o + \frac{\partial h_T}{\partial Atm}\,\Delta Atm + \frac{\partial h_T}{\partial V_E}\,\Delta V_E + \frac{\partial h_T}{\partial \gamma_E}\,\Delta \gamma_E + \frac{\partial h_T}{\partial \alpha_E}\,\Delta \alpha_E + \frac{\partial h_T}{\partial P_E}\,\Delta P_E + \frac{\partial h_T}{\partial \chi_E}\,\Delta \chi_E + \frac{\partial h_T}{\partial C_{P_b}}\,\Delta C_{P_b} + \frac{\partial h_T}{\partial Env}\,\Delta Env + \ldots \qquad (2)$$

The altitude h_o is the altitude at the $M = 1.0$ point in the trajectory produced by a particular set of values for the independent variables; say, Atm_o, V_{Eo}, etc. This altitude is referred to as the "null altitude." The delta (Δ) quantities represent the variations in the independent variables from the specified values; e.g., $\Delta V_E = V_E - V_{Eo}$. The three dots represent second and higher order terms in the Taylor expansion which are neglected in the analysis.

It may be observed that some of the quantities appearing in Eq. (2) have a rather problematical meaning; e.g., $\partial h_T / \partial Atm$. This problem is circumvented in the analysis by always working with the products of the partial derivatives and the associated Δ-quantities; e.g., $(\partial h_T / \partial Atm) \Delta Atm$. Clearly, these products (altitude-uncertainty components) can have significance. They are the altitude changes resulting from changes in the independent variables. Unless another meaning is specifically indicated, the phrase "altitude-uncertainty component" is defined to mean the <u>maximum</u> change from the null altitude due to the particular <u>independent</u> variable involved.

<u>The Procedure</u>

The procedure used in the analysis of each subsystem is as follows:

1. The operation of each subsystem is defined explicitly. At this stage in the study, it is impossible to make an exactly correct definition. This will become possible only when the combination of the independent variables that produces the most adverse effect is known. Therefore, for the sake of being explicit, the most correct definition for the eight corner runs is used.

2. The trigger altitudes for certain of the 18 runs listed in Table 1 are determined.

3. The altitude-uncertainty components due to the atmosphere, entry velocity and entry flight path angle uncertainties are determined. Table 9 summarizes the relations used in this computation.

TABLE 9, EQUATIONS USED TO COMPUTE THE FIRST THREE ALTITUDE-UNCERTAINTY COMPONENTS

$h_{av} \triangleq \frac{1}{8} \Sigma h_T$		(Sum over all 8 corner runs)
$h_{-8} \triangleq \frac{1}{4} \Sigma h_T$		(Sum over the 4 corner runs for which the atmosphere is VM-8)
$h_{HI} \triangleq \frac{1}{4} \Sigma h_T$		(Sum over the 4 corner runs for which V_E = 16,000 ft/sec)
$h_{-20} \triangleq \frac{1}{4} \Sigma h_T$		(Sum over the 4 corner runs for which γ_E = -20 deg)

$$\frac{\partial h_T}{\partial Atm} \Delta Atm = h_{-8} - h_{av}$$

$$\frac{\partial h_T}{\partial V_E} \Delta V_E = h_{HI} - h_{av}$$

$$\frac{\partial h_T}{\partial \gamma_E} \Delta \gamma_E = h_{-20} - h_{av}$$

NOTE: The term "corner runs" refers to the eight trajectory runs that are so named in Table 1. These runs correspond to the eight possible three-tuples composed of the atmosphere, entry velocity and flight path angle extremes specified in the final column of Table 2.

4. The altitude-uncertainty components associated with the entry angle of attack, the entry rolling velocity, the entry azimuth angle, the base pressure coefficient and the operational-environmental effects are computed. The equations used in this computation are shown in Table 10. As noted in this table, these equations are for computing low altitude uncertainties only.

5. Finally, the null altitude is computed. The relation used to make this computation is

$$h_o = h_{AV} - \frac{\partial h_T}{\partial \alpha_E} \Delta\alpha_E - \frac{\partial h_T}{\partial P_E} \Delta P_E + \frac{\partial h_T}{\partial \chi_E} \Delta\chi_E - \frac{\partial h_T}{\partial C_{P_b}} \Delta C_{P_b} - \frac{\partial h_T}{\partial Env} \Delta Env \quad (3)$$

4.2 SUBSYSTEM DEFINITIONS

The four subsystems utilized in the three Candidate Systems are defined in this subsection. In addition, an ideal, $M = 1.0$ system is defined.

4.2.1 ACCELERATION SUBSYSTEM

The operational sequence for this system is as follows:

1. The axial acceleration a'_X is sensed by an accelerometer in the lander vehicle during entry.

2. When the acceleration level exceeds a preset level, the trigger circuit is armed.

3. The trigger pulse is generated when the acceleration level falls below a second preset level.

Only the second preset level is critical with respect to the trigger event. This acceleration level is selected to be the smallest value of sensed acceleration in the eight corner runs when the lander vehicle Mach number $M = 1.0$. This occurs on Run 77 when the axial acceleration $a'_X = 15.11$ ft/sec^2.

TABLE 10, EQUATIONS USED TO COMPUTE THE REMAINING FIVE ALTITUDE-UNCERTAINTY COMPONENTS

$$\frac{\partial h_T}{\partial \alpha_E} \Delta\alpha_E = \frac{1}{2}\left(h_{T\ \text{Run 75}} - h_{T\ \text{Run 76}}\right)$$

$$\frac{\partial h_T}{\partial P_E} \Delta P_E = \frac{1}{2}\left(h_{T\ \text{Run 20}} - h_{T\ \text{Run 41}}\right)$$

$$\frac{\partial h_T}{\partial \chi_E} \Delta\chi_E = \frac{1}{2}\left(h_{T\ \text{Run 71}} - h_{T\ \text{Run 80}}\right)$$

$$\frac{\partial h_T}{\partial C_{P_b}} \Delta C_{P_b} = \frac{1}{2}\left(h_{-8\ \text{MIN}\ P_b/P_o} - h_{-8\ \text{MAX}\ P_b/P_o}\right)$$

$$\frac{\partial h_T}{\partial \text{Env}} \Delta \text{Env} = \frac{1}{2}\left(h_{-8\ \text{Max + Environmental errors}} - h_{-8\ \text{Max − Environmental errors}}\right)$$

NOTE: Equations in this table are for computing low altitude uncertainties only. Equations used for computing high altitude uncertainties are given in Table 19.

It may be noted that the preceding description specifies measurement of the axial acceleration instead of the total acceleration. This is because the two are essentially equal for the range of total angle of attack occurring at or near M = 1.0. Figure 10 was prepared with the aid of the lander vehicle characteristics shown in Figures 3 and 4. Figure 10 shows the percent error of the axial, sensed acceleration, compared to the total angle of attack. For an angle of attack of 12 deg (the highest value in any of the eight corner runs) the error amounts to 0.2%.

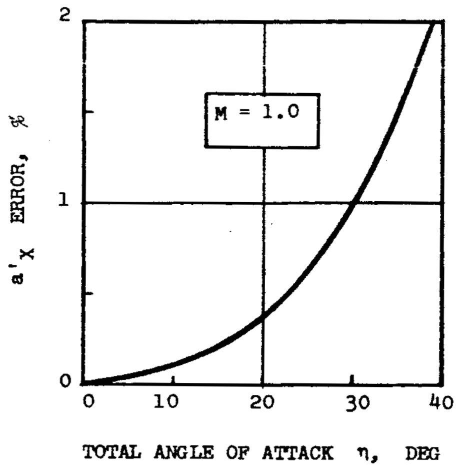

FIG. 10, ERROR IN AXIAL ACCELEROMETER VERSUS TOTAL ANGLE OF ATTACK

4.2.2 BASE PRESSURE SUBSYSTEM

The operational sequence for this system is as follows:

1. The base pressure P_b is sensed by a pressure transducer in the lander vehicle during entry.

2. The trigger pulse is generated when the base pressure rises above a preset value.

The preset value is selected to be the highest value of base pressure in the eight corner runs when the lander vehicle Mach number M = 1.0. This occurs on Run 70 when the ambient pressure $P_o = 6.40$ lb/ft^2. Figure 6 shows the maximum value at M = 1.0 for the ratio of base pressure to ambient pressure $(P_b/P_o)_{max} = 0.89$. The preset value for the base pressure is therefore $P_{bp} = 0.89 \times 6.40 = 5.69$ lb/ft^2.

In the Feasible Systems Study, it was suggested that the inside of the lander vehicle should be vented to the outside through ports in the base of the vehicle. In this way, the internal pressure would be made equal to the average pressure acting on the base of the vehicle and the designer would have complete freedom in choosing a location for the pressure sensor. It is estimated that eight 1-inch holes distributed over the base of the lander vehicle would be enough to assure that the pressure error due to lag is less than 0.2%.

4.2.3 BASE PRESSURE TO ACCELERATION RATIO SUBSYSTEM

The operational sequence for this system is as follows:

1. The base pressure P_b and the axial acceleration a'_X are sensed with appropriate sensors in the lander vehicle during entry.

2. The ratio of base pressure to axial acceleration P_b/a'_X is computed.

3. The trigger pulse is generated when this ratio rises above a preset value.

The preset value is computed with the following equation:

$$(P_b/a')_P = 2m(P_b/P_o)/C_D A \gamma M^2 \qquad (4)$$

Substituting the following values into this equation,

m	=	31.677 slugs	(1020 lb for $g = 32.2$ ft/sec^2)
(P_b/P_o)	=	0.89	(from upper curve in Figure 6b)
C_D	=	1.25	(from Figure 3, $\eta = 0$)
A	=	113.1 ft^2	(vehicle diameter $D = 12$ ft)
γ	=	1.37	(model atmosphere VM-8)
M	=	1.0	(the specified initiation condition)

gives the following preset (trigger) value:

$$(P_b/a')_P = 0.29 \text{ lb-sec}^2/\text{ft}^3.$$

4.2.4 ACCELERATION FUNCTION SUBSYSTEM

The operational sequence for this system is as follows:

1. The axial acceleration a'_X is sensed by an accelerometer in the lander vehicle during entry.

2. The maximum acceleration value is recognized and used to compute, with the aid of a simple preset function, a trigger value of the acceleration.

3. The trigger pulse is generated when the acceleration level falls below the computed trigger value.

Figure 11 presents a plot of acceleration at $M = 1.0$ versus maximum acceleration for the eight corner runs. The line drawn through the two lowest points, Runs 57 and 77, is defined as the trigger function for this system. A curved line could have been drawn through the three lowest data points to give somewhat better predictions, but this seems unjustifiable at present.

4.2.5 IDEAL M = 1.0 SYSTEM

This system is defined as one that triggers at exactly $M = 1.0$. It should be realized that although this system is assumed to have no altitude uncertainty associated with being able to recognize when $M = 1.0$, it does have uncertainty associated with the various mission uncertainties such as the atmosphere, entry velocity, entry path angle, etc.

4.3 MATRIX EQUATION DEFINED

In the previous subsection, five systems and subsystems are defined. These are summarized and identified with the numbers 1 through 5 in Table 11. Also, eight independent variables are defined. These are also summarized and identified with numbers 1 through 8 in Table 11.

Let the trigger altitude for each system/subsystem be denoted by h_{T_i} where i is the system/subsystem number. Likewise, let the altitude about which the Taylor expansion is presumed to be made be designated by h_{O_i}. Further, let these be used to form two 5 x 1 column vectors designated by $\underline{H}_T$ and $\underline{H}_O$ respectively. Finally, let the eight independent variables be designated by an 8 x 1 column vector $\underline{K}$. It follows that the five Taylor expansion equations for the five systems and subsystems can be written in very compact form as

$$\underline{H}_T = \underline{H}_O + (\partial H/\partial K)\ \underline{K}$$

where $(\partial H/\partial K)$ is a 5 x 8 matrix of partial derivatives.

4.4 PERFORMANCE ANALYSIS RESULTS

The analyses of the systems described in Subsection 4.2 were carried out in the fashion outlined in Subsection 4.1 The results are shown in Table 12 in terms of $\underline{H}_O$ and $(\partial H/\partial K)\underline{K}$. Also shown in Table 12 are $\underline{H}_{min}$ and the associated values of altitude reduction defined as the difference between h_{min} for the Ideal M = 1.0 System and h_{min}. Finally, the

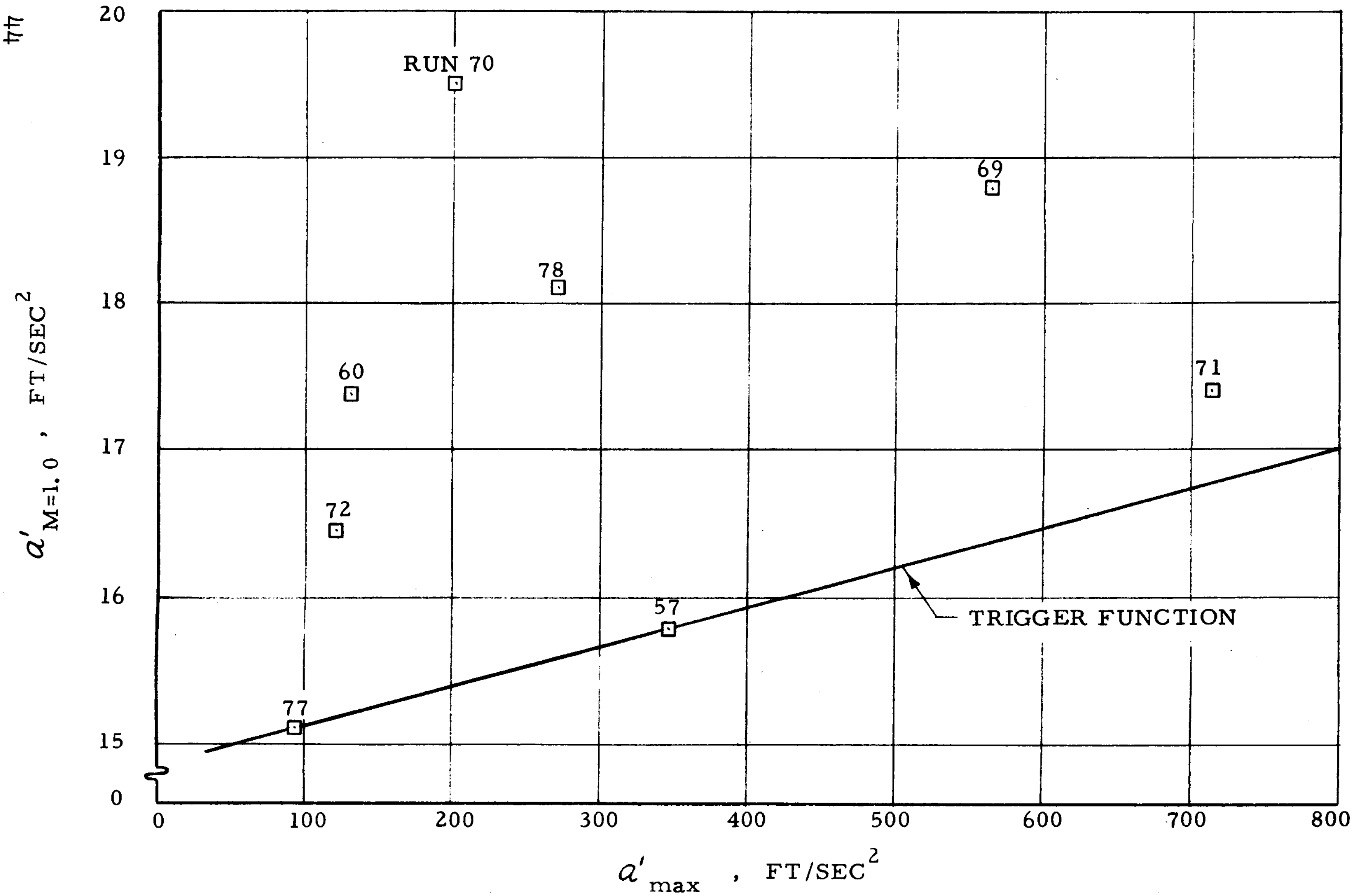

FIGURE 11. ACCELERATION AT M = 1.0 VERSUS MAXIMUM ACCELERATION FOR EIGHT CORNER RUNS

TABLE 11, SUMMARY OF THE FIVE SYSTEMS/SUBSYSTEMS AND EIGHT INDEPENDENT VARIABLES

(a) Systems/Subsystems

No.	Name
1	The Ideal M = 1.0 System
2	Acceleration Subsystem
3	Base Pressure Subsystem
4	Base Pressure To Acceleration Ratio Subsystem
5	Acceleration Function Subsystem

(b) Independent Variables

No.	Name
1	Mars Model Atmosphere Uncertainty
2	Entry Velocity Uncertainty
3	Entry Flight Path Angle Uncertainty
4	Entry Angle Of Attack Uncertainty
5	Entry Rolling Velocity Uncertainty
6	Entry Azimuth Angle Uncertainty
7	Base Pressure Coefficient Uncertainty
8	Environmental Factors Uncertainty

TABLE 12, SUMMARY OF ALTITUDE ERROR PERFORMANCE RESULTS FOR FIVE SYSTEMS/SUBSYSTEMS STUDIED IN PHASE 2

	H_o	$(\partial H/\partial K)K$								H_{Min}	Altitude Reduction	Altitude Reduction for Most Critical Run in Feasible Systems Study
System	h_{o_i}	$\left(\frac{\partial h_T}{\partial Atm}\right)_i \Delta Atm$	$\left(\frac{\partial h_T}{\partial V_E}\right)_i \Delta V_E$	$\left(\frac{\partial h_T}{\partial \gamma_E}\right)_i \Delta \gamma_E$	$\left(\frac{\partial h_T}{\partial \alpha_E}\right)_i \Delta \alpha_E$	$\left(\frac{\partial h_T}{\partial P_E}\right)_i \Delta P_E$	$\left(\frac{\partial h_T}{\partial \chi_E}\right)_i \Delta \chi_E$	$\left(\frac{\partial h_T}{\partial C_{P_b}}\right)_i \Delta C_{P_b}$	$\left(\frac{\partial h_T}{\partial Env}\right)_i \Delta Env$	$h_{o_i} - (\partial H/\partial K)K$	$h_{Min\ i=1} - h_{Min_i}$	
i = 1 Ideal M = .1.0 System	43,300 Ft	25,000 Ft	1,000 Ft	2,400 Ft	300 Ft	900 Ft	100 Ft	0 Ft	0 Ft	13,600 Ft	0 Ft	
i = 2 Acceleration Subsystem	29,500	19,100	1,500	2,700	300	900	500	0	4,300	200	13,400	(Feasible System N) 3,400 Ft
i = 3 Base Pressure Subsystem	39,400	25,000	300	300	200	0	200	400	1,000	12,000	1,600	(Feasible System R) 2,020
i = 4 Base Pressure to Acceleration Ratio Subsystem	41,500	25,000	1,000	2,400	300	900	100	800	2,000	8,000	5,600	(Feasible System J) 1,340
i = 5 Acceleration Function Subsystem	31,500	18,800	1,300	1,800	500	600	500	0	4,300	3,700	9,700	(Feasible System 0) 2,720

last column shows the corresponding values of altitude reduction for the most critical run (Run 57) that occurred in the Feasible Systems Study. The values of the eight independent variables that yield the null altitude and the minimum altitude are shown in Table 13.

It may be noticed that minimum altitudes of from 200 to 13,600 feet are predicted for the five systems shown in Table 12. These minimum altitudes, it should be emphasized, are predicted on the basis of linear mathematical models for the various systems. Not only are these systems nonlinear, at least with respect to the eight independent variables, but in most cases it is necessary to evaluate the altitude-uncertainty components at flight conditions far different than the minimum altitude flight condition.

Table 12 shows that the Base Pressure Subsystem has the smallest minimum altitude reduction, 1600 feet, followed in second place by the Base Pressure to Acceleration Subsystem, 5600 feet. This sequence is the opposite of what was indicated in the Feasible Systems Study; see last column in table. Also, this table shows the Acceleration Function Subsystem and the Acceleration Subsystem to rank third and fourth place respectively with reductions of 9900 and 13,400 feet respectively.

The largest single altitude uncertainty component is clearly associated with the atmosphere uncertainty. The next largest component depends on the system. For the Acceleration Subsystem, the Base Pressure Subsystem and the Acceleration Function Subsystem, it is the component associated with environmental effects. For the Base Pressure to Acceleration Ratio Subsystem, it is the component associated with the entry flight path angle. In all cases, the uncertainty components associated with the entry angle of attack and the entry azimuth angle are relatively small.

4.5 PRIME SENSOR TRADE STUDIES

Trade studies were conducted to establish the availability and suitability of pressure transducers and accelerometers for application in the Candidate Systems. The results of these trade studies are presented in this subsection.

TABLE 13, SUMMARY OF VALUES FOR INDEPENDENT VARIABLES GIVING THE NULL ALTITUDE AND THE MINIMUM ALTITUDE FOR THE PHASE 2 STUDY CONDITIONS

INDEPENDENT VARIABLE, K	VALUE FOR MINIMUM ALTITUDE	VALUE FOR NULL ALTITUDE
Atm	VM-8	Halfway between VM-3 and VM-8
V_E	12,500 FPS	14,250 FPS
γ_E	-20 deg	-17 deg
α_E	± 105 deg	± 50 deg
χ_E	± 1 rad/sec	$\pm 1/2$ rad/sec
p_E	+90 deg	0
C_{P_b}	Lower curve in Figure 6b	Middle curve in Figure 6b
Env	$(P_b)_{ACT} = 1.05\ (P_b)_{IND}$ $(a'_{X_B})_{ACT} = 0.95\ (a'_{X_B})_{IND}$	$(P_b)_{ACT} = (P_b)_{IND}$ $(a'_{X_B})_{ACT} = (a'_{X_B})_{IND}$

4.5.1 ACCELEROMETERS

The results of a trade study on accelerometers are summarized in Table 14. Shown in this table are representative performance specifications for six different types of accelerometers. These accelerometer types are identified as (a) Piezoelectric, (b) Hydraulic-Servo, (c) Quartz, Photo Diode and Light Source, (d) Cantilever Seismic Mass, (e) Strain Gauge and (f) Force Balance Electronic Servo.

A preliminary appraisal of the accelerometer types shown in Table 14 indicates that all but one are suited to the application being considered. This is the piezoelectric type. A piezoelectric accelerometer is more suited to measuring a rapidly changing, transient phenomena. Of the five remaining types, the strain gauge accelerometer has the most attractive combination of characteristics. It has fewer parts and is simpler; in addition, it is believed to be more reliable. Some of the other units can provide greater accuracy, but the accuracy available with a strain gauge accelerometer is believed to be adequate.

The accuracy of the strain gauge accelerometer is approximately 1.0% of full scale and should therefore not exceed 2% in the planned application. The weight of a unit with an output of 0 to 5V (with an output impedance of 2000 ohms) is approximately 4.0 oz. This type of transducer typically operates with a 28 $\pm$ 2 V power supply.

4.5.2 PRESSURE TRANSDUCERS

Table 15 summarizes the pressure transducers investigated. Five basically different types of sensors are shown in this table. These are identified as (a) Capacitive, (b) Strain Gauge, (c) Thermoconductive, (d) Piezoelectric and (e) Bourdon Tube - Bellows - Diaphram type pressure transducers. As noted in the table, the latter two types are unsuited for the application here under consideration.

The third transducer shown in Table 15 is a gas thermoconductivity measuring device. This device is small, light weight and potentially quite reliable. However, it is sensitive to gas composition and can not be considered feasible at this time.

TABLE 14, TRADE STUDY MATRIX FOR SIX ACCELEROMETERS

CHARACTERISTICS	ACCELERATION SENSOR TYPES		
	Piezoelectric	Hydraulic-Servo	Quartz, Photo Diode, Light Source
Ranges	± 1000 g and ± 10,000 g	10^{-6} g to 30 g	± 10 g
Sensitivity	4 to 60 MV/g	Shaft rotation 100 RPM/g	IV/g
Material	Stainless Steel and/or Aluminum	Unknown	Unknown
Temperature	-65°F to +250°F and -320°F to +500°F	60°F to 120°F operation -80°F to 212°F storage	Unknown
Accuracy	± 1% linearity. ± 4% over temperature range	Linearity 3×10^{-5} g to 1 g & 3×10^{-5} of reading to 30 g	Linearity 5×10^{-5} g to 1 g 10^{-2} g to 10 g
Weight	.3 ounces to 1.2 ounces	1.9 pounds	5 ounces acceleration and 4 ounces amplifier
Tri-Axial Model	Available	Yes	Unknown
Power, External	None	25W peak, heater } 28V 18W peak, servo } 26V, 400 CPS, 1 Ø 15W Peak	± 22V at 50 MA 3V at 60 MA
	Cantilever Seismic Mass	Strain Gauge	Force Balance Electronic Servo
Ranges	± 5 g to ± 500 g	± 1 g to ± 500 g	± 1 g to ± 80 g
Sensitivity	AC Bridge with 20 mh coils in unit	± 5 Volts F.S.	± 15 Volts F. S.
Material	Unknown	Unknown	Unknown
Temperature	0-165°F	-70°F to 300°F	-65°F to 212°F
Accuracy	Linearity ± ½% best straight line + ½% acceleration excursion for Hysteresis	± 1.0% F.S.	.02% Hysteresis. .05% non-linearity. .01% non-repeatability
Weight	1 to 3 ounces	1 to 4 ounces	Unknown
Tri-Axial Unit	Unknown	Yes	Unknown
Power, External	Excitation for bridge, 400 CPS to 20,000 CPS	28 VDC	± 28 VDC at ± 15 MA

TABLE 15, TRADE STUDY MATRIX FOR FIVE TYPES OF PRESSURE TRANSDUCERS

CHARACTERISTICS	PRESSURE TRANSDUCER TYPES				
	Capacitive Transducer	Strain Gage	Thermoconductivity	Piezoelectric	Bourdon Tube-Bellows-Diaphragm Types
Pressure Range	0.05 to 3.0 PSI-FS	± 0.05 to 0-5K PSID	.0005 PSI to 0.6 PSI	Present state-of-the-art shows no low pressure devices of the piezoelectric type currently available	State-of-art precludes the possibility of using any of the mechanical type of pressure transducers shown in this column.
Overpressure Max.	15 PSI	1000% F.S.	No Limit		
Accuracy	1.0% of Full Scale	0.6%	1.0%		
Linearity	± 1%	0.075%	.001%		
Hysteresis	.1%	0.075%	.001%		
Overpressure Susceptibility	Medium	Medium	None		
Repeatability	0.01% at const. temp.	0.05%	1 Micron at 30K Microns		
Frequency Response	3 DB Down at 330 CPS	0-500 CPS	50 M_a		
Resolution	Infinite	Infinite	Infinite		
Exitation Required	28 ± 5 VDC	5.0 VDC	28 VDC ± 3 V		
Maximum Temperature Range (Operating and Non-Operating)	$-60^{\circ}F$ to $+190^{\circ}F$	$-65^{\circ}F$ to $+250^{\circ}F$	$-65^{\circ}F$ to $+165^{\circ}F$		
Thermal Sensitivity Shift	Typical 0.03%/°F	0.01%/°F	Not Available		
Thermal Zero Shift	0.5 Mv/°F referred to the output	0.01%/°F	Not Available		
Type of Output (Switch-Voltage or Impedance)	0-5 VDC	3.5 Mv/VFS 350 ∿	Switch Function		
Shock	50 g	50 g			
Vibration	± 20 g 20-2000 CPS	± 15 g 0-500 CPS	± 20 g 20-2000 CPS		
Weight	2.33 lbs.	3.8 lbs.	16 oz. total		

The second transducer in Table 15 employs unbonded strain gauges as the sensing elements. It is rather well suited to the application being considered in all respects except one. This is the overpressure limitation. As noted in the table, the maximum overpressure rating is 1000% of full scale. For a pressure transducer with a full scale range of 0.05 PSIA, this is a maximum overpressure of only 0.5 PSI. This limitation is too severe for the present application.

The selected pressure sensor is the first transducer shown in Table 15. This is a capacitive transducer, and it employs a flat diaphram spaced midway between the two flat condenser plates. One side of the diaphram is heremetically sealed at essentially zero absolute pressure. The other side is connected to the lander vehicle interior compartment (or other region as required). A preliminary investigation of this unit indicated that the pre-operational environment specified in Table 3 would not have an adverse effect on this transducer. Also, the unit appears to be well suited for functioning in the operational environment specified in this same table.

4.6 CANDIDATE SYSTEMS RANKING

An evaluation matrix was used in order to establish a rational means for ranking the three Candidate Systems. Three primary evaluation criteria were used for this purpose: Performance, Reliability and Development Risk. These criteria were broken down into subitems and weighting factors were utilized. Whereas performance and reliability were assigned approximately equal weighting, development risk was apportioned about half as much weighting. Of all the factors considered, altitude dispersion -- a subitem of the performance criteria -- was given the largest weighting factor.

The results of the evaluation analysis are presented in Table 16. This table shows that the scores for the three systems are extremely close. Candidate System No. 2, which scored 318 merit points, is followed by Candidate System No. 1 with 314 merit points and Candidate System No. 3 with 313 merit points. In this regard, it should be realized that the three systems are very similar; namely, their secondary subsystems are identical and their primary subsystems all use an accelerometer.

TABLE 16, EVALUATION MATRIX FOR THE CANDIDATE SYSTEMS

EVALUATION FACTOR		Candidate System No. 1		Candidate System No. 2		Candidate System No. 3	
TOTAL MERIT POINTS		314		318		313	
A. PERFORMANCE — SUBTOTAL		100		150		108	
1. Altitude Dispersion	10	4	40	10	100	5	50
2. System Weight	3	10	30	8	24	10	30
3. Power Demand	2	10	20	9	18	9	18
4. Total Mission Versitility	1	10	10	8	8	10	10
B. RELIABILITY — SUBTOTAL		140		105		132	
1. Functional Simplicity	5	10	50	7	35	9	45
2. Degree of Redundancy	4	10	40	7	28	10	40
3. Failure Rate	3	10	30	8	24	9	27
4. Environment Suitability	2	10	20	9	18	10	20
C. DEVELOPMENT RISK — SUBTOTAL		74		63		73	
1. Development Time	3	10	30	9	27	9	27
2. Component Availability	2	10	20	7	14	10	20
3. Mission Compatability	2	8	16	8	16	10	20
4. System Concept Status	1	8	8	6	6	6	6

SCORE

FACTOR

WEIGHTING FACTOR

An inspection of Table 16 shows that the performance score for Candidate System System No. 2 is significantly higher than for the other two systems. This is a reflection of the fact that this system does in fact measure Mach number instead of an indication of Mach number. An opposite effect is shown by the reliability score. In the Degree of Redundancy subitem, the low grade for Candidate System No. 2 results from a consideration that, if a condition could exist that would create a failure in one of the pressure transducers, a failure in the other pressure transducer might also be induced. In addition, the state-of-the-art of components for long space storage and subsequent operation is considered less advanced for pressure transducer systems than for accelerometer systems. This is reflected in the scores for the failure rate and availability subitems.

Based primarily on the above considerations, Candidate System No. 2 was selected for further analysis in Phase 3 of the study. In addition to the above considerations, it could be pointed out that this system has almost all the components that are used in the other two candidate systems. Thus, much of the detailed information generated in the final study phase would be applicable if a change were made to one of the other two candidate systems at some future time.

5.0 FINAL SYSTEM STUDY (PHASE 3)

The Final System features a primary subsystem and a secondary subsystem acting in parallel. The primary subsystem is also referred to as the Base Pressure to Acceleration Ratio Subsystem, and the secondary subsystem is also referred to as the Base Pressure Subsystem. In the Feasible Systems Study, these subsystems are referred to as System J and System R. In the Candidate Systems Study, this configuration of subsystems is System No. 2.

5.1 PERFORMANCE ANALYSIS

Two changes in the assumptions used in the Candidate Systems Study are made. First, the environmental uncertainties are changed to be ± 10.6% for the Base Pressure to Acceleration Ratio Subsystem and ± 5.5% for the Base Pressure Subsystem. A detailed explanation giving the basis for these error values is presented in Section 5.2.4. Second, the preset value of the base pressure used in the Secondary Subsystem is slightly changed. Otherwise, the subsystem descriptions presented in Section 4.0 still apply insofar as this performance analysis is concerned.

5.1.1 PERFORMANCE ANALYSIS APPROACH

The approach used in the performance analysis is the same as that used in the Candidate Systems Study with certain improvements. Two additional independent variables are now considered. Interpolation procedures are used with the computer generated tables in order to improve the accuracy of the computations. Finally, an improved equation is used to compute the null altitude h_o.

The ten independent variables used in this analysis are independent in the way they appear in the trigger altitude equation,

$$h_T = h_T(\text{Atm}, V_E, \gamma_E, \alpha_E, p_E, \chi_E, C_{P_b}, \text{Env}, \text{Wind}, C_D) \qquad (5)$$

The quantities Wind and C_D are the two additional variables standing for maximum wind profile and lander vehicle drag coefficient. The ten independent variables and their ranges are listed in Table 17.

TABLE 17, SUMMARY OF THE TEN INDEPENDENT VARIABLES CONSIDERED IN THE FINALY SYSTEM STUDY

Independent Variables (Vector K)	Assumed Limiting Values
1. Atm	VM-3 to VM-8
2. V_E	12,500 to 16,000 ft/sec
3. γ_E	-14 to -20 deg
4. α_E	-105 to +105 deg
5. p_E	-1 to +1 rad/sec
6. χ_E	-90 to +90 deg
7. C_{P_b}	Same as Candidate Systems Study; see Figure 6.
8. Env	$(P_b/a')_{ACT} = 0.894\ (P_b/a')_{IND}$ to $1.106\ (P_b/a')_{IND}$ $(P_b)_{ACT} = 0.945\ (P_b)_{IND}$ to $1.055\ (P_b)_{IND}$
9. Wind	See Section 2.3
10. C_D	See Section 2.2

The Taylor expansion for the trigger altitude in terms of the ten independent variables, disregarding terms of second order and higher, is

$$h_T = h_o + \frac{\partial h_T}{\partial Atm} \Delta Atm + \frac{\partial h_T}{\partial V_E} \Delta V_E + \frac{\partial h_T}{\partial \gamma_E} \Delta \gamma_E + \frac{\partial h_T}{\partial \chi_E} \Delta \alpha_E$$

$$+ \frac{\partial h_T}{\partial p_E} \Delta p_E + \frac{\partial h_T}{\partial \chi_E} \Delta \chi_E + \frac{\partial h_T}{\partial C_{P_b}} \Delta C_{P_b} \qquad (6)$$

$$+ \frac{\partial h_T}{\partial Env} \Delta Env + \frac{\partial h_T}{\partial Wind} \Delta Wind + \frac{\partial h_T}{\partial C_D} \Delta C_D$$

<u>The Primary and Secondary Subsystems</u>

The steps taken in computing the performance of each subsystem include those described in Section 4.0 with certain additions and modifications. These are itemized as follows:

1) The low altitude-uncertainty components associated with the maximum wind profile and drag coefficient effects are computed with the equations shown in Table 18.

2) The high altitude-uncertainty components associated with the entry angle of attack, the entry rolling velocity, entry azimuth angle, the base pressure coefficient, the operational environmental effects, the wind and the drag coefficient are computed. The equations used in this computation are shown in Table 19.

3) The null altitude is computed. The relations used to make this computation are

$$h_o = h_{AV} - \left| \frac{\partial h_T}{\partial p_E} \Delta p_E \right| + \left| \frac{\partial h_T}{\partial \chi_E} \Delta \chi_E \right| , \quad \text{low altitudes}$$

$$(7)$$

$$h_o = h_{AV} - \left| \frac{\partial h_T}{\partial p_E} \Delta p_E \right| - \left| \frac{\partial h_T}{\partial \chi_E} \Delta \chi_E \right| , \quad \text{high altitudes}$$

TABLE 18, EQUATIONS FOR COMPUTING TWO ADDITIONAL LOW ALTITUDE-UNCERTAINTY COMPONENTS

$$\frac{\partial h_T}{\partial \text{Wind}} \Delta \text{Wind} = h_{T\,\text{Run 81}} - h_{T\,\text{Run 69}}$$

$$\frac{\partial h_T}{\partial C_D} \Delta C_D = h_{T\,\text{Run 86}} - h_{T\,\text{Run 71}}$$

TABLE 19, EQUATIONS FOR COMPUTING SEVEN HIGH ALTITUDE-UNCERTAINTY COMPONENTS

$$\frac{\partial h_T}{\partial \alpha_E} \Delta \alpha_E = \frac{1}{2}(h_{T_{\text{Run 74}}} - h_{T_{\text{Run 73}}})$$

$$\frac{\partial h_T}{\partial P_E} \Delta P_E = \frac{1}{2}(h_{T_{\text{Run 24}}} - h_{T_{\text{Run 44}}})$$

$$\frac{\partial h_T}{\partial \chi_E} \Delta \chi_E = \frac{1}{2}(h_{T_{\text{Run 60}}} - h_{T_{\text{Run 79}}})$$

$$\frac{\partial h_T}{\partial C_{P_b}} \Delta C_{P_b} = \frac{1}{2}(h_{-3_{\text{MIN } P_b/P_o}} - h_{-3\ \text{MAX } P_b/P_o})$$

$$\frac{\partial h_T}{\partial \text{Env}} \Delta \text{Env} = \frac{1}{2}(h_{-3_{\text{Max + Environmental errors}}} - h_{-3_{\text{Max − Environmental}}})$$

$$\frac{\partial h_T}{\partial \text{Wind}} \Delta \text{Wind} = h_{T_{\text{Run 82}}} - h_{T_{\text{Run 72}}}$$

$$\frac{\partial h_T}{\partial C_D} \Delta C_D = h_{T_{\text{Run 85}}} - h_{T_{\text{Run 60}}}$$

Equation (7) represents a substantial improvement over Equation (3) used in the Candidate Systems Study. The equation used previously yields overly conservative results. The reason a different equation is required for each altitude range is due to the fact that $\chi_E = +90^o$ is associated with both the minimum altitude entry trajectory and the maximum altitude entry trajectory.

The computations for the Final System performance analyses are done using approximate values for the preset base pressure to acceleration ratio $(P_b/a')_P$ and the base pressure $(P_b)_P$. These values are derived on the basis of the eight corner runs and are as follows:

$$(P_b/a')_P = 0.29 \text{ PSFA/FPSS}$$

$$(P_b)_P = 5.55 \text{ PSFA}$$

In addition to the altitude-uncertainty components and the null altitude h_o, certain secondary computational results are presented. The quantities computed and the equations used to make these computations are presented in Table 20.

The Ideal M = 1.0 System

The Ideal M = 1.0 System's performance is included in order to provide a basis for evaluating the performance of the Final System's two subsystems. Equations (6) and (7) are also used in computing h_T and h_o for this system. It should be realized that for this system, the trigger altitude h_T is the altitude at which M = 1.0.

5.1.2 FINAL SYSTEM PERFORMANCE ANALYSIS RESULTS

The results of the performance computations for the low altitude range and for the high altitude range are presented in Tables 21 and 22. A comparison of these tables with the corresponding table in the Candidate Systems Study, Table 12, indicates that a substantial improvement in accuracy is effected by using interpolation procedures. Also, it is seen that the two added uncertainty components are quite important. The wind-uncertainty component is, in fact, second in size after the atmosphere-uncertainty component.

TABLE 20, EQUATIONS FOR THE SECONDARY COMPUTATIONS

$$\underline{H}_{\substack{MIN\\MIN}} = \underline{H}_o - (\partial H/\partial K)\underline{K}$$

$$\begin{pmatrix}\text{MAXIMUM}\\\text{MIN.-ALT.}\\\text{UNDERSHOOT}\end{pmatrix}_{\text{SYSTEM } i} = \begin{pmatrix}h_{\substack{MIN\\MIN}}\end{pmatrix}_{\substack{\text{IDEAL}\\\text{SYSTEM}}} - \begin{pmatrix}h_{\substack{MIN\\MIN}}\end{pmatrix}_{\text{SYSTEM } i}$$

$$\underline{H}_{\substack{MAX\\MIN}} = \underline{H}_{\substack{MIN\\MIN}} + 2\left(\frac{\partial h}{\partial C_{P_b}} \Delta C_{P_b} + \frac{\partial h}{\partial Env} \Delta Env\right)$$

$$\begin{pmatrix}\text{MINIMUM}\\\text{MIN.-ALT.}\\\text{UNDERSHOOT}\end{pmatrix}_{\text{SYSTEM } i} = \begin{pmatrix}h_{\substack{MAX\\MIN}}\end{pmatrix}_{\substack{\text{IDEAL}\\\text{SYSTEM}}} - \begin{pmatrix}h_{\substack{MAX\\MIN}}\end{pmatrix}_{\text{SYSTEM } i}$$

$$\underline{H}_{\substack{MAX\\MAX}} = \underline{H}_o - (\partial H/\partial K)\underline{K}$$

$$\begin{pmatrix}\text{MINIMUM}\\\text{MAX.-ALT.}\\\text{UNDERSHOOT}\end{pmatrix}_{\text{SYSTEM } i} = \begin{pmatrix}h_{\substack{MAX\\MAX}}\end{pmatrix}_{\substack{\text{IDEAL}\\\text{SYSTEM}}} - \begin{pmatrix}h_{\substack{MAX\\MAX}}\end{pmatrix}_{\text{SYSTEM } i}$$

$$\underline{H}_{\substack{MIN\\MAX}} = \underline{H}_{\substack{MAX\\MAX}} - 2\left(\frac{\partial h}{\partial C_{P_b}} \Delta C_{P_b} + \frac{\partial h}{\partial Env} \Delta Env\right)$$

$$\begin{pmatrix}\text{MAXIMUM}\\\text{MAX.-ALT.}\\\text{UNDERSHOOT}\end{pmatrix}_{\text{SYSTEM } i} = \begin{pmatrix}h_{\substack{MIN\\MAX}}\end{pmatrix}_{\substack{\text{IDEAL}\\\text{SYSTEM}}} - \begin{pmatrix}h_{\substack{MIN\\MAX}}\end{pmatrix}_{\text{SYSTEM } i}$$

TABLE 21, SUMMARY OF LOW ALTITUDE ERROR PERFORMANCE RESULTS (ALTITUDES BELOW H_O)

	H_o	$(\partial H/\partial K)K$										$H_{Min \atop Min}$	Maximum Min.-Alt. Reduction	$H_{Max \atop Min}$	Minimum Min.-Alt Reduction
System	h_{o_i}	$\left(\frac{\partial h_T}{\partial Atm}\right)\Delta Atm$	$\left(\frac{\partial h_T}{\partial V_E}\right)\Delta V_E$	$\left(\frac{\partial h_T}{\partial \gamma_E}\right)\Delta\gamma_E$	$\left(\frac{\partial h_T}{\partial \alpha_E}\right)\Delta\alpha_E$	$\left(\frac{\partial h_T}{\partial P_E}\right)\Delta P_E$	$\left(\frac{\partial h_T}{\partial x_E}\right)\Delta x_E$	$\left(\frac{\partial h_T}{\partial C_{P_b}}\right)\Delta C_{P_b}$	$\left(\frac{\partial h_T}{\partial Env}\right)\Delta Env$	$\left(\frac{\partial h_T}{\partial Wd}\right)\Delta Wd$	$\left(\frac{\partial h_T}{\partial C_D}\right)\Delta C_D$	$h_{o_i} - (\partial H/\partial K)K$	(a)	(b)	(c)
i = 1 Ideal System M = 1.0	43,950 Ft	24,870 Ft	1,070 Ft	2,330 Ft	230 Ft	700 Ft	250 Ft	0 Ft	0 Ft	4,060 Ft	1,250 Ft	9,190 Ft	0 Ft	9,190 Ft	0 Ft
i = 2 Base Pressure to Acceleration Ratio Subsystem	(43,950)	24,870	1,070	2,330	230	700	250	730	2,600	4,060	1,250	(5,860)	(3,330)	(12,520)	(-3,330)
i = 3 Base Pressure Subsystem	(41,410)	24,850	180	440	70	60	30	450	1,220	2,060	370	(10,680)	(-1,490)	(14,020)	(-4,830)

NOTES: (a) = $\left(h_{Min \atop Min}\right)_{Ideal\ Syst.} - \left(h_{Min \atop Min}\right)_{Syst._i}$, (b) = $H_{Min \atop Min} + 2\left(\frac{\partial h}{\partial C_{P_b}}\Delta C_{P_b} + \frac{\partial h}{\partial Env}\Delta Env\right)$, (c) = $\left(h_{Max \atop Min}\right)_{Ideal\ Syst} - \left(h_{Max \atop Min}\right)_{Syst_i}$

TABLE 22, SUMMARY OF HIGH ALTITUDE ERROR PERFORMANCE RESULTS (ALTITUDES ABOVE H_O)

	H_o	$(\partial H/\partial K)K$										$H_{Max \atop Max}$	Minimum Max.-Alt. Reduction	$H_{Min \atop Max}$	Maximum Max.-Alt. Reduction
System	h_{o_i}	$\left(\frac{\partial h_T}{\partial Atm}\right)\Delta Atm$	$\left(\frac{\partial h_T}{\partial V_E}\right)\Delta V_E$	$\left(\frac{\partial h_T}{\partial \gamma_E}\right)\Delta\gamma_E$	$\left(\frac{\partial h_T}{\partial \alpha_E}\right)\Delta\alpha_E$	$\left(\frac{\partial h_T}{\partial P_E}\right)\Delta P_E$	$\left(\frac{\partial h_T}{\partial x_E}\right)\Delta x_E$	$\left(\frac{\partial h_T}{\partial C_{P_b}}\right)\Delta C_{P_b}$	$\left(\frac{\partial h_T}{\partial Env}\right)\Delta Env$	$\left(\frac{\partial h_T}{\partial Wd}\right)\Delta Wd$	$\left(\frac{\partial h_T}{\partial C_D}\right)\Delta C_D$	$h_{o_i} + (\partial H/\partial K)K$	(d)	(e)	(f)
i = 1 Ideal System M = 1.0	42,750 Ft	24,870 Ft	1,070 Ft	2,330 Ft	240 Ft	1,520 Ft	130 Ft	0 Ft	0 Ft	6,550 Ft	620 Ft	80,080 Ft	0 Ft	80,080 Ft	0 Ft
i = 2 Base Pressure to Acceleration Ratio Subsystem	(42,750)	24,870	1,070	2,330	240	1,520	130	1,330	4,950	6,550	620	(86,360)	(-6,280)	(73,800)	(6,280)
i = 3 Base Pressure Subsystem	(41,160)	24,850	180	440	30	270	10	1,030	2,030	1,150	40	(71,190)	(8,890)	(65,070)	(15,010)

NOTES: (d) = $\left(h_{Max \atop Max}\right)_{Ideal\ Syst.} - \left(h_{Max \atop Max}\right)_{Syst._i}$, (e) = $H_{Max \atop Max} + 2\left(\frac{\partial h}{\partial C_{P_b}} + \frac{\partial h}{\partial Env}\Delta Env\right)$, (f) = $\left(h_{Min \atop Max}\right)_{Ideal\ Syst} - \left(h_{Min \atop Max}\right)_{Syst._i}$

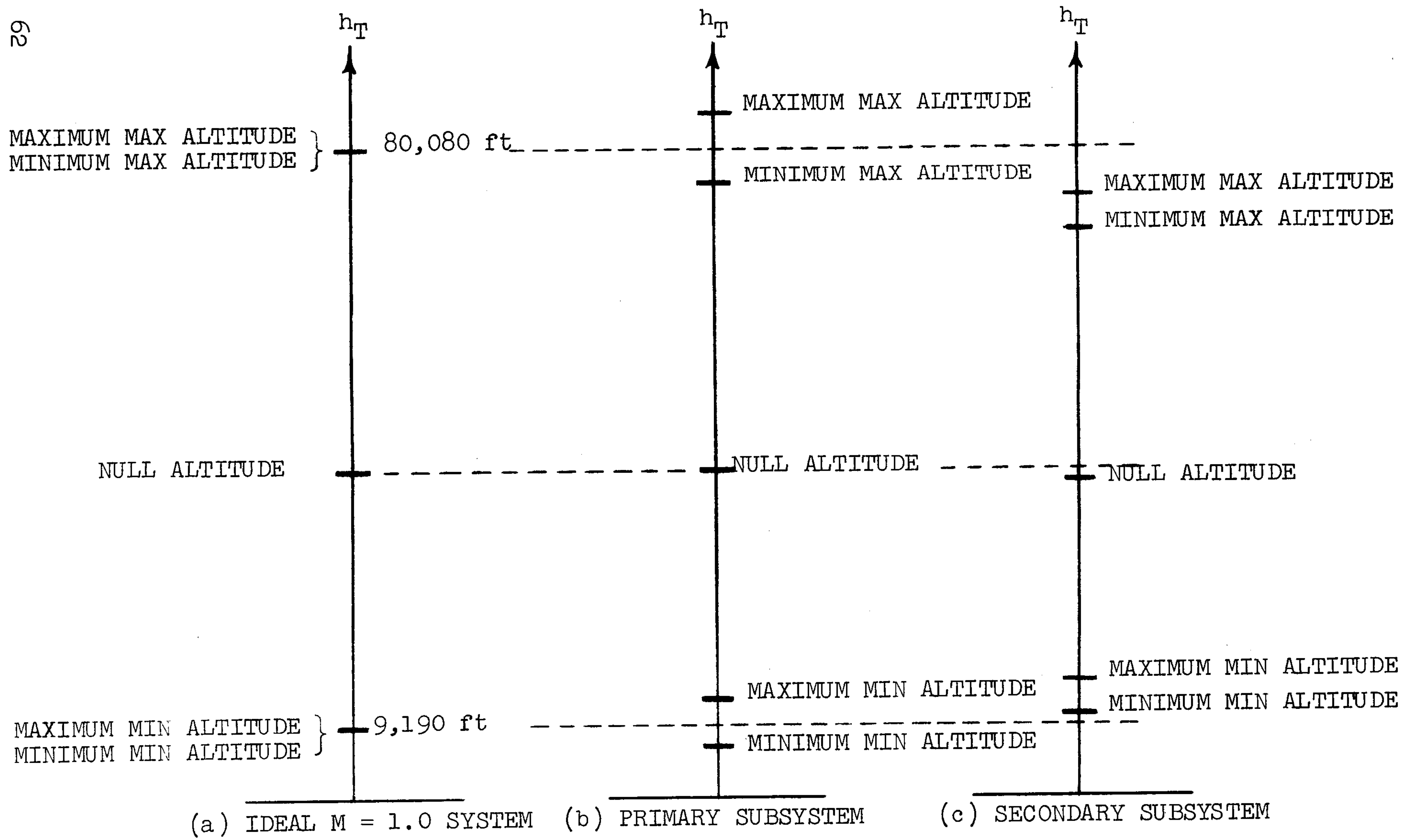

FIGURE 12, SCHEMATIC DIAGRAMS ILLUSTRATING THE PERFORMANCE RESULTS

The final four columns in Tables 21 and 22 contain the most interesting performance results. These results are organized in diagram form in Figure 12. This figure shows, in a schematic way, the minimum, null and maximum trigger altitudes for the Primary and Secondary Subsystems together with the corresponding altitudes for the Ideal M = 1.0 System. Two minimum altitudes and two maximum altitudes are shown for each system. These two altitudes at each extreme are due to the base pressure and environmental uncertainties. The two minimum altitudes are called the minimum min and maximum min in this discussion. Likewise, the two maximum altitudes are called minimum max and maximum max. The values of the independent variables corresponding to each of these altitudes is shown in Table 23.

Figure 12 (or Tables 21 and 22) shows that the maximum min trigger altitudes for both the Primary and Secondary Subsystems are above the M = 1.0 altitude. Also, the maximum max altitude for the Primary Subsystem is above the M = 1.0 altitude. This means that these subsystems, as they are specified with the preset values given on Page 59, may trigger at too high an altitude. In other words, they may trigger at a Mach number greater than 1.0. This is due simply to the fact that the preset values have not been properly chosen. Future analysis can develop improved preset values on the basis of the computational results presented herein. Thus, it should be realized that the parenthesized numbers in these tables are subject to change. Future analysis can, in addition, use the improved approach developed in this phase of the study to update the analysis results of the previous study phase.

The Extreme Cases

The last four runs indicated in Table 1 are referred to as the extreme cases. These are Runs 94 - 97. They were made available for the explicit purpose of checking the accuracy of the performance results developed in the study.

Table 24 summarizes the trigger altitude h_T for the Ideal M = 1.0 System and each of the Final System's two subsystems. Also shown in this table are the altitudes predicted by Equation (6) with the values given in Tables 21 and 22 (assuming no base pressure or environmental errors). Reasonably good agreement is indicated; the mean deviation is 414 ft for the 12 cases shown in this table.

TABLE 23, SUMMARY OF VALUES FOR INDEPENDENT VARIABLES GIVING MINIMUM, NULL AND MAXIMUM TRIGGER ALTITUDES

Independent Variable, K	$H_{min\ min}$	$H_{max\ min}$	H_o	$H_{min\ max}$	$H_{max\ max}$
(1) Atm	VM-8	VM-8	Note (a)	VM-3	VM-3
(2) V_E	12,500 FPS	12,500 FPS	14,250 FPS	16,000 FPS	16,000 FPS
(3) γ_E	-20 deg	-20 deg	-17 deg	-14 deg	-14 deg
(4) α_E	$\pm$105 deg	$\pm$ 105 deg	$\pm$ 50 deg	0	0
(5) ρ_E	$\pm$1rad/sec	$\pm$ 1 rad/sec	$\pm\frac{1}{2}$ rad/sec	0	0
(6) χ_E	+ 90 deg	+ 90 deg	0	+ 90 deg	+90 deg
(7) Cp_b	Note (b)	Note (c)	Note (d)	Note (b)	Note (c)
(8) Env	Note (e)	Note (f)	No Error	Note (e)	Note (f)
(9) Wind	Note (g)	Note (g)	No Wind	Note (h)	Note (h)
(10) C_D	3% Low	3% Low	No Error	3% High	3% High

NOTES:
- (a) Halfway between VM-3 and VM-8
- (b) (P_b/P_o) is lower curve in Figure 6b
- (c) (P_b/P_o) is upper curve in Figure 6b
- (d) (P_b/P_o) is a mid-curve in Figure 6b
- (e) $(P_b)_{ACT} = 1.055\ (P_b)_{IND}$ and $(P_b/a')_{ACT} = 1.106\ (P_b/a')_{IND}$
- (f) $(P_b)_{ACT} = 0.945\ (P_b)_{IND}$ and $(P_b/a')_{ACT} = 0.894\ (P_b/a')_{IND}$
- (g) Wind is toward the East; V_W = 220 FPS and h_s = 16,100 ft
- (h) Wind is toward the West; V_W = 155 FPS and h_s = 80,780 ft

TABLE 24, SUMMARY OF TRIGGER AND PREDICTED ALTITUDES FOR THE EXTREME CASES (RUNS 94-97)

RUN	IDEAL M = 1.0 SYSTEM		PRIMARY SUBSYSTEM		SECONDARY SUBSYSTEM	
	TRIGGER	PREDICTED*	TRIGGER	PREDICTED*	TRIGGER	PREDICTED*
94	13,566	14,500	13,566	14,500	14,867	15,780
95	14,885	15,000	14,885	15,000	15,389	15,840
96	72,025	72,650	72,025	72,650	66,758	66,920
97	72,918	72,910	72,918	72,910	66,849	66,940

* Using Equation (6) with the values in Tables 21 and 22 and assuming no base pressure or environmental errors.

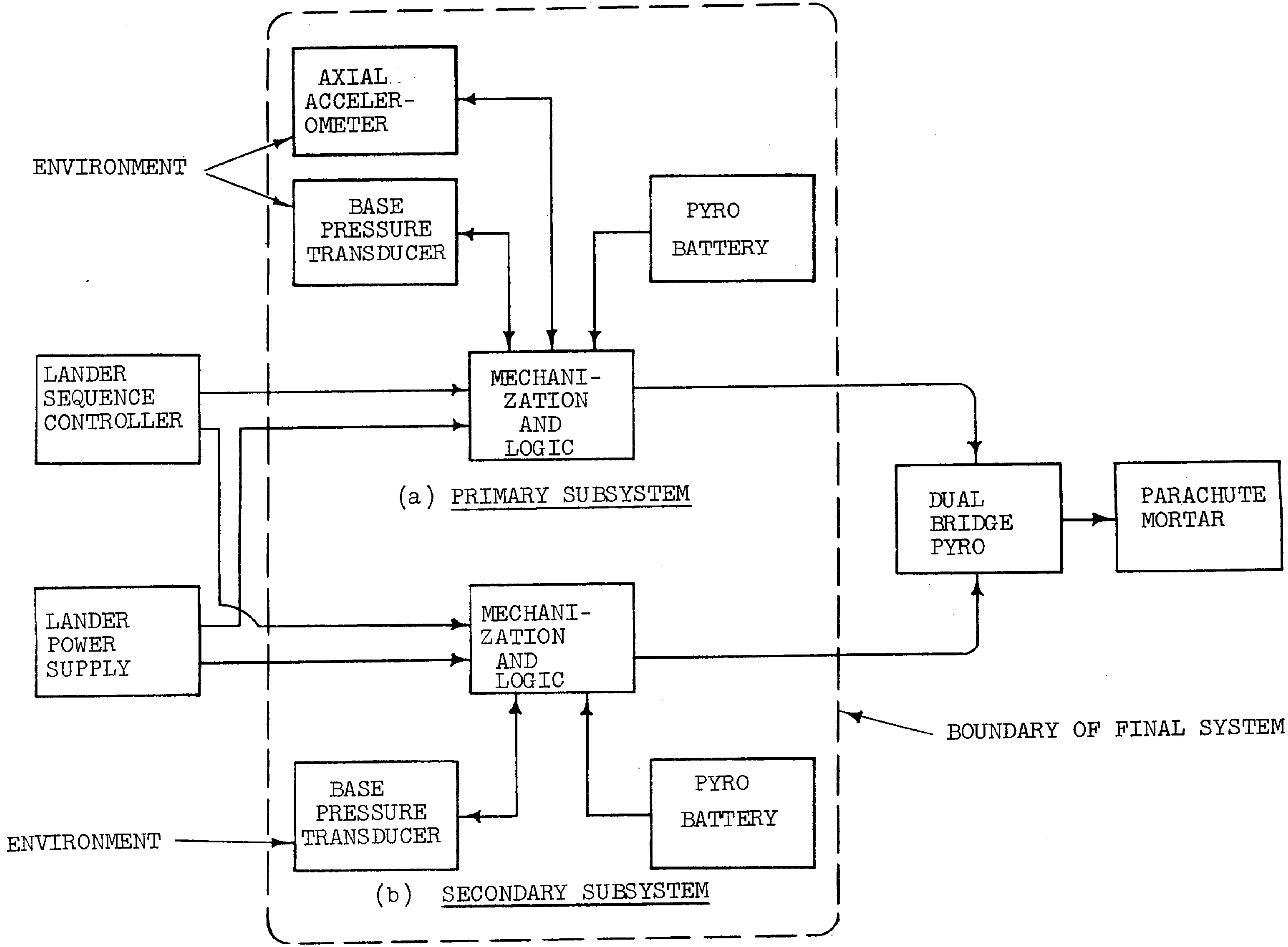

FIGURE 13, BLOCK DIAGRAM OF FINAL SYSTEM

5.2 ELECTRICAL DESIGN

The material presented in this section gives the electrical design details for the Final System. A method for arming the Base Pressure to Acceleration Ratio Subsystem is explained. Circuit diagrams are presented and interpreted. Error analyses are made. A parts list is given. A weight breakdown is shown, and the total system weight is estimated. And finally, a reliability analysis is presented.

5.2.1 INTRODUCTORY REMARKS

The Final System is shown schematically in relation to other lander vehicle components in Figure 13. The electrical inputs are shown to consist of a line from the lander sequence controller to each subsystem and a line from the lander power supply to each subsystem. The lander sequence controller is assumed to activate the system after the deorbit event when the lander vehicle is in a state of "free fall." The lander power supply is assumed to have negligible internal impedance and to provide three direct current voltage sources of +28, +12 and -6 volts.

The outputs from the two subsystems go to the opposite sides of a dual pyro bridge. Each side of this dual bridge is capable of actuating the parachute mortar (or other deceleration system component). The current (power) required to initiate one side of this dual bridge is taken to have a value of 4.5 amperes (4.5 watts). The corresponding "no fire" value for each bridge is normally 1.0 ampere (1.0 watt).

5.2.2 ARMING OF THE PRIMARY SUBSYSTEM

The reason the Base Pressure to Acceleration Subsystem must include an arming circuit is as follows. The inputs to the differential amplifier are a voltage proportional to the base pressure and a voltage equal to 0.29 times the acceleration; the output is a voltage equal to the amplifier gain times $(P_b - 0.29\ a')$. When the two inputs become equal, their difference is zero and the output of the amplifier is equal to zero. This occurs when the flight Mach number equals 1.0. At this time, the base pressure is increasing and the acceleration is decreasing. Thus, the output of the amplifier changes from a negative value to a positive value. However, it is estimated that the output of the amplifier could drift by as much as 1/2 volts positive (due most likely to a few millivolts of drift in one of the amplifier's two inputs). This amount of drift would not produce a serious error if the flight Mach number was approaching 1.0. However, early in the trajectory when both the base pressure and the acceleration are essentially equal to zero, this amount of drift would cause the trigger pulse to be generated prematurely if there were no arming circuit.

The first arming method conceived used a peak acceleration detecting circuit. The output from an accelerometer was used to charge an R-C circuit that had a very small (short) charging time constant and a very large (long) discharging time constant. For the case of a rather flat trajectory such as Run 77, the maximum sensed acceleration is approximately 90 ft/sec^2 and the rate of change of acceleration at this time is approximately 0.3 ft/sec^3. The ratio of these two quantities, (90 ft/sec^2)/(0.3 ft/sec^3) = 300 sec. The discharge time constant required in the peak detecting circuit must be several factors larger. Exactly how much larger depends on the sensitivity, gain and drift characteristics of the accelerometer and amplifier being used. If a one microfared capacitor is being used, an effective resistance in the R-C circuit of over 300 megohms is required. Although this level of resistance can be achieved by careful selection of the amplifier, blocking diode, and wiring; the internal leakage of the capacitor may itself present a limitation. Even the possibility of selecting a larger capacitor might not help because of the probability of an attendant larger internal leakage.

Another problem inherent in the peak acceleration arming method should be mentioned. This problem is the fact that the peak acceleration may be almost two orders of magnitude larger than the acceleration level at which the specified flight condition occurs. Thus, it is implied that either (a) the accelerometer operate over both a low range and a high range, or (b) there be two accelerometers: one for low range operation and one for high range operation. The first alternative is not attractive because an accuracy loss in the low range is inevitable. The second alternative, while more feasible, introduces additional complexity.

An alternative, simple arming method for the primary subsystem was evolved when it was realized that the peak acceleration arming circuit might not be satisfactory. This method employs the output from the base pressure transducer and consists simply of a circuit that recognizes when this output exceeds a preset value. This arming method is easily mechanized and apparently entirely satisfactory from the standpoint of reliability.

5.2.3 CIRCUIT OPERATION

The circuit diagram for the Final System is presented in Figure 14. Its principle of operation is described below.

The Primary Subsystem

The upper portion of Figure 14 shows the circuit diagram for the primary subsystem. Base pressure transducer MT1, differential amplifier AR1, "and" gate G1, and the reference voltage circuit at the very top of the figure perform the arming function. Resistance R1 and zener diode CR1 of this arming circuit provide a precision voltage of about 6 volts. A zener diode with this voltage rating is chosen due to the excellent temperature compensation inherent in such a unit. The small capacitor C1 provides filtering and the precision resistors R2 and R3 scale the zener voltage to about 1.5 volts. (It may be noted that a small error in this voltage does not affect the accuracy of this subsystem as a sensor.) This reference voltage is connected to the inverting input of the differential amplifier AR1. The base pressure transducer MT1 is selected to have an output of 5.000 volts when the pressure is 0.05000 PSIA. The output from this pressure transducer is connected to the non-inverting input of the differential amplifier. When this output becomes slightly larger than the reference voltage, the output of the differential amplifier AR1 becomes positive, the "and" gate G1 is turned on, and the arming of the primary subsystem is completed. The output voltage from the pressure transducer required for this event is approximately 1.510 volts, the exact value depending on the gain in AR1 and the voltage gain or loss in G1. A base pressure transducer output of 1.510 volts would be produced by a pressure of 0.0151 PSIA (2.17 PSFA).

The trigger pulse is to be generated when the base pressure, in units of PSFA, becomes equal to 0.29 times the sensed acceleration, in units of ft/sec^2 (FPSS). As noted above, the base pressure transducer MT1 is selected to have an output of 5.000 volts when the pressure is 0.05000 PSIA. In equation form, this is equivalent to:

$$P_b = (1.44 \text{ PSFA/volt})\, V_b$$

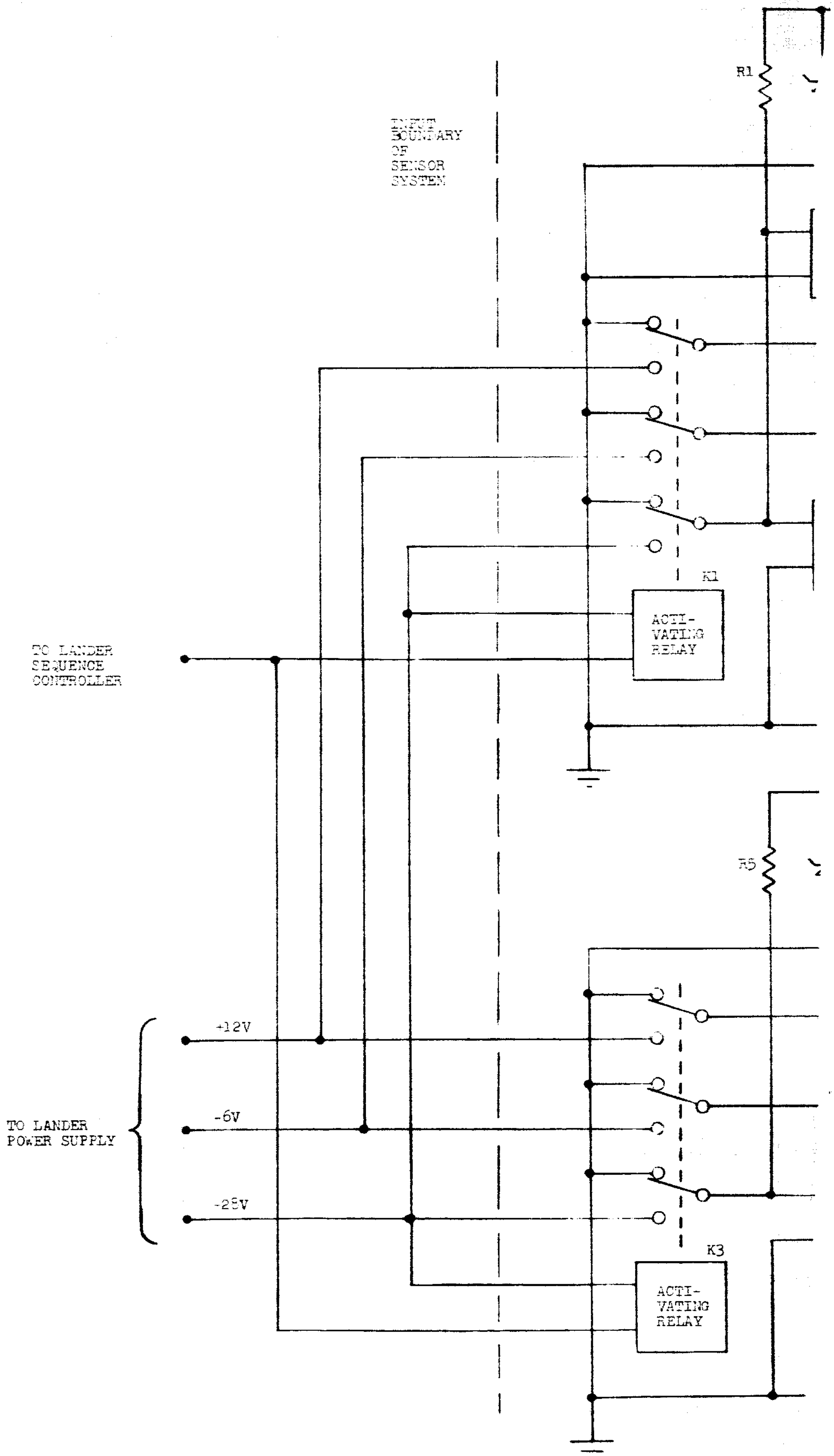

PRECEDING PAGE BLANK NOT FILMED.

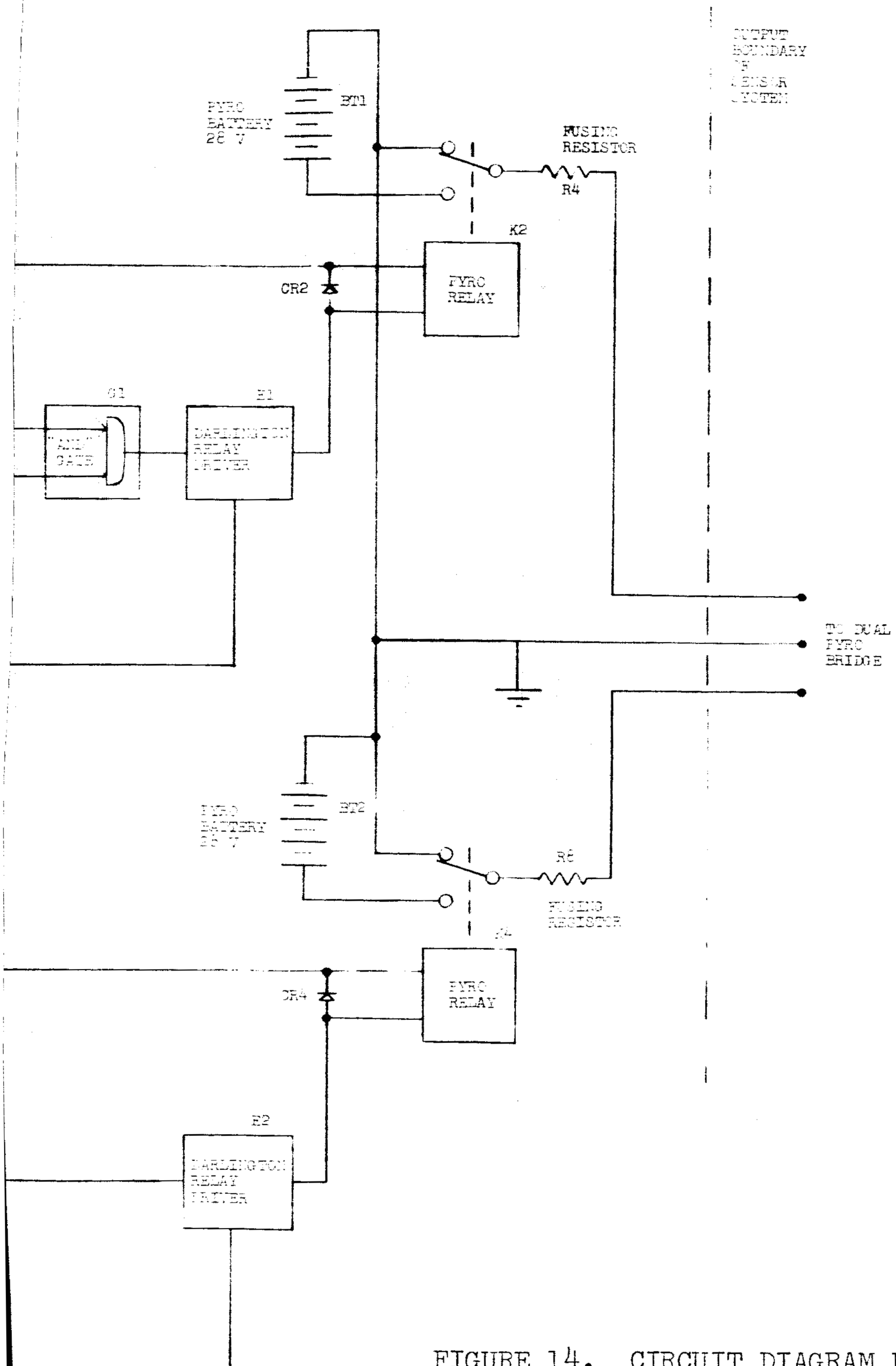

FIGURE 14, CIRCUIT DIAGRAM FOR FINAL SYSTEM.

To compute the scale factor for the accelerometer output, let it be assumed that the sensed acceleration is related to the output voltage by the following equation

$$a'_X = (S.F.)\ V_{a'}$$

where (S.F.) is the scale factor to be determined. Substituting the above two equations into the trigger relation,

$$P_b/a'_X = 0.29 \text{ PSFA/FPSS} \qquad (8)$$

and solving for the scale factor gives

$$(S.F.) = 4.97 \text{ FPSS/volt}$$

Thus, the full scale voltage output for the accelerometer, corresponding to 32.2 FPSS, is

$$(V_{a'})_{F.S.} = \frac{32.2 \text{ FPSS}}{4.97 \text{ FPSS/volt}} = 6.48 \text{ volts}$$

This is rounded to 6.5 V in subsequent discussion.

The output of accelerometer A1 is connected to the inverting input of the differential amplifier AR2, and the output of the pressure transducer MT1 is connected to the noninverting input. The output of this amplifier is essentially zero near the beginning of the entry trajectory because both the sensed acceleration and the base pressure are very nearly zero. As the lander vehicle begins to enter the atmosphere, the acceleration and the base pressure both begin to rise. The output from the accelerometer rises more rapidly than the base pressure, and the output of the differential amplifier is negative. The acceleration continues to rise until it reaches a peak value, and then it begins to decline. During this period, the base pressure continues to rise; when a preset value is reached, the "and" gate G1 is armed as described previously. When the acceleration decreases sufficiently and the base pressure increases sufficiently to satisfy the trigger relation, Equation (8), the output of the differential amplifier AR2 passes through zero and then becomes positive. At this instant, the amplifier acts somewhat like a switch due to its gain, and the "and" gate is actuated.

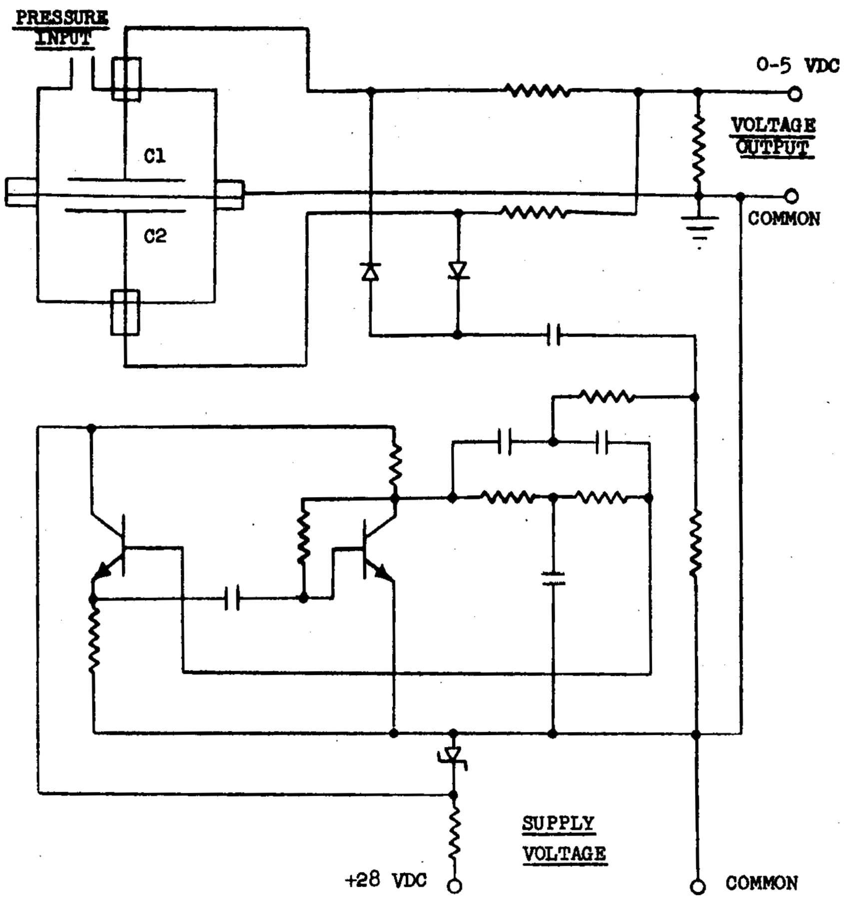

FIGURE 15, SCHEMATIC DIAGRAM FOR TYPICAL CAPACITIVE PRESSURE TRANSDUCER

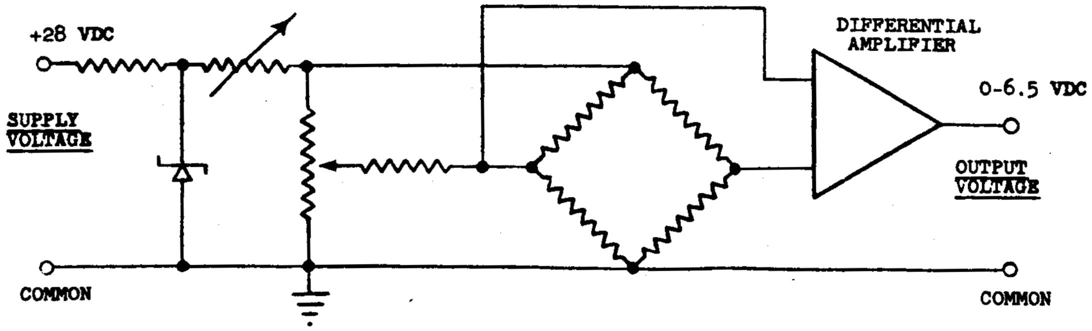

FIGURE 16, SCHEMATIC DIAGRAM FOR TYPICAL STRAIN GAUGE ACCELEROMETER

The term "'and' gate" is used in this discussion because it identifies the function of component G1. This component may be a conventional diode network, an integrated circuit, transistorized "and" gate, an integrated circuit "nor" gate (used with the inverted outputs of the amplifier), or a more complex logic function type component composed of integrated circuits. All of these approaches would apparently fulfill the requirement, and the final choice should be based on reliability, cost and availability considerations. At this point, a dual DTL "Nand" gate type integrated circuit module seems like a logical choice.

Actuation of the "and" gate provides a positive voltage to the input of the Darlington relay driver E1. This component is an integrated circuit and is used to provide sufficient current to ensure positive operation of the mechanical relay K2. Diode CR2 across relay K2 provides protection to the Darlington relay driver E1. Relay K2 actuates the pyro battery circuit which provides the trigger pulse. The trigger circuit includes a nickel-cadmium battery BT1, a fusing resistor R4, and one half of the dual pyro bridge. A nickel-cadmium battery is selected for BT1 because of its high current producing capabilities and resistance to environmental conditions.

Schematic diagrams for a typical capactive pressure transducer, strain gage accelerometer, differential amplifier, "Nand" gate, and Darlington relay driver are presented in Figures 15 through 19 respectively.

The Secondary Subsystem

The lower portion of Figure 14 shows the circuit diagram for the secondary subsystem. No arming function is required for this subsystem. The operational functions of the components in this subsystem are similar to the functions just explained for the corresponding components in the primary subsystem. For this reason, a description for the operation of this system is not felt to be necessary.

Other Remarks

The system being presented consists of discrete components and integrated circuits that are available as off-the-shelf items or as items with reasonably short delivery schedules. In particular, it is estimated that the longest lead time for any item would not exceed 120 days.

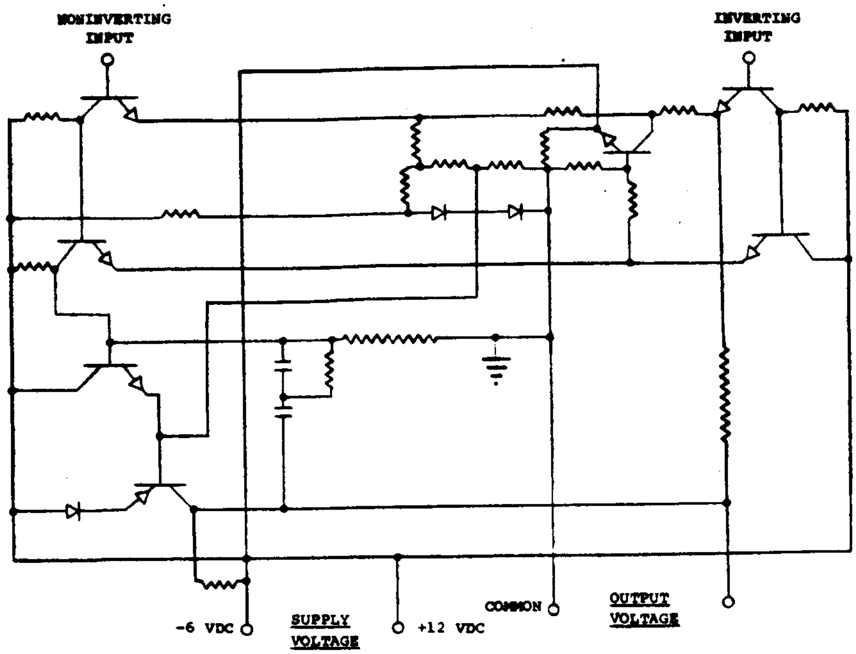

FIGURE 17, SCHEMATIC DIAGRAM FOR TYPICAL DIFFERENTIAL AMPLIFIER

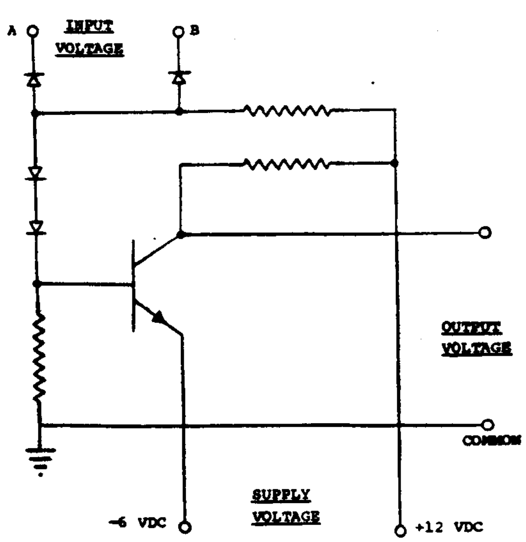

FIGURE 18, SCHEMATIC DIAGRAM FOR TYPICAL "NAND"GATE

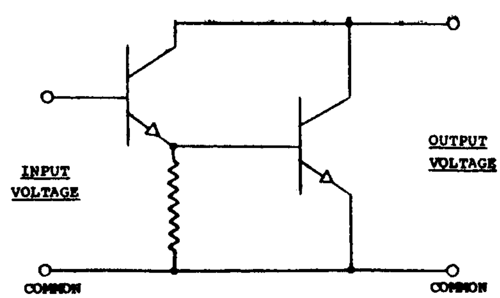

FIGURE 19, SCHEMATIC DIAGRAM FOR TYPICAL DARLINGTON RELAY DRIVER

The integrated circuits proposed for this application are manufactured by the Westinghouse Electric Company. These units are designed for military applications and appear to have the required operating and storage temperature ranges. Their operating temperature range is -55°C to +125°C and their storage temperature range is -65°C to +175°C.

5.2.4 ERROR ANALYSIS

In the following error analyses, all errors are converted into equivalent voltage errors at the inputs to the differential amplifiers AR2 and AR3. Timing errors such as the time lag of the pressure transducer and the pull times of the various relays are converted into equivalent voltage errors. For the purpose of this analysis, the trigger flight condition is assumed to occur when the outputs of both prime sensors are 3 volts. Also, the temperature uncertainty range is assumed to be ±50°F. The transconductance of the Darlington relay driver is unknown; therefore, it is assumed that the circuit will pull in the pyro relay with a small positive input voltage and that there is no error from this source. In appraising the following error estimates, it should be remembered that full scale (F.S.) for the accelerometer and the pressure transducers corresponds to 6.5 and 5.0 volts respectively.

Primary Subsystem

Accelerometer	Error at Input to Diff. Amplifier
Noise (± 5 MVRMS = 7 MV peak)	7 MV
Nonlinearity and Hysteresis (± 1% F.S. = 0.01 x 6.5).	65
Thermal Sensitivity Shift (0.02%/°F = 0.0002 x 3 x 50)	30
Thermal Zero Shift (0.02% F.S./°F = 0.0002 x 6.5 x 50) . .	65
Misalignment of X Axis to Flight Path (0.2% = 0.002 x 3).	6
Pressure Transducer	
Hysteresis and Noise (0.1% F.S. = 0.001 x 5).	5
Linearity (± 1% F.S. = 0.01 x 5).	50

Thermal Sensitivity Shift (0.03%/°F = 0.0003 x 50 x 3) . .	45
Thermal Zero Shift (0.5 MV/°F = 0.5 x 50) . . .	25
Supply Voltage Effect on Sensitivity (Assume supply voltage is 28 ± 2 VDC, 0.02%/V = 0.0002 x 3 x 2)	1.2
Time Lag (0.2% = 0.002 x 3)	6
<u>Differential Amplifier</u>	
Loading Effect on Transducers (none assumed; can be calibrated out)	0
D. C. Off-Set at Output (0.5 volts is typical with a transducer output impedance of 100 ohms. Because this application employs a transducer with a different output impedance, assume 1 volt. Reflected to the input, with a minimum gain of 220, this is 1/220). . . .	4.5
Drift Due to Temperature (10 μV/°C = 5/9 x 50 x 10)	0.3
<u>"Nand" Gate</u>	
Trigger voltage = 1.45 ± 0.85 volts (reflected to input = 0.85/220).	3.9
<u>Darlington Circuit</u>	
(Acts as a switch and will contribute negligible error; i.e., the "Nand" gate circuit will drive the Darlington circuit to saturation).	0
<u>Relay</u>	
The error contributed by the relay is a time function. A nominal time delay of 5 to 10 milliseconds can be expected. The estimated equivalent voltage at the amplifier input is 0.0025 volts	2.5
TOTAL	317 MV

The maximum transducer and electrical error of this system is 317 millivolts. This represents an error of 10.6% at a trigger value of 3 volts. The RMS sum of the listed error is 121 millivolts. This represents a one sigma error of 4.3% at the 3 volt trigger value.

Secondary Subsystem

Pressure Transducer	Error at Input to Diff. Amplifier
Hysteresis and Noise (0.1% F.S. = 0.001 x 5)	5 MV
Linearity (± 1% F.S. = 0.01 x 5).	50
Thermal Sensitivity Shift ($0.03\%/^{o}F$ = 0.0003 x 50 x 3)	45
Thermal Zero Shift ($0.5\ MV/^{o}F$ = 0.5 x 50).	25
Supply Voltage Effect on Sensitivity (Assume supply voltage is 28 ± 2 VDC, 0.02%/V = 0.0002 x 3 x 2)	1.2
Time Lag (0.2% = 0.002 x 3)	6
Differential Amplifier	
Loading Effect on Transducers (none assumed; can be calibrated out).	0
D.C. Off-Set at Output (0.5 volts is typical with a transducer output impedance of 1000 ohms. This application employs a transducer that may have slightly less impedance; however, assume 0.5 volts. Reflected to the input, with a minimum gain of 220 this is 0.5/220). . .	2.2
Drift Due to Temperature ($10\ \mu V/^{o}C$ = 5/9 x 50 x 10).	0.3
Reference Voltage	
The reference voltage can be adjusted to almost any degree of accuracy; 1% is assumed (0.01 x 3).	30
TOTAL	165 MV

TABLE 25, PARTS LIST AND WEIGHT ESTIMATE FOR FINAL SYSTEM

① NUMBER REQUIRED	② COMPONENT	③ MANUFACTURER AND MODEL NUMBER	④ WEIGHT (each)	⑤ ① x ④
1	Accelerometer (A1)	Statham Instruments, Inc., Mod. A 404 TC	4.0 oz	4.0 oz
3	Differential Amplifier (AR)	Westinghouse Electric Corp. WS123Q	0.004	0.01
1	"and" Gate (G1)	Westinghouse Electric Corp. WM241G	0.01	0.01
2	Darlington Relay Driver (E)	Westinghouse Electric Corp. WS153Q	0.01	0.02
2	Zener Diode (CR)	Texas Instruments, Inc. 1N709A-62	0.01	0.04
2	Diode (CR)	Texas Instruments, Inc. 1N1696	0.01	0.02
2	Capacitor (C)	Sprague, Type CS13BF334M (33 mfd, 35 vdc)	0.45	0.90
6	Resistor (R)	I.R.C. Type MEA-TE Mil Type RN 60C	0.03	0.20
2	Activating Relay (K)	Filters Relay Co. BRVS 26SRA-J 12A (4P2T)	2.59	5.18
2	Pyro Relay (K)	Filters Relay Co. SPRJS 26E116A-1 (2P2T)	0.53	1.06
2	Pyro Battery (BT)	Nickel-Cadmium Type	8.0	16.0
2	Pressure Transducer (MT)	Lion Research Corp. LRC Series 110	37.0	74.0
1	Circuit Board, etc.		8.6	8.6

Final System Total Weight 110.0 oz

The maximum transducer and electrical error of this system is 165 millivolts. This represents an error of 5.5% at a trigger value of 3 volts. The RMS sum of the listed error is 78 millivolts. This represents a one sigma error of 2.6%.

5.2.5 PARTS LIST AND WEIGHT ESTIMATE

Table 25 presents a detailed parts list for the Final System. The specific components listed in this table are believed to be capable of meeting the mission requirements, but do not represent the results of detailed trade-off studies. Also presented in this table are the weights for each component. The total weight for the Final System, as described in Subsection 5.2, is estimated to be 110 ounces.

(The two pyro batteries are required for only a brief instant of time; and, undoubtedly, they will be used to provide power for some other function subsequent to providing the trigger pulses. In other words, uncertainty exists as to whether it is proper to include the total weight of these components as sensor system weight. The weight of the Final System, less the two pryo batteries, is 94 ounces.)

The heaviest component by far is the pressure transducer. It seems quite likely that the weight of this component could be markedly reduced. Also, it should be noted that a further weight reduction could be achieved by going to an all-integrated-circuit design.

5.3 RELIABILITY ANALYSIS

The Mars Atmospheric Sensing System involves the use of small numbers of component parts operating for short time durations without on-board maintenance. These factors, combined with unique environmental conditions and the requirement for high initial mission reliability, limit the usefulness of conventional reliability prediction techniques. These prediction techniques, based on component part failure rates, assume that all parts in a population are equally bad, while actual experience shows that failures are most often caused by individually defective parts. Parts representative of the true capabilities of a reliable design may actually exhibit zero failure rates. Therefore, the major portion of the reliability effort is directed toward identifying, controlling and eliminating defective parts and system failure modes critical to mission success. By locating and correcting design weaknesses during development, fabrication and testing, it is expected that the probability of success will be significantly greater than what can be predicted by conventional reliability statistics.

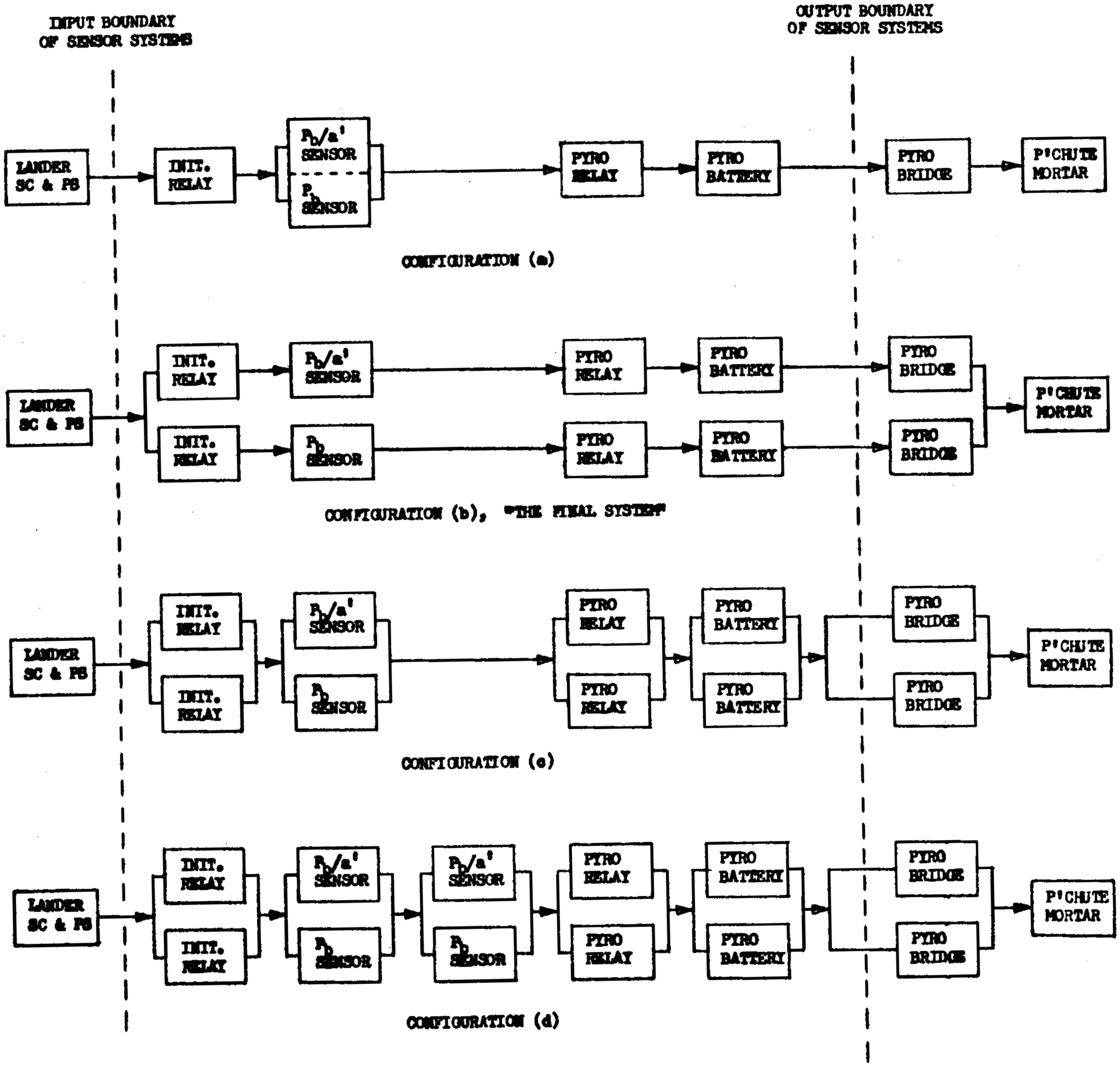

FIGURE 20, FOUR SENSOR SYSTEM CONFIGURATIONS FEATURING AT LEAST ONE EACH OF: AN INITIATING RELAY, BOTH A P_b/a' SENSOR AND A P_b SENSOR, A PYRO RELAY, AND A PYRO BATTERY

The design-oriented reliability work described herein is based on the following definitions:

(a) A subsystem is a major functioning entity and consists of the following components: initiating relay, environmental sensor, pyro relay and pyro battery.

(b) A system is the total end-item sensor configuration. It consists of one or more subsystems and employs a minimum of two environmental sensor components (one base pressure sensor and one base pressure to acceleration ratio sensor).

The following considerations are based on the reliability block diagrams presented in Figure 20.

5.3.1 REDUNDANCY CONSIDERATIONS

A sensor system utilizing series component redundancy as shown below increases the probability of late deployment (or no deployment). Failure of a sensor component to provide the trigger signal for parachute deployment may be overcome by a trigger signal from a parallel component. Parallel redundancy however, increases the probability of a premature trigger signal. Component failure resulting in a premature trigger signal (and premature parachute deployment) cannot be overcome by a "back-up" component or subsystem. Thus, the application of a parallel "back-up" component may fail to improve system reliability; multiple parallel redundancy eventually degrades system reliability.

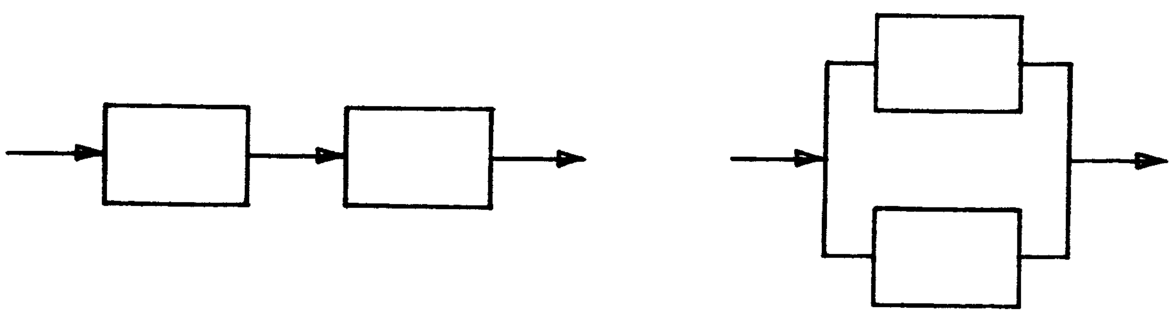

(a) Series Redundancy (protects against premature operation)

(b) Parallel Redundancy (protects against late operation)

FIGURE 21, THREE MODES OF REDUNDANCY

The use of parallel and/or series redundancy to improve reliability in any given application depends on the predominant component failure modes. Preliminary analysis of the environmental sensing components under consideration does not indicate a significant tendency for either "open" or "short" failures. Under these conditions, four sensor components in series-parallel (as shown below and in Figure 20d) provides optimum reliability. The use of a crossover (as shown) depends somewhat on the predominant failure mode.

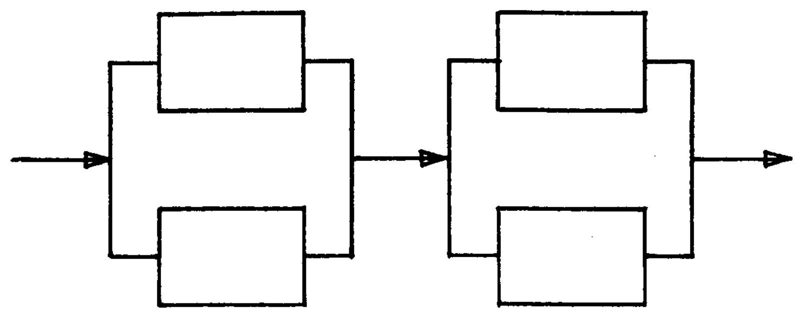

FIGURE 21 CONCLUDED, (c) Series-Parallel Redundancy (protects against both premature and late operation)

The following example illustrates these redundancy consideration where there are two modes of component failures with

f_s = probability of premature operation (short)

f_o = probability of no operation (open)

For the series redundant configuration, the probability of failure by premature operation is

$$F_s = f_s^2$$

and the probability of no operation is

$$F_o = 1 - (1 - f_o)^2$$

Assuming, for example, that $f_s = f_o = 0.001$, then

$$F_s = 0.000001$$

$$F_o = 0.002$$

The series arrangement, while greatly decreasing the probability of premature operation, doubles the probability of no operation.

When the two components are arranged in parallel, the situation is reversed:

$$F_s = 1 - (1 - f_s)^2$$

$$F_o = f_o^2$$

For the series-parallel arrangement of four components, the probabilities of premature and no operation failures are given by:

$$F_s = \left[1 - (1 - f_s)^2 \right]^2$$

$$F_o = 1 - (1 - f_o^2)^2$$

Assume again, that $f_s = f_o = 0.001$. Then, for a single component, the total probability of failure is

$$f_s + f_o = 0.002,$$

while for the series-parallel arrangement of four components the total probability of failure is

$$F_s + F_o = 0.000006.$$

These outstanding variations in "component system" reliability are illustrated in Table 26.

The preceding examples of redundancy may be applied to any of the components in this system. Parallel redundancy is recommended where the predominant failure mode is "failure-to-operate", e.g., pyro batteries. Quadrature redundancy is particularly applicable to the environmental sensor components, where less reliability data is available and where the predominant failure modes may be difficult to determine. The feasibility of quadrature component redundancy for this application appears realistic in view of the small weight and volume of the parts involved, particularly if solid state circuits are used. The use of redundancy in this manner allows the inherent weakness of one sensing technique to be off-set by strengths in another. These strengths and weaknesses can be exposed as analysis, design, and evaluation proceeds.

5.3.2 SYSTEM DESIGN

The functional block diagrams shown in Figure 20 illustrate four possible system configurations--all based on the use of the circuit designs previously discussed in Section 5.2. These four system configurations represent a sequential increase in system reliability (and system weight) from (a) thru (d). Configuration (b) is the Final System, as presented in the previous section of this report. It provides

TABLE 26, SYSTEM RELIABILITY AS A FUNCTION OF COMPONENT CONFIGURATION

CONFIG.	RELIABILITY BLOCK DIAGRAM AND MATH. MODEL FOR ENVIRONMENTAL SENSOR	NUMERICAL EXAMPLE (WHERE $f_s = f_o \cong 0.001$)			
		PROBABILITY OF PREMATURE OPERATION (F_s)	PROBABILITY OF NO OPERATION (F_o)	TOTAL PROBABILITY OF FAILURE ($F=f_s+f_o$)	RELIABILITY ($1-F$)
1.	 $F_s = f_s$, $F_o = f_o$	0.001	0.001	0.002	0.998
2.	 $F_s = f_s^2$, $F_o=1-(1-f_o)^2$	0.000001	0.002	0.002001	0.998
3.	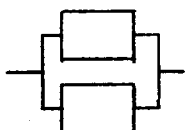 $F_s=1-(1-f_s)^2$, $F_o = f_o^2$	0.002	0.000001	0.002001	0.998
4.	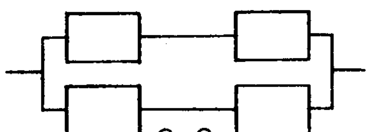 $F_s=1-(1-f_s^2)^2$, $F_o=[1-(1-f_o)^2]^2$	0.000002	0.000004	0.000006	0.999994
5.	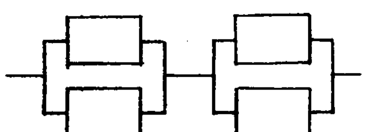 $F_s=[1-(1-f_s)^2]^2$, $F_o=1-(1-f_o^2)^2$	0.000004	0.000002	0.000006	0.999994

fully redundant and independent functional subsystems. The estimated weight for this configuration is 110 oz (6.9 lb).

Configuration (a) is the minimum system that still embodies both the Base Pressure to Acceleration Ratio and the Base Pressure type concepts. Now, however, only one prime sensor of each type is used and all other components are reduced in number to the absolute minimum. The estimated weight for this system is 60 oz (3.75 lb).

Configuration (c) employs essentially the same components as the Final System, but it features crossovers at four points and has improved reliability since alternate paths are provided for each component function. (This is based on a preliminary analysis assumption that the components involved have a predominant "failure-to-operate" tendency.) The estimated weight of Configuration (c) is 116 oz (7.25 lb).

Configuration (d) illustrates how still more reliability can be achieved. In this configuration, protection is provided against both premature and late operation. This is accomplished by introducing a series-parallel arrangement of sensor element components as discussed in the preceding subsection. The estimated weight for this configuration is 197 oz (12.3 lb).

Figure 21 shows a crossover circuit for pyrotechnic initiation. The principle illustrated in this figure is fairly typical. This crossover incorporates the following advantageous features:

(a) All pyrotechnic contacts are shorted prior to initiation.

(b) A signal from either sensor activates both relays (and both pyrotechnic bridges).

(c) Failure of one relay, one battery or one pyrotechnic bridge does not result in a system failure.

5.3.3 FAILURE MODE AND EFFECTS ANALYSIS

The anticipated environmental conditions and functional performance requirements were used as the basis for a preliminary Failure Mode and Effects Analysis. In this analysis, it was attempted to ascertain the reliability advantages and disadvantages for the various system configurations shown

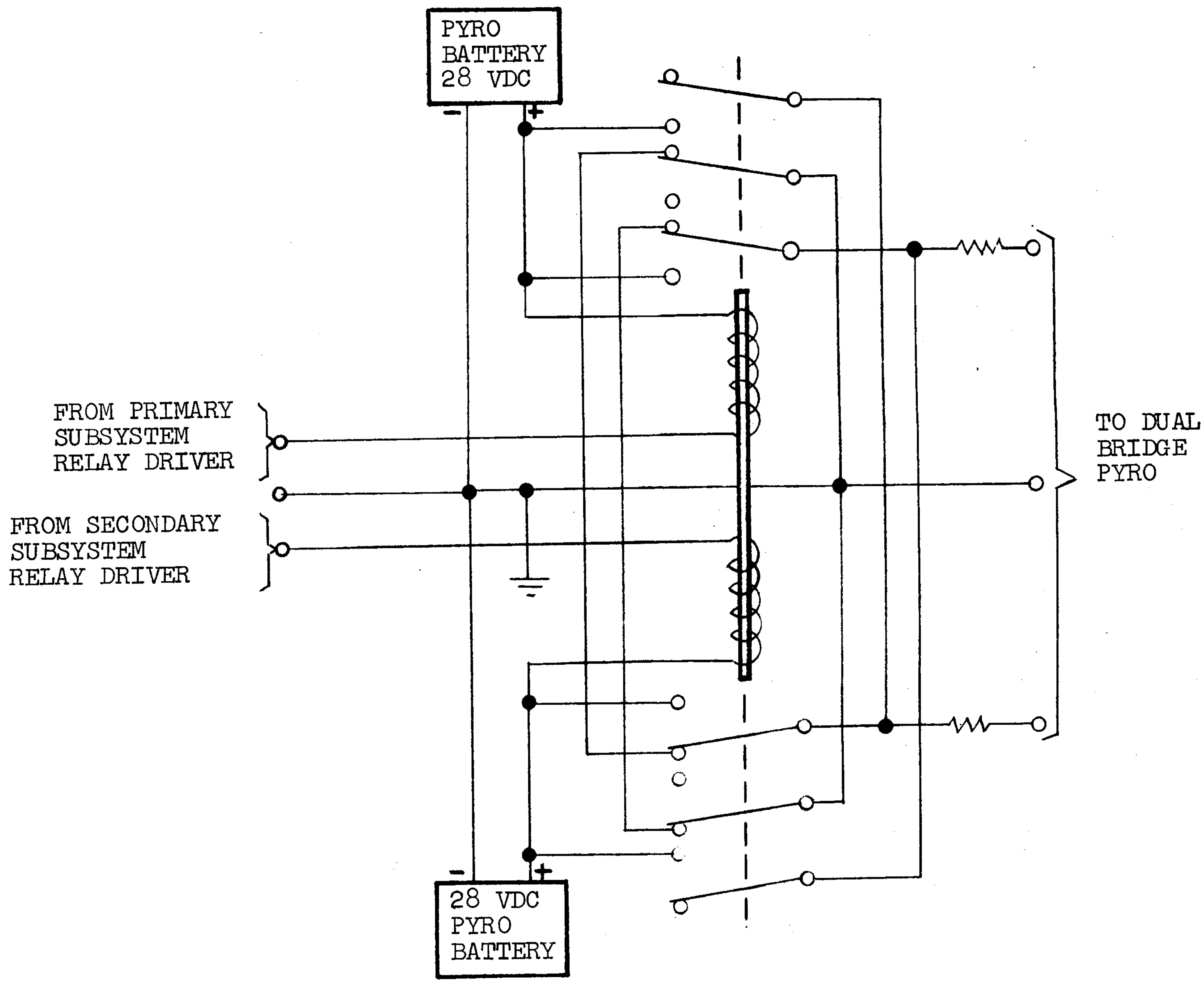

FIGURE 22, TYPICAL CROSSOVER NETWORK FOR PYROTECHNIC INITIATION in Figure 20. The results of this analysis are summarized in Table 27. This table presents the following information:

(a) potential subsystem failure modes

(b) probable causes for each of the failure modes

(c) the effect of these failures on subsystem and system performances

(d) techniques used to overcome each potential failure mode

(e) the system configurations (Figure 20) which employ each of the given corrective techniques

This information identifies the important reliability advantages and disadvantages of the various system configurations.

5.3.4 RELIABILITY RECOMMENDATIONS

The reliability concepts described herein can aid design personnel in developing a sensor system with a high degree of inherent reliability. In addition, it provides data for future trade-off studies based on weight, reliability, performance, and other criteria. Final selection of a system configuration depends upon these trade-offs which involve overall mission requirements yet undefined.

Component part application for this program should be based on the use of design techniques to retain and enhance the high inherent reliability of the components selected. These design techniques should include component derating, redundancy and environmental protection. Parts required but not listed in References 20 and 21 should be selected for their ability to meet the functional and environmental system requirements based on test data and previous use in similar applications. Techniques should be employed to evaluate potential component vendors and to maintain cognizance over subcontractor design, manufacturing and testing procedures.

Reliability work on the next phase of development should include:

(a) Component Engineering - To evaluate light-weight parts and assist with component application.

TABLE 27, SUMMARY OF FAILURE MODE AND EFFECTS ANALYSIS

No.	Failure Mode	Probable Cause	Functional Effect	Corrected By	Config.
1.	Activating relay fails to operate on signal from lander sequence controller.	Damage to coil or contacts by vibration or shock. High contact resistance.	Failure to provide power to sensor subsystem - with resultant failure to provide trigger and pyro signal.	Parallel redundant subsystems. Parallel redundant relays.	b c,d
2.	Environmental sensor operates prematurely.	a. P_b/a' amplifier drift during early system operation when both acceleration and base pressure are zero. b. Accelerometer or pressure transducer failure.	a. Premature trigger signal-possible system failure. b. Premature trigger signal-possible system failure.	a. Arming circuit-using base pressure sensor b. Series redundant sensors.	a,b,c,d d
3.	Environmental sensor fails to operate (or operates late).	Accelerometer or pressure transducer failure.	Failure to provide trigger/pyro signal.	Parallel redundant environmental sensors Parallel redundant subsystems.	a,c,d b
4.	Pyro relay operates prematurely.	Contact closure due to vibration or shock during lander launch from Mars vehicle.	Premature trigger/pyro signal.	Careful relay selection and testing. Relay mounting with sensitive axis opposed to direction of shock.	a,b,c,d
5.	Pyro relay fails to operate on signal from sensor circuit.	Damage to coil or contacts by vibration or shock.	Failure to provide trigger/pyro signal.	Parallel redundant subsystems. Parallel redundant relays.	b c,d
6.	Pyro battery fails	Deterioration resulting from environmental exposure.	Failure to provide pyro power.	Parallel redundant subsystems. Parallel redundant batteries.	b c,d

(b) Testing - To evaluate component/system reliability as a basis for reliability estimates and design improvements.

(c) Failure Analysis and Corrective Action - To identify, control and eliminate failure mechanisms critical to mission success.

6.0 CONCLUSIONS

The following conclusions are presented, based on the results of this study.

1) This study, encompassing an analysis of sensor systems suitable for initiating parachute deployment on a Mars entry vehicle, shows conclusively that today's technology and hardware can provide a sensor system with sufficient flexibility to assure accurate sensing over the wide range of possible Martian atmospheres, entry conditions, and environmental conditions currently postulated for the mission.

2) A variety of sensor systems are feasible. Of the many sensor concepts analyzed in Phase 1 of the study, sixteen are suitable in various degrees. In general, sensor systems employing an accelerometer seem to have the most satisfactory performance over the ranges of deployment conditions and entry modes studied.

3) Of the four feasible sensor systems selected for more detailed analysis in Phase 2 of the study, two employ an accelerometer, one employs a base pressure transducer, and one employs both an accelerometer and a base pressure transducer. A trade study of these two types of prime sensors indicates that a strain gauge accelerometer and a capacitive pressure transducer are the most satisfactory in this application. A matrix established for evaluation of the four sensor systems revealed that all four would be suitable for development within the specified guide lines.

4) The Final System, selected for detailed analysis and design in Phase 3 of the study, features two sensor subsystems operating in parallel: a sensor subsystem utilizing the ratio of base pressure to sensed acceleration, and a sensor subsystem utilizing base pressure by itself. This system represents the most promising deployment prediction capability.

5) The performance analysis of the Final System is based on the requirement that parachute deployment should be initiated at or below (but not above) the specified Mach number $M = 1.0$. The altitude at which this Mach number occurs can be expressed rather accurately as a simple function of eight variables. These eight variables are: the atmosphere model, entry velocity, entry flight path angle, entry azimuth angle, entry angle of attack, entry rolling velocity, maximum wind profile and vehicle drag coefficient. The altitudes at which the Final System's two sensor subsystems trigger parachute deployment can be expressed similarly but require the inclusion of terms for two additional variables; the subsystems' operational errors, and the base pressure coefficient errors.

6) The largest deployment altitude-uncertainty component is due to the atmospheric-properties-uncertainty range, exemplified by Mars model atmospheres VM-3 and VM-8. This amounts to approximately $\pm$ 25,000 feet of altitude uncertainty. The next largest altitude-uncertainty components (maximum wind profile, environment effects and entry flight path angle) are approximately an order of magnitude smaller.

7) The design of the Final System employs existing components conservatively. Short operating times and component derating minimize the common problem of wear-out failures. These factors provide a system with high inherent reliability.

8) Additional reliability improvement can be obtained by adding more redundancy and crossover networks. These improvements may be incorporated as additional data on mission requirements and failure modes become available.

7.0 RECOMMENDATIONS

Based on the results of this study, the following recommendations are presented:

1) The performance analysis, as developed in Phase 3 of the study, should be carried to completion. This analysis approach should also be used to substantiate the results obtained with the somewhat less complete approach used in Phase 2 of the study.

2) The results presented in this report should be used as the basis for additional development effort. This additional effort should consist of: a more detailed design analysis, additional component trade studies, tests to evaluate both components and complete subsystems in order to provide a basis for additional reliability analysis and design improvements, and a more detailed failure mode and effects study to identify and eliminate potential problems critical to mission success.

3) At an early date, the results of the two preceding recommendations should be combined; and the development and qualification of the two subsystems of the Final System should be undertaken.

REFERENCES

1. Stone, Irving, "Atmosphere Data to Alter Voyager Design," Space Technology International, Vol. 9, No. 1, Jan. 1966 (pp 36-38)

2. Seiff, Alvin and David E. Reese, Jr., "Defining Mars' Atmosphere -- A Goal for the Early Missions," Astronautics and Aeronautics, Vol. 3, No. 2, Feb. 1965 (pp 16-21)

3. Krase, W. H., "Mars Environmental Measurements in Support of Future Manned Landing Expeditions," Rand Corporation Memorandum RM-4437-NASA, April 1965

4. Kiely, John R. (editor), "SAMPLER: Standford Advanced Mars Project for Life Detection, Exploration and Research," Stanford University Engineering Department Report, June 1965

5. Peterson, Victor L., "Analysis of the Errors Associated with the Determination of Planetary Atmosphere Structure from Measured Accelerations of an Entry Vehicle," NASA TN R-225, July 1965

6. Beuf, F.G., G.D. Katz and R.J. Kern, "Earth Entry Flight Test of Mars Entry Vehicles, "Journal of Spacecraft and Rockets, Vol. 3., No. 2, April 1966 (pp 498-503)

7. Ranftl, J.W., "Use of Radiation Gauging Methods to Measure Atmospheric Density During Martian Entry," Rand Corporation Memorandum RM-4434-NASA

8. Cato, Glenn, "Measurement of Free Air Properties from Onboard a Large Launch Vehicle," AIAA Paper No. 64-326, (Presented at the 1st AIAA Annual Meeting at Washington, D.C., June 29 - July 1964)

9. Boobar, M.G. and B.A. McElhoe, "Indirect Speed Measurement for Planetary Entry," AIAA Journal, Vol. 3., No. 8, August 1965 (pp 1527-9)

10. Worth, R.N., "The Voyager Descent System, Parametric Analyses and Development Status Report," Northrop Ventura Report 3946, Sept. 1965

11. Duncan, Robert Clifton, Dynamics of Atmospheric Entry, McGraw-Hill Book Co., New York, 1962 (pp 47-48)

12. Chapman, Dean, "An Analysis of Base Pressure at Supersonic Velocities and Comparison with Experiments," NASA Report 1051, May 1950

13. Cubbage, James M., Jr., "Jet Effects on Base and Afterbody Pressures of a Cylindrical Afterbody at Transonic Speeds," NACA RM L56C21, May 1956

14. Spahr, J. Richard and Robert R. Dickey, "Effect of Tail Surfaces on the Base Pressure of a Body of Revolution at Mach Numbers of 1.5 and 2.0," NACA TN 2360, 1951

15. Reller, John O. Jr., and Frank M. Hamaker, "An Experimental Investigation of the Base Pressure Characteristics of Non-Lifting Bodies of Revolution at Mach Numbers from 2.73 to 4.98," NACA TN 3393, March 1955

16. Love, Eugene S., "Base Pressure at Supersonic Speeds on Two-Dimensional Airfoils and on Bodies of Revolution with and Without Fins Having Turbulent Boundary Layers," NACA TN 3819, Jan. 1957

17. McFall, John C. Jr., "Drag Measurements of a Reentry Body with Rocket-Boosted Models in Free Flight at Mach Numbers from 2.8 to 0.6," NASA TM X-1, August 1959

18. ----, "Monthly Progress Report No. 3, 10 February - 10 March 1966," NVT/66-38, 10 March 1966

19. ----, "Monthly Progress Report No. 4, 10 March - 25 April 1966," NVT/66-51, 25 April 1966

20. Visser, J., "Electronic Part Sterilization Candidates for Spacecraft Applications," JPL Spec. ZPP-2010-SPL-B, 1 December 1965

21. Visser, J., "JPL Preferred Parts List," JPL Spec ZPP-2061-PPL-G, 1 July 1965

APPENDIX A

NOMENCLATURE

SYMBOLS

A	$= \frac{1}{4}\pi D^2$	Reference area equal to entry vehicle's base area, ft^2
$\underline{a}$		Acceleration with respect to inertial space, ft/sec^2
a'	$= \lvert \underline{a}-\underline{G} \rvert$	Magnitude of sensed acceleration (the quantity that is measured by an accelerometer), ft/sec^2
a'_X		Magnitude of sensed acceleration component in X axis direction, ft/sec^2
Atm		Generalized variable representing the effect of changing from one Mars model atmosphere to another
C_A, C_N, C_Y		Axial, normal and side force coefficients
C_ℓ, C_m, C_n		Rolling, pitching and yawing moment coefficients
C_{ℓ_p}, C_{m_q}, C_{n_r}		Damping derivatives (dimensionless)
C_D		Generalized variable representing the effect of changing the level of the entry vehicle's force coefficients
C_{P_b}		Entry vehicle's base pressure coefficient
D		Entry vehicle's reference dimension equal to base diameter, ft
E		Entry point (arbitrarily defined as the point in trajectory having an altitude of 805,000 ft)
Env		Generalized variable representing sensor system operational errors due (primarily) to preoperational and operational environmental conditioning
ETO		Ethylene oxide
F_o		Series/parallel configuration probability of late or no operation (open type failure)

F_s	Series/parallel configuration probability of premature operation (short type failure)
F.S.	Full scale
f	Frequency, CPS
f_o	Component probability of late or no operation (open type failure)
f_s	Component probability of premature operation (short type failure)
G	Gravitational specific force, ft/sec^2
"g"	Unit of acceleration equal to 32.2 ft/sec^2
$\underline{H}$	Altitude column vector equal to $(h_1\ h_2\ \ldots)'$, see Subsection 4.3
h	Altitude, ft
$\underline{K}$	Independent variable column vector equal to $(ATM\ V_E\ \ldots)'$, see Subsection 4.3
M	Free stream Mach number
m	Entry vehicle mass, SLUGS
P	Pressure, lb/ft^2
P_{S_2}	Stagnation pressure aft of shock, lb/ft^2
p, q, r	Rolling, pitching and yawing velocities, rad/sec
R	Radius of curvature, ft
t	Time, sec
V	Velocity, ft/sec
V_A	Aerodynamic velocity (w/t local "air), ft/sec
VM	Voyager-Mars atmosphere model
w/t	With respect to
Wind	Generalized variable representing the effect of wind

X, Y, Z	Entry vehicle body axes
ΔX_N	Distance aft of nose to center of pressure, ft
α, β	Angle of attack and angle of sideslip
γ	Flight path angle, deg (or specific heat ratio)
γ_E and γ_{IE}	Entry flight path angle (w/t inertial space), deg
η	Total angle of attack, deg (see page 10)
Λ	Latitude, deg
λ	Longitude, deg
ρ	Density, slugs/ft^3
χ	Azimuth angle, deg
ω	Planet rate of rotation, rad/sec

SUBSCRIPTS

A	Aerodynamic; i.e., w/t the local "air"
ACT	Actual
AV, -8, HI, -20	See definitions in Table 9
b	Base
c.p.	Center of pressure
dep	Deployment initiation
E	Entry Point E
F.S.	Full scale
I	Inertial (also ideal)
IND	Indicated
i	System/Subsystem number
max	Maximum
min	Minimum

O	Null
o	Free stream
P	Preset
S	Specified
s	Shear
T	Trigger
w	Wind
X	X body axis

NOTE: Underlined symbols are vector quantities

Northrop Corporation, Ventura Division

JPL Contract No. 951174

RE-ORDER No. 66-418

NVR 4062 Errata Sheet

1) Page 2: The equation should read

$$\frac{a_{dep}}{a_{max}} = -2e \left(\frac{V_{dep}}{V_E}\right)^2 \log_e \left(\frac{V_{dep}}{V_E}\right)$$

2) Page 10, footnote: The equation should read

$$\eta = \arccos(\cos\alpha \cos\beta)$$

3) Page 36, Equation (2), **second line**

$$\frac{\partial h_T}{\partial P_E} \Delta P_E \text{ should be } \frac{\partial h_T}{\partial p_E} \Delta p_E$$

4) Page 39, Equation (3), **first line**

same correction as 3)

5) Page 46, The last entry into the "Altitude Reduction" column:

9,700 should be 9,900

6) Page 48, First column of table: The symbols "X_E" and p_E should be interchanged.

7) Page 57, Equation (6), **first line**

$$\frac{\partial h_T}{\partial X_E} \Delta\alpha_E \text{ should be } \frac{\partial h_T}{\partial \alpha_E} \Delta\alpha_E$$

8) Page 58, Table 19, second equation:

$$\frac{\partial h_T}{\partial P_E} \Delta P_E \text{ should be } \frac{\partial h_T}{\partial p_E} \Delta p_E$$

Page 58, Table 19, fifth equation: Add the word "errors" to the subscript on the last symbol.

9) Pages 2, 10, 36, 39, 46, 48, 57, and 58 were also changed to reflect improvements in textual construction and when supplied reflect the changes listed in paragraphs 1) through 8) above.

10). Pages 9, 30, 35, 37, 47, 54, and 93 when supplied reflect improvements in textual construction and presentation only.

AUG 8 1966

A number of ideas have been presented in prior literature on how to measure various flight and atmospheric conditions from onboard an entry vehicle while it is descending through the Martian atmosphere. Some of these are:

a) The velocity and altitude can be obtained by integrating data from accelerometers (2) - (6). During the terminal portion of the descent, such a scheme can be augmented by a more direct measurement method employing the ratio of two vehicle surface pressures.

b) Density can be measured directly by a back-scattering technique (7) or computed with the aid of accelerometer data (2) - (6).

c) During the terminal descent phase, both ambient and stagnation pressures and temperatures can be measured by sensors located judiciously on the surface of the entry vehicle.

Also of interest in regard to making measurements from onboard a vehicle while traveling at supersonic speed, although not concerned with Martian entry, is Reference 8.

At least two previous studies have dealt with the central question considered in this report: What is the best method, in a Mars entry vehicle, to sense the flight condition at which parachute deployment should be initiated? Boobar and McElhoe (9) analytically derived the following expression to show how a simple accelerometer, aligned with the longitudinal axis of a non-lifting entry vehicle, could be used for this purpose:

$$\frac{a_{dep}}{a_{max}} = -2e\left(\frac{V_{dep}}{V_E}\right)^2 \log_e\left(\frac{V_{dep}}{V_E}\right)^{*}$$

The quantities a and V are for acceleration and velocity respectively; the subscripts dep, max, and E stand for deployment initiation, maximum and initial entry respectively. Foreknowledge of the velocity ratio (V_{dep}/V_E) permits the right hand side of this equation to be evaluated prior to entry. Thus, it is seen that the deployment initiation condition occurs when the acceleration is equal to a predetermined

* This equation provides the analytic basis utilized as the principle of operation for the Acceleration Function System (9).

TABLE 1b, SUMMARY OF TRAJECTORY DATA AT M = 1.0

RUN	TIME FROM ENTRY PT	ALTITUDE	VELOCITY (AERO)	FL. PATH ANGLE (AERO)	ACCELER-ATION (SENS)	DYNAMIC PRESS.	STAGNA-TION PRESS.	PITCH ANGLE AMP.	PRESS. (AMB)	DENSITY (AMB)	TEMPERA-TURE (AMB)	MACH NUMBER (ACTUAL)
	t	h	V_A	γ_A	a'	q	P_{s2}	$\bar{\eta}$	P	$\rho \times 10^6$	T	M
	(sec)	(ft)	(fps)	(deg)	(fpss)	(psf)	(psf)	(Deg)	(psf)	(scf)	(°R)	-
TYPICAL ORBITAL TRAJECTORIES, ALL SIX MODEL ATMOSPHERES												
44	315.463	72,452	890.25	- 47.75	16.665	3.7305	10.34	± 3.5	5.50	9.0	360	1.0004
43	321.296	57,134	911.27	- 46.66	16.303	3.6444	9.66	± 3.5	5.30	8.0	373	1.0055
45	327.698	42,111	948.96	- 46.07	15.654	3.4065	9.40	+ 3.6	5.00	7.8	405	1.0052
42	303.163	40,810	620.03	- 43.88	15.028	3.3872	8.79	+ 3.2	4.80	18.0	228	1.0039
40	311.382	31,666	645.87	- 45.88	14.752	3.3252	9.18	+ 3.6	4.90	16.0	265	1.0054
41	317.666	23,374	679.54	- 45.91	14.782	3.3262	9.18	+ 3.2	4.90	14.4	291	1.0123
60	349.119	71,528	899.04	- 47.22	17.378	3.8803	10.53	± 3.3	5.60	10.0	360	1.0103
59	355.126	55,170	911.18	- 46.53	16.759	3.7518	10.44	+ 3.3	5.50	9.0	377	[illegible]
61	360.278	39,933	952.79	- 46.03	16.124	3.6355	9.96	+ 3.[illegible]	5.30	8.0	410	1.0035
56	332.336	39,359	627.43	- 42.11	16.103	3.6316	9.93	+ 3.7	5.20	18.5	233	1.0057
56	338.884	30,422	656.75	- 43.40	16.016	3.5690	9.55	+ 3.8	5.10	16.7	270	1.0153
57	345.559	21,252	680.27	- 44.45	15.779	3.5302	9.74	+ 3.9	5.20	15.5	298	1.0027
TYPICAL HYPERBOLIC ENTRY TRAJECTORIES												
55	211.625	71,089	892.57	- 43.19	17.051	3.8115	10.53	+ 3.5	5.60	[illegible]	360	1.0036
53	185.426	39,606	622.49	- 39.57	15.720	3.5471	9.55	± 3.4	5.00	1.67	232	.9995
54	200.904	21,756	676.55	- 42.05	15.397	3.4447	9.74	+ 3.5	5.20	1.50	295	.9997
52	77.101	19,677	706.70	- 46.20	35.735	7.0759	[illegible]	+ 3.6	11.30	31.5	295	1.0000
51	IMPACT	AT MACH	1.10 -	- - - -	- - - -	- - - -	- - - -	- - - -	- - - -	- - - -	- - - -	- - - -
THE EIGHT "CORNER RUNS"												
60	349.119	71.528	899.04	- 47.22	17.378	3.8803	10.53	± 3.3	5.60	10.0	360	1.0103
70	244.749	65,662	894.88	- 45.07	19.508	4.3579	12.03	+ 3.3	6.40	11.2	360	1.0056
72	399.374	72,677	890.09	- 51.20	16.453	3.7113	10.34	± 3.5	5.50	9.6	360	1.0003
78	231.121	66,302	890.75	- 43.96	18.105	4.0809	11.26	+ 3.3	6.00	10.5	360	1.0010
57	345.559	21,252	680.27	- 44.45	15.779	3.5302	9.74	+ 3.9	5.20	15.5	298	1.0027
69	234.404	16,049	696.05	- 41.89	18.795	4.2447	11.61	+ 4.2	6.20	17.5	313	1.0017
77	532.454	22,519	676.79	- 52.26	15.110	3.3770	9.18	± 3.4	4.90	14.7	294	1.0039
71	218.668	18,876	691.66	- 40.82	17.406	3.8864	10.49	± 3.9	5.60	16.4	305	1.0076
ENTRY ROLL VELOCITY P_E = 1 RAD/SEC												
24	317.000	69,660	892.97	- 47.95	16.811	3.9840	11.09	±15.2	5.90	10.3	360	1.0035
20	320.056	21,521	676.59	- 47.27	14.770	3.4876	9.55	+14.6	5.10	15.5	296	1.0015
ENTRY ANGLE OF ATTACK, α_E = -5 AND -105 DEG												
74	349.778	71,293	893.39	- 47.66	17.232	3.8510	10.62	± 1.2	5.65	10.0	360	1.0040
75	218.350	19,163	694.03	- 40.52	17.377	3.8835	10.40	± 0.9	5.60	16.2	304	1.0125
73	349.086	71,260	898.99	- 47.20	17.234	3.9021	10.62	+ 6.2	5.65	10.0	360	1.0103
76	218.818	18,505	691.65	- 40.78	17.210	3.9239	10.58	+ 6.7	5.65	16.5	305	1.0058
ENTRY ANGLE OF AZIMUTH, χ_E = -90 DEG (RETROGRADE ENTRY)												
79	351.708	71,243	898.55	- 46.02	17.343	3.8998	10.72	± 3.2	5.70	10.0	360	1.0065
80	221.331	19,157	685.60	- 41.70	16.818	3.7904	10.49	± 3.1	5.60	16.5	304	1.0002
WIND ONSET INSTANTANEOUS WITH CONSTANT WIND VELOCITY TO SURFACE												
81	243.970	11,726	702.81	- 38.92	21.409	4.8087	13.30	+13.2	7.10	19.5	325	.9901
82	408.770	66,263	892.11	- 48.96	18.742	4.2758	11.56	+ 9.8	6.15	11.0	360	1.0025
83	399.070	72,905	894.18	- 51.12	16.610	3.7272	10.04	± 3.6	5.34	9.5	360	1.0046
84	235.289	15,913	690.35	- 42.23	18.456	4.1790	11.61	+ 4.2	6.20	17.5	314	.9916
LANDER VEHICLE C_A AND C_N VARIATION = + 3% (NOMINAL)												
85	345.787	75,489	938.53	- 46.50	18.141	3.8857	9.59	+ 4.0	5.10	9.0	360	1.0547
86	218.987	17,144	685.92	- 40.83	17.293	3.9975	11.24	+ 3.2	6.00	17.2	310	.9910
EXTREME CASES												
94	235.470	13,575	704.07	- 42.39	18.850	4.8103	12.55	+19.7	6.70	18.5	320	1.0003
95	238.170	14,805	697.98	- 42.54	18.235	4.3934	12.10	+17.4	6.46	18.0	316	.9973
96	395.131	71,836	887.89	- 51.79	16.797	3.7598	10.30	± 0.9	5.48	9.60	360	.9978
97	399.170	72,938	890.06	- 51.23	16.472	3.6903	10.04	+ 0.6	5.34	9.50	360	1.0602

AUG 8 1969

2.2 THE LANDER VEHICLE

The shape of the lander vehicle is that of a blunt cone with rounded shoulders and a flat base. A side view of the lander vehicle is shown in Figure 2. The lander vehicle is symmetrical about its longitudinal axis, both geometrically and with respect to its mass distribution. The moment center is located one quarter of a diameter aft of the nose.

The mass of the lander vehicle is assumed to be a constant 31.677 slugs (the mass loss due to ablation is negligible). Its moments of inertia about the X, Y and Z axes are 300, 270 and 270 slug-ft^2, respectively and the products of inertia are zero. The base diameter (reference dimension) is taken to be $D = 12$ ft.

The lander vehicle's static aerodynamic characteristics were specified in the computer program by three two-dimensional tables organized as follows:

$$C_A = F_1 (M,\alpha) \qquad M = 0.3,\ 0.5,\ ..\ ,\ 50.0$$
$$C_N = F_2 (M,\alpha) \qquad \alpha = 0,\ 10,\ ..\ ,\ 180 \text{ deg}$$
$$\Delta X_N/D = F_3 (M,\alpha)$$

where $\Delta X_N/D = (X_{nose} - X_{c.p.})/D$. The quantities X_{nose} and $X_{c.p.}$ are the distances along the X axis at which the nose of the vehicle and the center of pressure occur. (All values in this table were for an angle of sideslip $\beta = 0$.) For values of M and α not in the table, a linear interpolation was made.

Plots prepared from the aerodynamic tables are presented in Figures 3, 4 and 5. Figure 3 presents axial force coefficient C_A (positive in the $-X$ direction) versus Mach number for seven values of total angle of attack η from 0 to 180 degrees.* Figure 4 presents normal force coefficient C_N (positive in the $-Z$ direction) versus Mach number for seven values of angle of attack α from 0 to 180 degrees. Figure 5 presents similar curves for the center of pressure location C_m/C_N. This is, in effect, the position (in units of D) at

---

* The total angle of attack η is the resultant angle associated with α and β. In the strictest sense, it is computed with the relation

$$\eta = \arccos (\cos \alpha \cos \beta)$$

by the Stagnation to Base Pressure System (I). The Stagnation Pressure and Timer System (V) and the Stagnation Pressure to Acceleration Ratio System (T) yield approximately the same performance. The use of a preset acceleration value as in the Acceleration System (N) gives comparable results at the low altitude end but has poorer performance as the Mach number 1.0 altitude increases in the denser atmosphere models. Some improvement is obtained by computing the acceleration level as in the Acceleration Function System (O) or the Acceleration Matrix Fit System (B). It is interesting to note that the Altimeter and Timer System (C) and the Stagnation Pressure and Timer System (V) are feasible for the orbital entry, specified Mach number 1.0 conditions only.

For orbital entry and Mach number 2.5 specified, the best performance across the board is provided by the Acceleration System (N), the Stagnation to Base Pressure Ratio System (I), the Inertial Path Angle System (F), and the Base Pressure to Acceleration Ratio System (J). Showing somewhat less performance are the Stagnation Pressure System (U) and the Base Pressure System (R).

For orbital entry and Mach number 5.0 specified, the best performance across the board is provided by the Acceleration Function System (O) followed closely by the Acceleration System (N). Next, with significantly less performance, are the Time after Maximum Acceleration System (P), the Towed Body System (H), the Stagnation to Base Pressure Ratio System (I), and the Base Pressure to Acceleration Ratio System (J).

For hyperbolic entry, deployment could be accomplished at the Mach numbers of 2.5 and 5.0 for all entry conditions. Deployment at a Mach number of 1.0 is not considered feasible since this condition does not occur above 1000 ft in Run 51. The best performing systems for the hyperbolic entry mode are the Time Function of Maximum Acceleration System (Q), the Base Pressure to Acceleration Ratio System (J), and the Stagnation to Base Pressure Ratio System (I). Next, with somewhat less performance, are the Acceleration System (N), the Towed Body System (H), and the Acceleration Function System (O).

Comparison of all sixteen systems across the board for suitability of all Mach numbers and entry modes shows the Stagnation to Base Pressure Ratio System (I) and the Base Pressure to Acceleration on Ratio System (J) to have the smallest altitude errors. The Acceleration Function System (O) also gives rather good performance across the board.

It appears that sensor systems employing an accelerometer generally have the most satisfactory performance over the ranges of deployment conditions and entry modes studied.

4.0 CANDIDATE SYSTEMS STUDY (PHASE 2)

The performance results obtained in the Feasible Systems Study were combined with other considerations preparatory to deciding on the specific sensor configurations to be analyzed in Phase 2 of the study. These other considerations included reliability and development risk factors. On this basis, three configurations of sensor systems were selected and approved by JPL. Each was selected to consist of two independent subsystems acting in parallel; i.e., each candidate system comprises two sensor subsystems. For convenience sake, these subsystems are identified as primary and secondary, although in reality, they act in parallel. The three candidate systems are as follows:

Candidate System Number	Primary Subsystem	Secondary Subsystem
1	Acceleration (Feasible System N)	Base Pressure (Feasible System R)
2	Base Pressure To Acceleration Ratio (Feasible System J)	Base Pressure (Feasible System R)
3	Acceleration Function (Feasible System O)	Base Pressure (Feasible System R)

It may be noted that each candidate system uses the same two types of prime sensors: an accelerometer and a base pressure sensor.

At this point in the study, the specified Mach number for initiating parachute deployment was restricted to the one Mach number, $M_S = 1.0$. Also, it was decided that a one-stage parachute system could be assumed for the remainder of the study.

The error performances for the candidate systems are determined by analyzing the performances of the four subsystems. In the feasible systems study, these are Systems J, N, O and R as noted above. Following an explanation of the approach used in the analysis, the results of the performance analysis and the results of trade studies on the two types of prime sensors are presented.

4.1 PERFORMANCE ANALYSIS APPROACH

The performance analysis used in this phase of the study expresses the maximum altitude reduction due to the uncertainty in each of the independent variables acting individually. These are utilized to estimate the maximum overall altitude reduction due to the uncertainty in all the independent variables acting simultaneously.

The Assumed Functionality

Let the initiation altitude due to the operation of a sensor system be referred to as the trigger altitude, h_T. In this analysis, this trigger altitude is viewed as a function of eight independent variables as follows:

$$h_T = h_T\,(Atm,\ V_E,\ \gamma_E,\ \alpha_E,\ \rho_E,\ \chi_E,\ C_{P_b},\ Env) \qquad (1)$$

where, in addition to the symbol meanings given in Table 2, the symbols Atm, C_{P_b} and Env are used to represent atmosphere model, base pressure coefficient and environmental effects respectively.

Equation (1) states that the trigger altitude is a function of eight independent variables: atmosphere model, entry velocity, etc. Assuming that this functionality is "well behaved", Eq. (1) can be written as a Taylor expansion about an altitude h_o as follows:

$$h_T = h_o + \frac{\partial h_T}{\partial Atm}\,\Delta Atm + \frac{\partial h_T}{\partial V_E}\,\Delta V_E + \frac{\partial h_T}{\partial \gamma_E}\,\Delta\gamma_E$$
$$+ \frac{\partial h_T}{\partial \alpha_E}\,\Delta\alpha_E + \frac{\partial h_T}{\partial \rho_E}\,\Delta\rho_E + \frac{\partial h_T}{\partial \chi_E}\,\Delta\chi_E$$
$$+ \frac{\partial h_T}{\partial C_{P_b}}\,\Delta C_{P_b} + \frac{\partial h_T}{\partial Env}\,\Delta Env + \ldots \qquad (2)$$

The altitude h_o is the Mach number 1.0 altitude occurring in the trajectory produced by a particular set of values for the independent variables; say, Atm_o, V_{Eo}, etc. This altitude is referred to as the "null altitude." The delta (Δ) quantities represent the variations in the independent variables from the specified values; e.g., $\Delta V_E = V_E - V_{Eo}$. The three dots represent second and higher order terms in the Taylor expansion which are neglected in the analysis.

It may be observed that some of the quantities appearing in Eq. (2) have a rather problematical meaning; e.g., $\partial h_T / \partial Atm$. This problem is circumvented in the analysis by always working with the products of the partial derivatives and the associated Δ-quantities; e.g., $(\partial h_T / \partial Atm) \Delta Atm$. Clearly, these products (altitude-uncertainty components) can have significance. They are the altitude changes resulting from changes in the independent variables. Unless another meaning is specifically indicated, the phrase "altitude-uncertainty component" is defined to mean the maximum change from the null altitude due to the particular independent variable involved.

The Procedure

The procedure used in the analysis of each subsystem is as follows:

1. The operation of each subsystem is defined explicitly. At this stage in the study, it is impossible to make a quantitatively accurate definition. This will become possible only when the combination of the independent variables that produces the most adverse effect is known. Therefore, for the sake of being explicit, the most correct definition for the eight corner runs is used.

2. The trigger altitudes for certain of the 18 runs listed in Table 1 are determined.

3. The altitude-uncertainty components due to the atmosphere, entry velocity and entry flight path angle uncertainties are determined. Table 9 summarizes the relations used in this computation.

4. The altitude-uncertainty components associated with the entry angle of attack, the entry rolling velocity, the entry azimuth angle, the base pressure coefficient and the operational-environmental effects are computed. The equations used in this computation are shown in Table 10. As noted in this table, these equations are for computing low altitude uncertainties only.

5. Finally, the null altitude is computed. The relation used to make this computation is

$$h_o = h_{AV} - \frac{\partial h_T}{\partial \alpha_E} \Delta\alpha_E - \frac{\partial h_T}{\partial p_E} \Delta p_E + \frac{\partial h_T}{\partial \chi_E} \Delta\chi_E - \frac{\partial h_T}{\partial C_{P_b}} \Delta C_{P_b} - \frac{\partial h_T}{\partial Env} \Delta Env \qquad (3)$$

4.2 SUBSYSTEM DEFINITIONS

The four subsystems utilized in the three Candidate Systems are defined in this subsection. In addition, an ideal, $M = 1.0$ system is defined.

4.2.1 ACCELERATION SUBSYSTEM

The operational sequence for this system is as follows:

1. The axial acceleration a'_X is sensed by an accelerometer in the lander vehicle during entry.

2. When the acceleration level exceeds a preset level, the trigger circuit is armed.

3. The trigger pulse is generated when the acceleration level falls below a second preset level.

Only the second preset level is critical with respect to the trigger event. This acceleration level is selected to be the smallest value of sensed acceleration in the eight corner runs when the lander vehicle Mach number $M = 1.0$. This occurs on Run 77 when the axial acceleration $a'_X = 15.11$ ft/sec^2.

TABLE 12, SUMMARY OF ALTITUDE ERROR PERFORMANCE RESULTS FOR FIVE SYSTEMS/SUBSYSTEMS STUDIED IN PHASE 2

	H_o	$(\partial H/\partial K)K$								H_{Min}	Altitude Reduction	Altitude Reduction for Most Critical Run in Feasible Systems Study
System	h_{o_i}	$\left(\frac{\partial h_T}{\partial Atm}\right)_i \Delta Atm$	$\left(\frac{\partial h_T}{\partial V_E}\right)_i \Delta V_E$	$\left(\frac{\partial h_T}{\partial \gamma_E}\right)_i \Delta \gamma_E$	$\left(\frac{\partial h_T}{\partial \alpha_E}\right)_i \Delta \alpha_E$	$\left(\frac{\partial h_T}{\partial P_E}\right)_i \Delta P_E$	$\left(\frac{\partial h_T}{\partial x_E}\right)_i \Delta x_E$	$\left(\frac{\partial h_T}{\partial C_{P_b}}\right)_i \Delta C_{P_b}$	$\left(\frac{\partial h_T}{\partial Env}\right)_i \Delta Env$	$h_{o_i} - (\partial H/\partial K)K$	$h_{Min_{i=1}} - h_{Min_i}$	
i = 1 Ideal M = .1.0 System	43,300 Ft	25,000 Ft	1,000 Ft	2,400 Ft	300 Ft	900 Ft	100 Ft	0 Ft	0 Ft	13,600 Ft	0 Ft	
i = 2 Acceleration Subsystem	29,500	19,100	1,500	2,700	300	900	500	0	4,300	200	13,400	(Feasible System N) 3,400 Ft
i = 3 Base Pressure Subsystem	39,400	25,000	300	300	200	0	200	400	1,000	12,000	1,600	(Feasible System R) 2,020
i = 4 Base Pressure to Acceleration Ratio Subsystem	41,500	25,000	1,000	2,400	300	900	100	800	2,000	8,000	5,600	(Feasible System J) 1,340
i = 5 Acceleration Function Subsystem	31,500	18,800	1,300	1,800	500	600	500	0	4,300	3,700	9,900	(Feasible System 0) 2,720

last column shows the corresponding values of altitude reduction for the most critical run (Run 57) that occurred in the Feasible Systems Study. The values of the eight independent variables that yield the null altitude and the minimum altitude are shown in Table 13.

It may be noticed that minimum altitudes of from 200 to 13,600 feet are predicted for the five systems shown in Table 12. These minimum altitudes, it should be emphasized, are predicted on the basis of linear mathematical models for the various systems. Not only are these systems non-linear, at least with respect to the eight independent variables, but in most cases it is necessary to evaluate the altitude-uncertainty components at flight conditions far different than the minimum altitude flight condition.

Table 12 shows that the Base Pressure Subsystem has the smallest minimum altitude reduction, 1600 feet, followed in second place by the Base Pressure to Acceleration Ratio Subsystem, 5600 feet. This sequence is the opposite of what was indicated in the Feasible Systems Study; see last column in table. Also, this table shows the Acceleration Function Subsystem and the Acceleration Subsystem to rank third and fourth place respectively with reductions of 9900 and 13,400 feet respectively.

The largest single altitude uncertainty component is clearly associated with the atmosphere uncertainty. The next largest component depends on the system. For the Acceleration Subsystem, the Base Pressure Subsystem and the Acceleration Function Subsystem, it is the component associated with environmental effects. For the Base Pressure to Acceleration Ratio Subsystem, it is the component associated with the entry flight path angle. In all cases, the uncertainty components associated with the entry angle of attack and the entry azimuth angle are relatively small.

4.5 PRIME SENSOR TRADE STUDIES

Trade studies were conducted to establish the availability and suitability of pressure transducers and accelerometers for application in the Candidate Systems. The results of these trade studies are presented in this subsection.

TABLE 13, SUMMARY OF VALUES FOR INDEPENDENT VARIABLES GIVING THE NULL ALTITUDE AND THE MINIMUM ALTITUDE FOR THE PHASE 2 STUDY CONDITIONS

INDEPENDENT VARIABLE, K	VALUE FOR MINIMUM ALTITUDE	VALUE FOR NULL ALTITUDE
Atm	VM-8	Halfway between VM-3 and VM-8
V_E	12,500 FPS	14,250 FPS
γ_E	-20 deg	-17 deg
α_E	±105 deg	±50 deg
p_E	±1 rad/sec	±1/2 rad/sec
χ_E	+90 deg	0
C_{P_b}	Lower curve in Figure 6b	Middle curve in Figure 6b
Env	$(P_b)_{ACT} = 1.05\ (P_b)_{IND}$ $(a'X_B)_{ACT} = 0.95\ (a'X_B)_{IND}$	$(P_b)_{ACT} = (P_b)_{IND}$ $(a'X_B)_{ACT} = (a'X_B)_{IND}$

AUG 8 1966

The performance score for Candidate System No. 2 is significantly higher than for the other two systems. This is a reflection of the fact that this system does inherently measure Mach number rather than an indirect relation to Mach number. An opposite effect is shown by the reliability score. In the Degree of Redundancy subitem, the low grade for Candidate System No. 2 results from a consideration that, if a condition could exist that would create a failure in one of the pressure transducers, a failure in the other pressure transducer might also be induced. In addition, the state-of-the-art of components for long space storage and subsequent operation is considered less advanced for pressure transducer systems than for accelerometer systems. This is reflected in the scores for the failure rate and availability subitems.

Based primarily on the above considerations, Candidate System No. 2 was selected, and approved by JPL, for further analysis in Phase 3 of the study. In addition to the above considerations, it could be pointed out that this system has almost all the components that are used in the other two candidate systems. Thus, much of the detailed information generated in the final study phase would be applicable if a change were made to one of the other two candidate systems at some future time.

The Taylor expansion for the trigger altitude in terms of the ten independent variables, disregarding terms of second order and higher, is

$$h_T = h_o + \frac{\partial h_T}{\partial Atm}\,\Delta Atm + \frac{\partial h_T}{\partial V_E}\,\Delta V_E + \frac{\partial h_T}{\partial \gamma_E}\,\Delta \gamma_E + \frac{\partial h_T}{\partial \alpha_E}\,\Delta \alpha_E$$

$$+ \frac{\partial h_T}{\partial p_E}\,\Delta p_E + \frac{\partial h_T}{\partial \chi_E}\,\Delta \chi_E + \frac{\partial h_T}{\partial C_{P_b}}\,\Delta C_{P_b} \qquad (6)$$

$$+ \frac{\partial h_T}{\partial Env}\,\Delta Env + \frac{\partial h_T}{\partial Wind}\,\Delta Wind + \frac{\partial h_T}{\partial C_D}\,\Delta C_D$$

The Primary and Secondary Subsystems

The steps taken in computing the performance of each subsystem include those described in Section 4.0 with certain additions and modifications. These are itemized as follows:

1) The low altitude-uncertainty components associated with the maximum wind profile and drag coefficient effects are computed with the equations shown in Table 18.

2) The high altitude-uncertainty components associated with the entry angle of attack, the entry rolling velocity, entry azimuth angle, the base pressure coefficient, the operational environmental effects, the wind and the drag coefficient are computed. The equations used in this computation are shown in Table 19.

3) The null altitude is computed. The relations used to make this computation are

$$h_o = h_{AV} - \left| \frac{\partial h_T}{\partial p_E}\,\Delta p_E \right| + \left| \frac{\partial h_T}{\partial \chi_E}\,\Delta \chi_E \right| \quad , \text{ low altitudes}$$

$$h_o = h_{AV} - \left| \frac{\partial h_T}{\partial p_E}\,\Delta p_E \right| - \left| \frac{\partial h_T}{\partial \chi_E}\,\Delta \chi_E \right| \quad , \text{ high altitudes} \qquad (7)$$

TABLE 18, EQUATIONS FOR COMPUTING TWO ADDITIONAL LOW ALTITUDE-UNCERTAINTY COMPONENTS

$$\frac{\partial h_T}{\partial Wind}\,\Delta Wind = h_{T\,Run\ 81} - h_{T\,Run\ 69}$$

$$\frac{\partial h_T}{\partial C_D}\,\Delta C_D = h_{T\,Run\ 86} - h_{T\,Run\ 71}$$

TABLE 19, EQUATIONS FOR COMPUTING SEVEN HIGH ALTITUDE-UNCERTAINTY COMPONENTS

$$\frac{\partial h_T}{\partial \alpha_E}\,\Delta \alpha_E = \frac{1}{2}(h_{T_{Run\ 74}} - h_{T_{Run\ 73}})$$

$$\frac{\partial h_T}{\partial p_E}\,\Delta p_E = \frac{1}{2}(h_{T_{Run\ 24}} - h_{T_{Run\ 44}})$$

$$\frac{\partial h_T}{\partial \chi_E}\,\Delta \chi_E = \frac{1}{2}(h_{T_{Run\ 60}} - h_{T_{Run\ 79}})$$

$$\frac{\partial h_T}{\partial C_{P_b}}\,\Delta C_{P_b} = \frac{1}{2}(h_{-3_{MIN\ P_b/P_o}} - h_{-3\ MAX\ P_b/P_o})$$

$$\frac{\partial h_T}{\partial Env}\,\Delta Env = \frac{1}{2}(h_{-3_{\text{Max + Environmental errors}}} - h_{-3_{\text{Max − Environmental errors}}})$$

$$\frac{\partial h_T}{\partial Wind}\,\Delta Wind = h_{T_{Run\ 82}} - h_{T_{Run\ 72}}$$

$$\frac{\partial h_T}{\partial C_D}\,\Delta C_D = h_{T_{Run\ 85}} - h_{T_{Run\ 60}}$$

6.0 CONCLUSIONS

The following conclusions are presented, based on the results of this study.

1) This study, encompassing an analysis of sensor systems suitable for initiating parachute deployment on a Mars entry vehicle, shows conclusively that today's technology and hardware can provide a sensor system with sufficient flexibility to assure accurate sensing over the wide range of possible Martian atmospheres, entry conditions, and environmental conditions currently postulated for the mission.

2) A variety of sensor systems are feasible. Of the many sensor concepts analyzed in Phase 1 of the study, sixteen are suitable in various degrees. In general, sensor systems employing an accelerometer seem to have the most satisfactory performance over the ranges of deployment conditions and entry modes studied.

3) All of the four feasible sensor systems selected for more detailed analysis in Phase 2 of the study would be suitable for development within the specified guide lines. Two of these systems employ an accelerometer, one employs a base pressure transducer, and one employs both an accelerometer and a base pressure transducer. A trade study of these two types of prime sensors indicates that a strain gauge accelerometer and a capacitive pressure transducer are the most satisfactory in this application.

4) The Final System, selected for detailed analysis and design in Phase 3 of the study, features two sensor subsystems operating in parallel: a sensor subsystem utilizing the ratio of base pressure to sensed acceleration, and a sensor subsystem utilizing base pressure by itself. This system represents the most promising deployment prediction capability.